Mast cells in pressure overload induced right ventricular remodeling

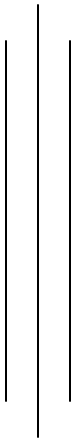

Inaugural dissertation submitted to the
Faculty of Medicine in partial fulfillment of the requirements
for the degree of Dr. hum. biol. from the Faculty of Medicine,
of the Justus Liebig University, Giessen

by
Himal Luitel
from
Sirsekot-7, Syangja, Nepal

Giessen, 2012

From the Medical Clinic II, Excellence Cluster of Cardio-Pulmonary System,
University of Giessen Lung Centre
Director/Chairman: Prof. Dr. med. Werner Seeger
of the Faculty of Medicine
of the Justus Liebig University Giessen

Supervisor: Prof. Dr. med. HA Ghofrani

Gutachter: Prof. Dr. med. HA Ghofrani
Gutachter: Prof. Dr. rer. nat. RT Schermuly

Date of Doctoral Defense: ……

CONTENTS

List of figures

List of schemes

ABBREVIATIONS

µg	Microgram
µL	Microliter
µm	Micrometer
ACE	Angiotensin converting enzyme
Ang-II	Angiotensin-II
ANP	Atrial natriuretic peptide
bFGF	Basic fibroblast growth factor
BNP	Brain natriuretic peptide
BSA	Bovine serum albumin
CI	Cardiac index
CO	Cardiac output
Col1	Collagen 1
Col3	Collagen 3
COPD	Chronic obstructive pulmonary disease
DAPI	4',6-diamidino-2-phenylindole
ECG	Electrocardiogram
ECM	Extracellular matrix
ECs	Endothelial cells
ET	Ejection time
ET-1	Endothelin-1
HR	Heart rate
Hrs	Hours
IB4-TRITC	Isolectin B4- Tetramethlylrhodamine isothiocynate
IL	Interleukin
IVCT	Isovolumic contraction time
IVRT	Isovolumic relaxation time
Kg	Kilogram
L	Liter

LV	Left ventricle
LVEDP	Left ventricular end diastolic pressure
LVSP	Left ventricular systolic pressure
MCP-4	Mouse mast cell protease 4
MCP-5	Mouse mast cell protease 5
MCs	Mast cells
MCT	Monocrotaline
mg	Milligram
min	Minute
mL	Milliliter
mm	Millimeter
O_2	Oxygen
PAB	Pulmonary artery banding
PAH	Pulmonary arterial hypertension
PAI-1	Plaminogen activator inhibitor-1
PCR	Polymerase chain reaction
PH	Pulmonary hypertension
RA	Right atrium
ROS	Reactive oxygen species
RV	Right ventricle
RVID	Right ventricular internal dimension
RVOT	Right ventricular outflow tract
RVSP	Right ventricular systolic pressure
RVWT	Right ventricular wall thickness
S	Septum
SAP	Systemic arterial pressure
Sec	Second
sGC	Soluble guanylyl cyclase
SVao	Aortic stroke volume
TAPSE	Tricuspid annular plane systolic excursion

TBS	Tris buffer solution
TDI	Tissue doppler imaging
TGF-β	Transforming growth factor-β
TL	Tibial Length
TNF-α	Transforming growth factor alpha
VEGF	Vascular endothelial growth factor
VEGFRII	Vascular endothelial growth factor receptor II
WGA-FITC	Wheat germ agglutinin-fluorescein isothiocynate

SUMMARY

Numerous studies have recently implicated mast cells in cardiovascular diseases. However, the role of mast cells in the development of right ventricular (RV) hypertrophy is not known. RV hypertrophy was induced in C57Bl/6 and WBB6F1/J-Kit^{W}/Kit^{W-v} (MC-deficient) and their wild type littermate mice by pulmonary artery banding (PAB). Mast cell stabilization in C57Bl/6 mice with cromolyn sodium was performed starting either from day 0 of PAB (early intervention) for 3 weeks or day 7 (late intervention) for 2 weeks. The functional changes of RV were assessed by high resolution ultrasound echocardiography. Hemodynamics, RV hypertrophy, RV mast cell density, mast cell activation/degranulation, RV interstitial fibrosis, cardiomyocyte hypertrophy, capillary density, mRNA expression of hypertrophic, profibrotic and mast cell specific genes were evaluated.

Pressure overload-induced RV remodeling in banded C57Bl/6 mice was characterized by significant interstitial fibrosis, increased mast cell activity and RV dysfunction. Inhibition of mast cell degranulation significantly reduced RV interstitial fibrosis and decreased mRNA expression of genes for collagen 1 and 3 and mast cell proteases 4 and 5. Moreover, these changes were associated with significantly improved RV function (cardiac output, myocardial performance index and tricuspid annular plane systolic excursion). Furthermore, we observed a beneficial RV remodeling characterized by the absence of interstitial fibrosis and chamber dilatation with preserved RV function in mast cell-deficient mice. These improvements were associated with decreased SMAD phosphorylation in mast cell-deficient mice.

Our data suggest that mast cells play a critical role in the pressure overload-induced RV remodeling. Stabilization of mast cells may represent a new approach in the RV-directed therapy.

ZUSAMMENFASUNG

Im Rahmen verschiedener Studien wurde das Auftreten von Mastzellen im Zusammenhang mit kardiovaskulären Erkrankungen bereits untersucht, allerdings ist ihre Rolle bei der Entwicklung von rechtsventrikulärer Hypertrophie bisher noch nicht hinreichend geklärt. Die rechtsventrikuläre Hypertrophie wurde mittels Pulmonalarteriellem Banding (PAB) in C57Bl/6- und WBB6F1/J-Kit^{W}/Kit^{W-v} (MC-defizienten)-Mäusen, sowie deren Wildtypen, induziert. Die Mastzell-Stabilisierung mittels Cromoglycinsäure wurde bei den C57Bl/6-Mäusen entweder ab Tag 0 der PAB-Operation (frühe Intervention) über einen Zeitraum von 3 Wochen oder ab Tag 7 (späte Intervention) über einen Zeitraum von 2 Wochen durchgeführt.Die Veränderungen der Funktionsparameter des rechten Ventrikels wurden mittels Echokardiographie (hoch auflösender Ultraschall) ermittelt. Ausgewertet wurden außerdem Hämodynamik, rechtsventrikuläre Hypertrophie, rechtsventrikuläre Mastzelldichte, Mastzell-Aktivierung/Degranulation, rechtsventrikuläre Fibrose, Kardiomyozyten-Hypertrophie, Kapillardichte und die mRNA-Expression der hypertrophen, profibrotischen und mastzellspezifischen Gene.

Das durch Druckbelastung induzierte rechtsventrikuläre Remodeling in den gebandeten C57Bl/6 Mäusen war gekennzeichnet durch signifikante interstitielle Fibrose, erhöhte Mastzellaktivität und rechtsventrikuläre Funktionseinschränkung. Die Hemmung der Mastzelldegranulation konnte die rechtsventrikuläre Fibrose signifikant reduzieren und die mRNA-Expression der Gene für Kollagen 1 und 3 sowie der Mastzellproteasen 4 und 5 deutlich senken.Zudem zeigte sich einesignifikanteVerbesserung der rechtsventrikulären Funktionsparameter (Herzzeitvolumen, MyocardialPerfomance Index und TricuspidAnnular Plane SystolicExcursion).Bezüglich des rechtsventrikulärenRemodelingskonnte in den Mastzell-defizienten Mäusen eine verminderte Ausprägung der interstitiellenFibrose und der Kammerdilatation beobachtet werden. Die festgestellten Verbesserungen gingen mit verminderter SMAD- Phosphorylierung einher.

Unsere Daten lassen vermuten, dass Mastzellen eine entscheidende Rolle bei der Ausprägung von rechtsventrikulärem Remodeling, bedingt durch Druckbelastung, spielen. Daher könnte die Mastzellstabilisierung einen neuen therapeutischen Ansatz im Rahmen der Behandlung der rechtsventrikulären Hypertrophie darstellen.

1 INTRODUCTION

1.1 Right ventricular remodeling

1.1.1 Background

Cardiac remodeling is an adaptive process by which the heart changes its shape, size and function in response to mechanical, neurohumoral or genetic factors[1]. It occurs during the normal growth or in response to hemodynamic stresses[2]. In response to an increase in load (volume or pressure overload or combination of both), the heart has to work harder than under normal physiological conditions. To counterbalance the chronic increase in wall stress, the cardiomyocytes enlarge which leads to an increase in size and mass of the heart[3-5]. In addition to cardiomyocytes, fibroblasts, extracellular matrix proteins and the coronary vasculature are also involved in the remodeling process[1]. Cardiac remodeling is associated with alterations of many mediators such as neurohumoral factors, cytokines, enzymes, ion channels, oxidative stress and mechanical stress. Although remodeling is initially an adaptive response to maintain normal cardiac function and cardiac output by ameliorating ventricular wall stress, it gradually becomes maladaptive and leads to progressive ventricular dilatation and heart failure.

Most of the current therapies are documented to be effective in reducing mortality and morbidity in left heart failure[6,7]. Beneficial effects of pharmacological and non-pharmacological therapies on prognosis in heart failure patients have been associated with favourable changes in cardiac geometry, suggesting that modulation of remodelling process is effective for preventing the progression of heart failure[8,9]. Recent research has attempted to elucidate underlying molecular mechanisms of cardiac remodeling and to develop novel therapeutic strategies to prevent heart failure[10-12].

Numerous recent studies have provided strong evidence to recognize the pivotal role of the right ventricle (RV) in heart diseases[13]. Thus, the performance of the RV defines prognosis in patients with congenital heart disease[14], pulmonary arterial hypertension (PAH)[15] myocardial infarction involving the RV[16], advanced left heart failure[17-19] and even in patients with stable cardiovascular diseases[20]. Although the response of the RV to chronic pressure or volume overload is an important determinant of patient outcome, very

little is known about the underlying mechanisms. For many years, the RV was viewed as less important than the left heart in the maintenance of normal overall hemodynamic performance[21]. Consequently, studying cardiac remodeling process has mainly been restricted to the left ventricle, whereas the role of the RV has remained comparatively ignored[22]. Only recently, after recognizing its key role in various physiological and pathological conditions, the forgotten chamber of the heart regained attention.

1.1.2 Etiology and epidemiology

The prevalence and severity of RV dysfunction differs depending on the etiology of the underlying disease[23]. It is commonly thought that RV hypertrophy is related to increased pulmonary artery pressure and RV hypertrophy is considered a consequence of pulmonary hypertension (PH). Clinically, PH is defined as the elevation of mean pulmonary arterial pressure of more than 25 mm Hg at rest and/or more than 30 mm Hg during exercise[24,25]. A variety of conditions can lead to the development of PH.

Idiopathic pulmonary arterial hypertension (PAH) is a rare disease characterized by remodeling of small pulmonary arteries leading to chronic pressure overload and associated volume overload with the development of tricuspid regurgitation. Pulmonary vascular disease may complicate untreated congenital heart diseases including ventricular septal defect, patent ductus arteriosus, atrial septal defect, as a result of increased pressure or volume overload or both[26]. After idiopathic PAH and PAH associated with connective tissue diseases, PAH associated with congenital heart defects is the third most common form of PAH in Group 1 of the PH classification[27].

PH associated with chronic parenchymal lung diseases in Group 3, including chronic obstructive pulmonary disease, interstitial lung diseases and sarcoidosis, is one of the most common forms of PH[28]. Chronic obstructive pulmonary disease is one of the leading causes of morbidity and mortality worldwide and represents thus a major public health issue[29]. The prevalence of PH in these patients depends on the population under study, the definitions applied and the tools used to evaluate patients[30]. Most studies have reported a prevalence of PH in between 30% and 70%[31]. In general, the degree of PH is low to moderate in magnitude. However, numerous studies have shown that the presence of even mild PH is of prognostic relevance in patients with COPD[30].

Left heart disease represents the most common cause of PH[32-34] and are summarized in Group 2. Heart failure is a major public health issue, with a prevalence of over 23 million worldwide[35]. Approximately 60% to 70% of patients with chronic heart failure develop pulmonary venous hypertension[17,18]. Over a period of time, an increase in pulmonary vascular resistance resulting from extensive remodeling of lung resistance vessels may ensue. The resulting increase in RV afterload may ultimately cause fatal RV failure. Moreover, in patients with chronic heart failure the presence of signs and/or symptoms of RV failure identify a subgroup of patients with a very poor prognosis.

RV hypertrophy and failure can also develop in various right-sided cardiac valvular diseases as a result of the adverse hemodynamic consequence of RV volume or pressure overload. In the past, right-sided cardiac valvular disease was considered less clinically important than left-sided valvular disease. However, with the recent advances in modern imaging techniques, it has been shown that detectable tricuspid regurgitation is very common. Recent studies suggest that right-sided valvular disease has a significant and independent impact on morbidity and mortality[36,37]. Tricuspid regurgitation is most frequently secondary to another disease process causing RV dilatation, distortion of the subvalvular apparatus, tricuspid annular dilatation, or a combination of these[36,37]. However, structural abnormality of the tricuspid valve of congenital (Ebstein anomaly, displasia or hypoplasia of the tricuspid valve) or acquired origin (endocarditis, trauma, rheumatic heart disease) can also cause tricuspid regurgitation[36,37]. High RV pressures can cause RV hypertrophy and eventually right-sided heart failure in several diseases with congenital or acquired obstruction to pulmonary blood flow (e.g. tetralogy of Fallot, pulmonary valve stenosis, pulmonary atresia and diGeorge's syndrome).

Thus, the etiological spectrum of RV hypertrophy and failure is very broad and the prevalence of some underlying diseases is very high representing a major public health issue. RV failure is a significant complication, which is frequently encountered and aggravates prognosis in these patients. Despite the recent recognition of an important role of the RV in heart diseases, there has been little interest in RV-targeted therapeutic approaches[38]. A better understanding of the mechanisms underlying the RV remodeling processes may provide important clues about possible candidate targets which will help us

develop novel therapeutic strategies directed specifically at RV and thus improve survival in patients.

1.1.3 Pathophysiology

The RV hypertrophy with subsequent failure may develop as a result of pressure or volume overload, intrinsic myocardial dysfunction, or preload reduction[39,40]. The underlying pathophysiological mechanisms may differ depending on the etiological factors. The mechanisms of pressure overload induced RV hypertrophy and failure will be described here.

According to the old paradigm, hypertrophy occurs as an adaptive response to normalize wall stress and compensate for an increased load. Cardiomyocytes increase in size and initiate remodeling of the entire ventricular chamber. However, recent studies in animal models of pressure overload indicate that hypertrophy is not a necessary adaptive response to elevated cardiac workload and inhibition of hypertrophy can, in fact, prevent rather than promote systolic dysfunction[41,42]. More recent studies suggest that modifying a particular signaling mechanism could exhibit more profound effects on the maintenance of cardiac function in response to hemodynamic overload than normalizing the wall stress. Indeed, cardiac hypertrophy occurs in response to a wide variety of stimuli, each of which activates an intricate network of signaling molecules[43]. These molecular pathways not only mediate cardiac hypertrophy but are also responsible for activation of deleterious or beneficial mechanisms for the heart, resulting in development of heart dysfunction and failure or maintained heart function, respectively. Therefore, the reduction of heart mass itself should not represent the main target in the treatment of cardiac hypertrophy. More important is the correction of the molecular pathways that account for complications associated with cardiac hypertrophy and/or the enhancement of the activity of cellular signals mediating cardioprotective actions.

The hypertrophy of individual cardiomyocyte requires a reinforcement of the fibrous scaffold of the heart or the extracellular matrix, which is sustained by deposition of collagen and other extracellular matrix proteins. Extracellular matrix, particularly fibrillar collagen, provides tensile strength that allows cardiac muscle to perform systolic and diastolic functions. Collagen is the predominant structural component of the extracellular matrix, forming an intricate network of fibers around individual cardiomyocytes and

interconnects myofibrils, muscle fibers and muscle bundles. An abnormal accumulation of collagen occurs within the interstitium and adventitia of intramyocardial coronary arterioles due to increase in collagen synthesis and/or decrease in collagen degradation. However, increased levels of interstitial collagen are detrimental for heart function, distorting tissue structure and causing abnormal myocardial stiffness.

Insufficient blood supply is another important issue in cardiac hypertrophy and failure. This may result from an inadequate growth of the capillary vascular bed while ventricular mass is increasing[44], an increase in diffusion distance due to cardiomyocyte hypertrophy and failure of cross-sectional area of the vascular bed to enlarge in proportion to the degree of hypertrophy[45]. Recent studies demonstrated that cardiac angiogenesis is crucially involved in the adaptive mechanism of cardiac hypertrophy and its impairment is essential for the transition from the compensated cardiac hypertrophy to heart failure[46].

Sustained pressure overload leads to dilatation of the hypertrophied RV (Scheme 1). Dilatation of the RV chamber leads to dilatation of the tricuspid annulus causing tricuspid regurgitation, resulting in volume overload and further exacerbating dilatation. As the RV dilates, the crescentic shape of the RV cavity is lost and the RV acquires a spherical shape. Because of interventricular interdependence, the interventricular septum bulges into the LV cavity resulting in impaired left ventricular filling and function. Furthermore, impaired left ventricular function leads to decrease of systemic and right coronary perfusion pressures, further compromising the RV function.

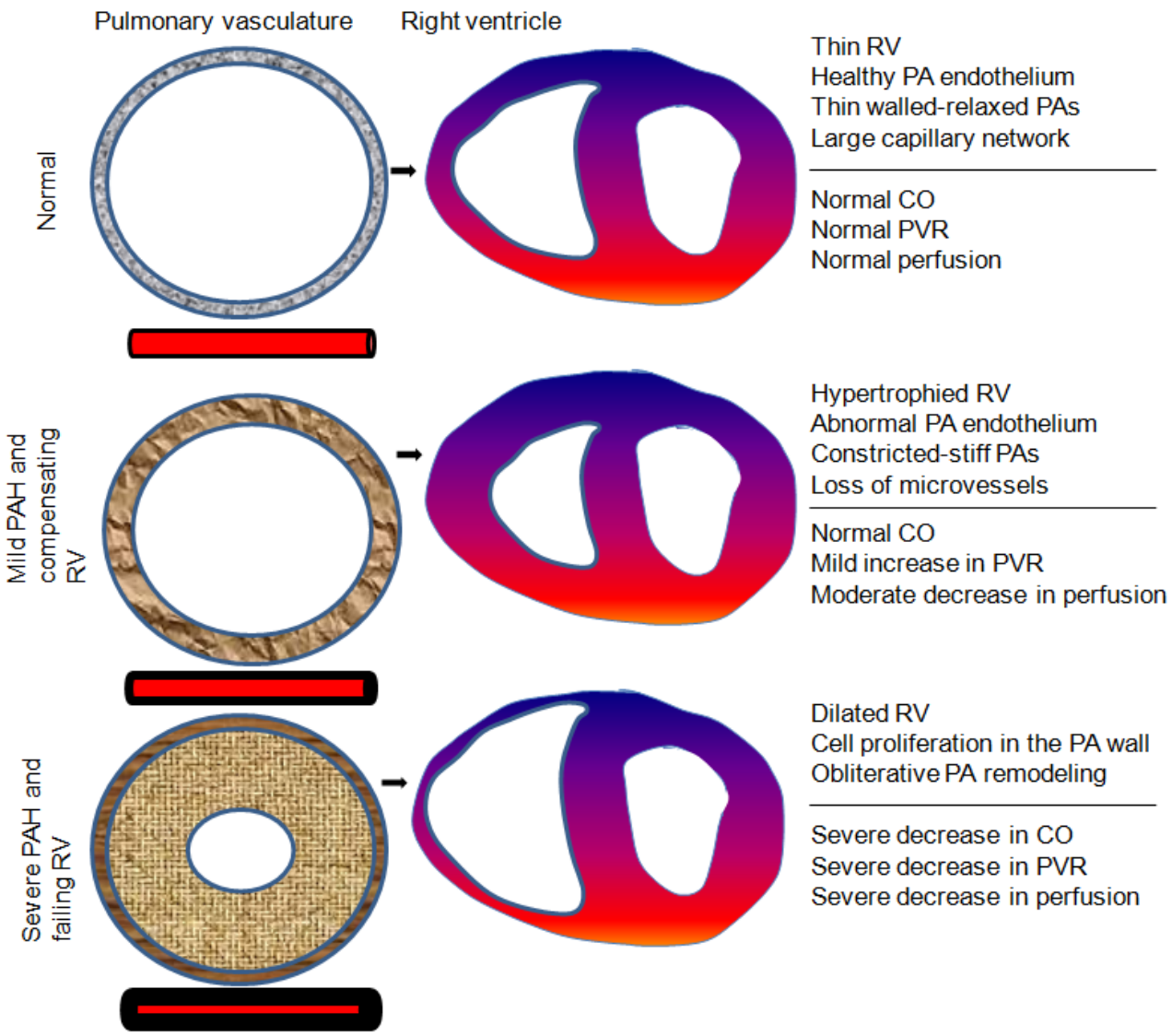

Scheme 1: Pulmonary hypertension and right ventricular remodeling
Modified from Champion *et al.*, 2009,[47]

1.2 Animal models of RV remodeling

A common approach for understanding the mechanisms underlying human diseases and for testing potential therapies is to mimic the disease in animal models. Various species from small to large animals have been used for cardiovascular research. Although, large animals have contributed to understanding of human diseases in the past, currently, large animal models are not as widely used as rodents. While large animals have anatomical and physiological similarities to humans, they are expensive and require substantial resources for housing and care. Additionally, in many countries, investigations on larger

animals are restricted due to ethical considerations. Small animals such as rodents offer many advantages like their easy availability and low maintenance cost. Moreover, with the advancement of genetically engineered animals, the popularity of the rodents has increased.

A number of rodent models of PH have been developed to study the underlying pathophysiological processes involved in the disease state and in the development of novel agents to treat the disease. The most commonly used animal models of PH are chronic exposure to hypoxia and injection of monocrotaline. As RV hypertrophy is the outcome of the PH, animal models of PH can also be used to study RV remodeling processes.

1.2.1 Hypoxia-induced PAH

Acute hypoxia induces hypoxic pulmonary vasoconstriction, an essential mechanism of the ventilation-perfusion matching in the lung. In contrast, chronic exposure of mice and rats to hypoxia leads to pulmonary vascular remodeling with subsequent PH and right heart hypertrophy. However, hypoxic PH is characterized by only mild-to-moderate PH and RV hypertrophy without development of RV failure[48,49]. Recently, combination of hypoxic exposure and VEGFRII inhibition was reported as a robust rodent model of PH characterized by pulmonary vascular lesions that resemble those found in human PAH and associated with fatal RV failure[50]. VEGF is a crucial pro-survival cytokine which keeps the endothelial cells alive. Single injection of SU5416, a VEGFRII antagonist followed by exposure to chronic hypoxia induces initial apoptosis of endothelial cells and selection of apoptosis-resistant endothelial cells with an extensive proliferative capacity[51]. Proliferation of pre-capillary endothelial cells results neointima formation and obliteration of pulmonary vasculature resulting severe PH which leads to RV hypertrophy and failure.

1.2.2 Monocrotaline-induced PAH

Monocrotaline, a pyrrolizidine alkaloid toxin present in the plant *Crotalaria spectabilis*, is quite often used to induce experimental PH in rodents. Several hours upon single subcutaneous or intraperitoneal injection of monocrotaline causes perivascular and interstitial lung edema and diffuse alveolar damage[52]. Monocrotaline-pyrrole released after hepatic metabolism of monocrotaline is a major metabolite responsible for vascular injury

in the pulmonary vessels[53,54]. Two weeks after monocrotaline injection, progressive remodeling of the pulmonary vasculature occurs finally leading to an increased pulmonary vascular resistance. This increased pulmonary vascular resistance results in increased workload to the right heart leading to RV hypertrophy and failure. Combination of pneumonectomy and monocrotaline injection has been proposed in order to develop more severe phenotype[55,56]. Recent evidence suggests that the monocrotaline causes myocarditis in rats, which complicates the study of the RV hypertrophy and failure[57] .

The model of monocrotaline-induced PH is best characterized in rats. Although, according to some publications, mice do not develop PH after monocrotaline exposure[58], this model was also applied in mice[59,60]. Nevertheless, hemodynamic changes after monocrotaline injection in mice are very mild and there is no evidence of heart failure.

1.2.3 Pulmonary artery banding (PAB)

RV hypertrophy with subsequent dysfunction has been the subject of extensive study. The underlying molecular mechanisms however remain elusive as experimental models of RV hypertrophy created by pulmonary artery banding (PAB) in the past involved mostly large animals[61-65].

With the advent of gene targeting technology, the mouse has rapidly become the most important model organism in cardiovascular research[66]. Recently, pressure overload-induced RV hypertrophy and failure have been produced by PAB in mice[67-74] and rats[75-81]. The availability of a murine model of PAB provides us with a valuable tool to explore the molecular mechanisms of hypertrophy as well as its transition to heart failure by application of pressure overload in various genetically modified mice. A better understanding of the mechanisms underlying the RV remodeling processes may provide important clues about possible candidate targets which will help us to develop novel therapeutic strategies directed specifically at RV. In contrast to the models of PH, this model allows investigating direct afterload-independent effects of therapy on RV remodeling and RV function.

Following PAB in mice, the heart is challenged with an immediate pressure overload and there is an initial increase in RV end-diastolic pressure at 6 h after PAB with following recovery by 24 h. Subsequently, the RV end-diastolic pressure further increases depending on the severity of the stenosis. Myocardial hypertrophy develops within 1

week[69]. Although, a similar degree of hypertrophy is induced by applying different degrees of pulmonary constriction, severe overload results in more significant RV dilation and depression of RV function[72]. Therefore, PAB can be used as a model of both pressure overload-induced compensated right heart hypertrophy and failure. Markedly enlarged RV chamber in severe pulmonary stenosis leads to flattening or bowing of the septum into the left ventricle (Figure 1) thus compromising the function of the left ventricle[67]. However, a detailed characterization of time course changes in RV morphology and function in response to pressure overload is still lacking.

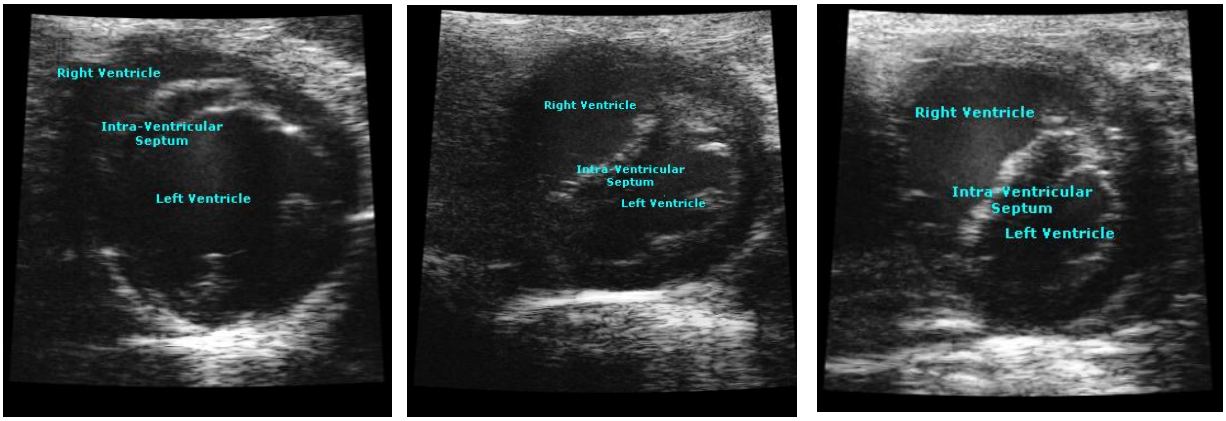

Sham Day 1 after PAB Day 35 after PAB

Figure 1: Representative Echocardiograms of sham and banded mice
Progressive increase in RV wall thickness, dilatation of the RV, flattening of the interventricular septum and compression of the left ventricle is shown. Left parasternal short-axis view.

1.3 Mast cell biology

Mast cells are multifunctional granular cells localized in various tissues throughout the body[82]. The mature mast cells activate inflammatory and tissue repair processes by releasing a variety of chemical substances including cytokines, proteases, leukotrienes and histamine[83]. Traditionally, mast cells were considered only as an early effecter cells of allergic diseases[84]. However biological functions of mast cells include also a role in innate and acquired immunity. Although mast cell functions have classically been related to allergic and non-allergic immune responses, a rapidly growing body of evidence has implicated these cells in a large variety of pathophysiologic processes including tissue repair, remodeling, pathological fibrosis and angiogenesis[85,86].

1.3.1 Mast cell heterogeneity

Although mast cells share many characteristics, they do not represent a homogeneous population. In rodents, two subtypes are distinguished: connective tissue mast cells localized in the sub-mucosa of the gastrointestinal tract, in the skin and in the peritoneum and mucosal mast cells, found in the mucosa of the gastrointestinal system and in the lamina propria of the respiratory tract. In addition to the tissue localization, there are also phenotypical differences between these mast cell subtypes, including cell size, histamine, protease, proteoglycan content and their function. In contrast to rodents, human mast cells have the major differences in protease content but not in histamine and proteoglycans. In humans, mast cells are classified according to the protease content. Mucosal type mast cells contain only tryptase, whereas connective tissue type mast cells produce both tryptase as well as chymases[87].

1.3.2 Mast cell activation and mediators release

Mast cells can be activated in two ways: immunologic and nonimmunologic activation. During the immunologic activation, stimulation of the mast cell activation is initiated either by interaction of the antigen specific antibodies or the antigen with the corresponding mast cell receptors[88,89]. Alternatively, mast cells can be activated by substances such as neuropeptides, basic compounds, cytokines and certain drugs[90,91]. This way of stimulation is called nonimmunologic activation. Both mechanisms lead to mast cells degranulation and release of mediators. Upon activation, mast cells release a large array of mediators which play a crucial role in different cellular responses. The mediators are broadly classified into three categories; namely preformed mediators (histamine, proteoglycans, serotonin, proteases), lipid derived mediators (prostaglandins and leukotrienes) and newly synthesized mediators (interleukins IL-1, 3, 4, 5, 6, 8, 10, 13, 16, tumor necrosis growth factor α, vascular endothelial growth factor, nerve growth factor)[92]. Tryptase, chymase, carboxypeptidase, cathepsin G are the mast cell proteases which play a critical role in extracellular matrix remodeling. Mast cell activation and release of mediators are shown in more detail in scheme 2.

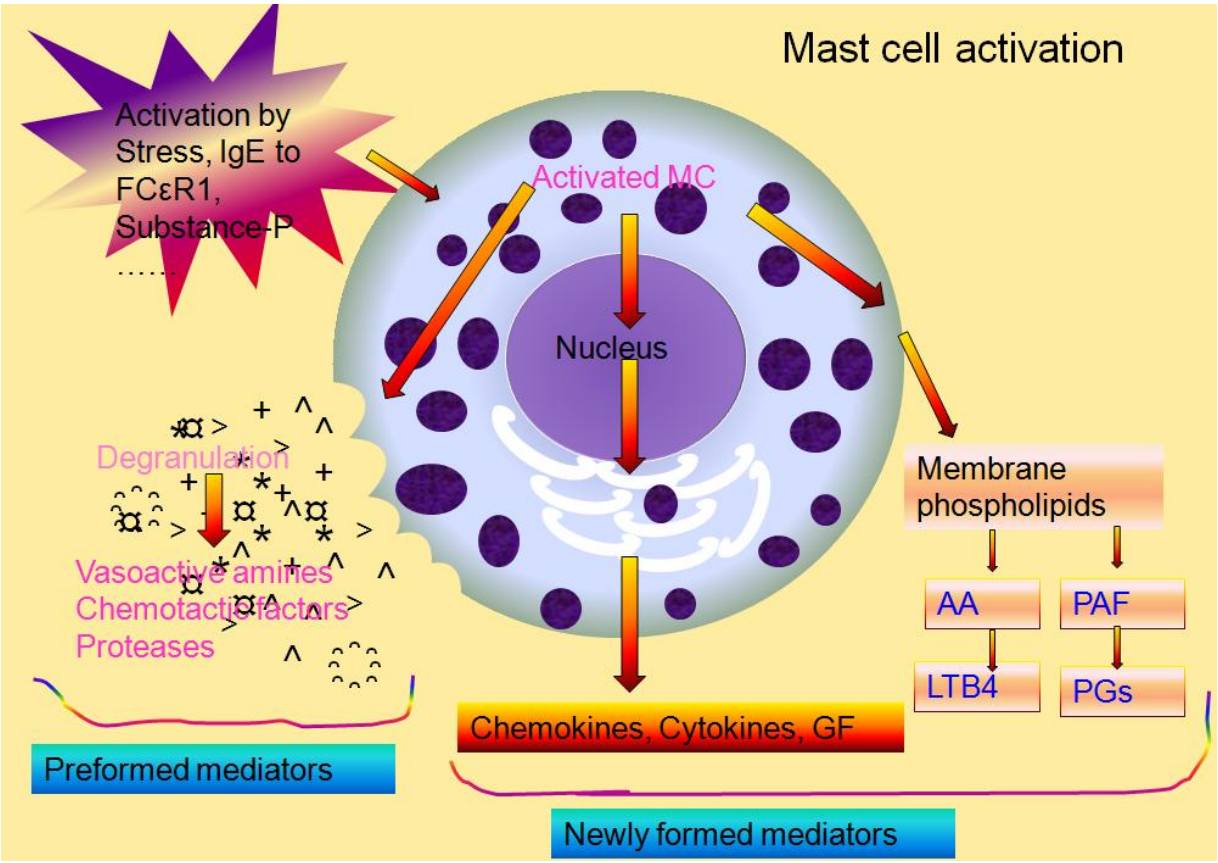

Scheme 2: Mast cell activation and mechanism of mediator release

Modified from Klueh *et al.*, 2010[90]

1.3.3 Mast cell in innate and adaptive immunity

Mast cells are commonly located at the sites that interface the external environments such as skin, alveolar surface, the gastrointestinal tract and in close proximity to nerves and blood vessels[93]. Mast cells act as sentinels ready at the first signal of the infection/trauma to release massive amount of preformed and newly synthesized mediators e.g. histamines, proteases, lipid mediators, cytokines and chemokines. So they work as a first line of defense like macrophages. The cytokines from mast cells induce other inflammatory cells such as neutrophils to release mediators and chemokines and play a role in recruiting inflammatory cells to the site of the injury[94].

Mast cells do play a role in host defense against bacterial and parasitic infection. Mast cells are the major source of inflammatory mediators and they are the only cells which store the pre-formed TNF-α which play important role in inflammation and host resistance to parasites[95] and promote lymph node hyperplasia[96]. Mast cell mediators are potential

vasodilators and increases vascular permeability. Mast cells are not only able to recruit effector cells, but by modulating vascular permeability also provide an optimal environment for the effective functioning of the complement cascade in the extravascular environment and for access of other innate effector mechanisms[97]. In addition, mast cells induce physiologic changes in the airways, such as bronchoconstriction and increased intestinal motility and epithelial sloughing[97]. Furthermore, mast cells respond through pathogen phagocytosis and production of antimicrobial peptides[97,93]. Although professional phagocytes such as neutrophils and macrophages are the major source of reactive oxygen species (ROS), several reports have shown that activated mast cells also generate intracellular ROS[98] which acts as potent antimicrobial agent and regulates the cell signaling and activation pathways. Mast cells play a role in antigen presentation via major histocompatibility complex [99-101] and dendritic cell maturation and recruitment[102].

1.3.4 Mast cell in cardiac remodeling

Although mast cell functions have classically been related to allergic and non-allergic immune responses, a rapidly growing body of evidence has implicated these cells in a large variety of pathophysiologic processes[103]. Mast cells are also present in the heart[104,105] and recent studies have identified critical roles for mast cells in cardiovascular diseases including atherosclerosis[106], progression of vascular aneurysms[107,108,109], pulmonary hypertension[110,111], myocardial infarction[112,113], left ventricular hypertrophy and failure[114,115]. Enhanced accumulation of mast cells in hypertrophied and failing hearts[116-118] suggests that mast cells play a role in the pathogenesis of these diseases. However, the molecular mechanisms by which cardiac mast cells may participate in such pathological processes remains unclear.

Mast cells are the major source of a whole host of growth factors, proteases, cytokines, chemokines, polypeptides, biogenic amines, proteoglycans and phospholipid metabolites including histamine, heparin, chymase, tryptase, phospholipases, kinins, tumour, tumor necrosis factor alpha and transforming growth factor[119]. Several of these mast cell mediators have been implicated in a number of cardiovascular pathologies. Chymase, a family of chymotrypsin-like serine proteases stored in secretory granules of mast cells, has been implicated in tissue remodeling through activation of endothelin 1 and matrix metalloproteinases[120-122], formation of angiotensin II[123-125] and activation of transforming

growth factor TGF-β[126]. Angiotensin II is a potent vasoactive peptide which also exerts direct growth-promoting effects on cardiac tissues, resulting in cardiomyocyte hypertrophy and mechanical dysfunction[127]. Most of the circulating angiotensin II is generated by plasma angiotensin I converting enzyme (ACE) but in the cardiac tissues, angiotensin II generation is chymase dependent. Angiotensin II promotes proliferation of cardiac fibroblasts coupled with collagen synthesis and expression of adhesion receptors which play a key role in myocardial remodeling process[128-131]. Recently, it was reported that mast cell chymase limits the cardiac efficacy of ACE inhibitor therapy in rodents[126]. Interestingly, Wei *et al*. demonstrated that combined chymase and ACE inhibition, relative to ACE inhibition alone, improved left ventricular function, decreased adverse cardiac remodeling and improved survival after myocardial infarction in hamsters[126]. Mast cell chymase inhibition has been shown to reduce atherosclerotic plaque progression[106], prevent cardiac fibrosis and improve diastolic dysfunction in the progression of heart failure[132-115].

TGF-β released by mast cells has also been involved in induction of cardiac hypertrophy and fibrosis[134]. Mast cell chymase is involved in the activation of latent TGF-β which is ultimately associated with increased collagen I and III expression in cardiac fibroblasts[116].

TNF-α plays an important role in the transition from compensated to decompensated hypertrophy[116]. Cardiac mast cells are involved in the regulation of cardiac growth during development of cardiac hypertrophy via activation of TNF-α/NF-kB/IL-6 signaling pathway.

In contrast, some studies suggest the protective role of mast cells in myocardial remodeling[135,136]. One explanation for this discrepancy is that the mast cells can release a wide range of mediators, cytokines and growth factors with multiple potential functions in relation to the target organ, so that may counteract the effects of each other with the resulting beneficial or detrimental outcome depending on the disease model. In addition, mast cells may be beneficial or harmful, depending on the stage of disease[137]. The discrepancy may also be explained by the functional heterogeneity of mast cell populations involved in pathological processes[138]. Indeed, the secondary increase in mast cells in failing myocardium under mechanical ventricular support was associated with an increase in chymase-negative mast cells and a change in phenotypic expression in mast cells with decreased myocardial basic fibroblast growth factor levels[139].

Thus, mast cells are involved in the development of left heart hypertrophy and failure. However, the role of mast cells in the development of RV hypertrophy has not been studied yet. A potential role of mast cells in cardiac hypertrophy is summarized in scheme 3 and 4.

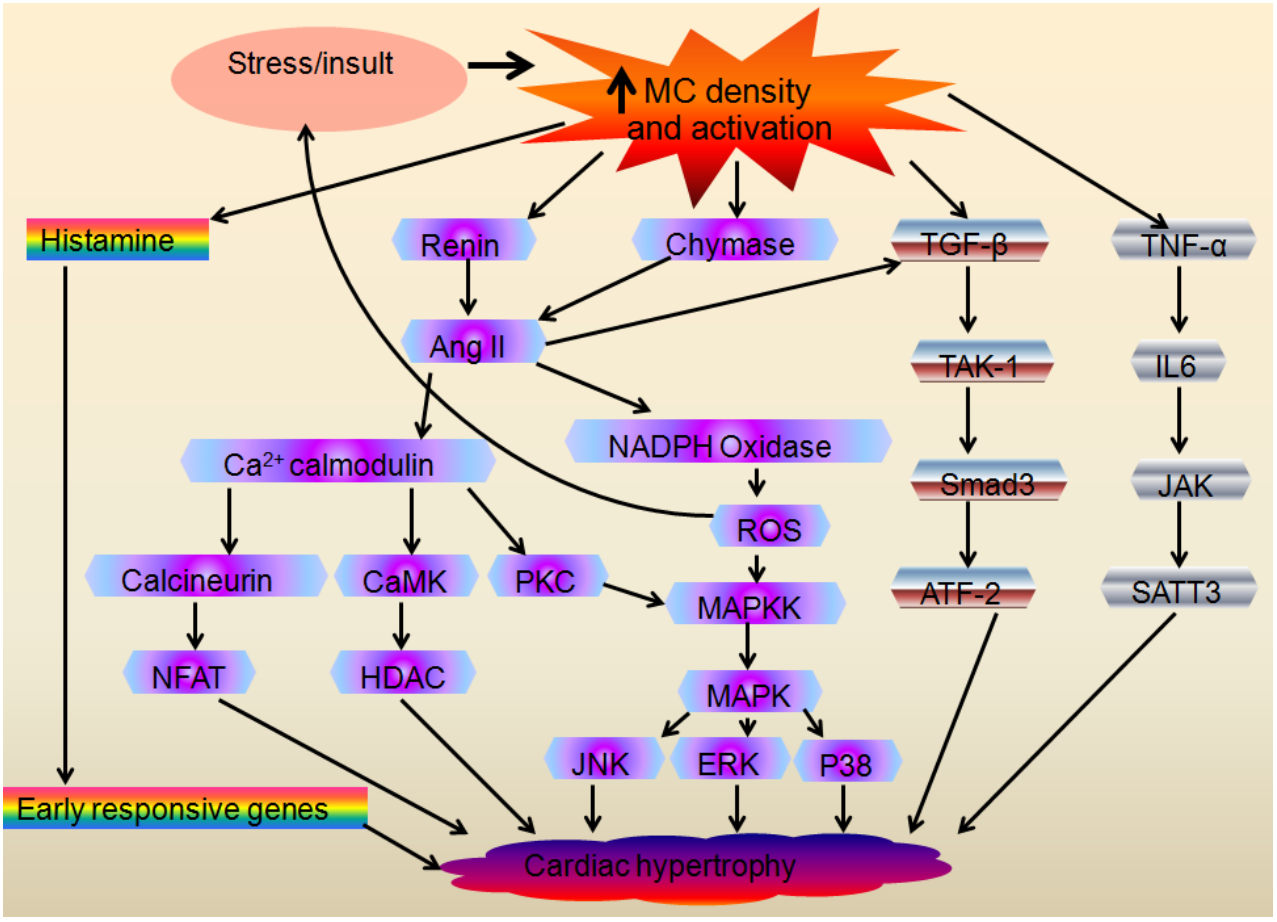

Scheme 3: Mast cell and their mediators in cardiac hypertrophy
Modified from Balkumar *et al.*[140].

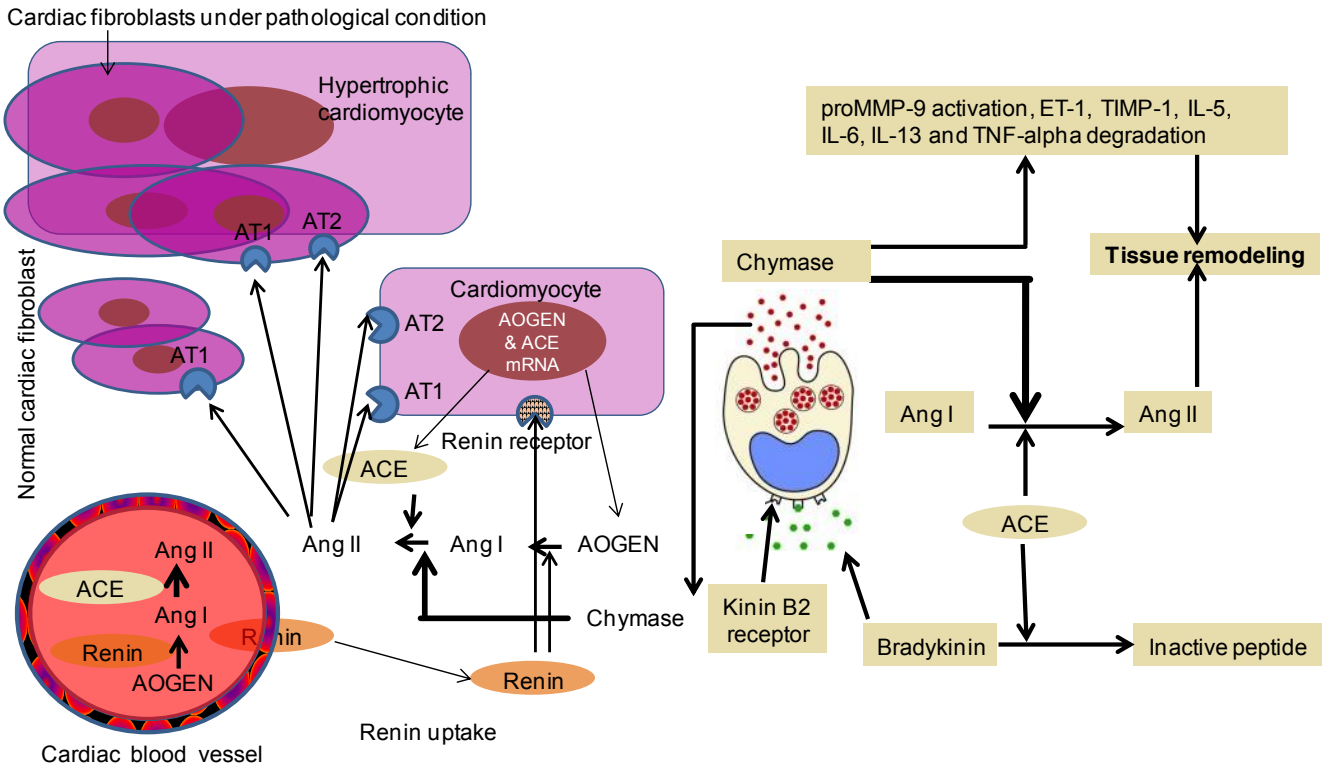

Scheme 4: Involvement of mast cell in cardiac remodeling,
Modified from Wei *et.al.*, *J Clin Invest.* 2010[126] and Paul M *et al.* Physiol Rev 2006[141].

1.4 Aims of the study

According to our hypothesis, mast cells are causally involved in the deleterious RV remodeling in response to pressure overload and represent therefore an interesting target for a novel therapeutic strategy directed specifically at RV. The objectives of this study are, therefore, to investigate the role of mast cells in RV remodeling process in response to pressure overload and to explore potential of a clinically available mast cell-stabilizing agent as a novel therapeutic strategy directed specifically at RV.

2 MATERIALS AND METHODS

2.1 Materials

2.1.1 Solutions and substances

Isoflurane	Forene® Abbott, Wiesbach, Germany
Physiological saline solution	DeltaSelect GmbH, Dreieich, Germany
Baytril 2.5%	Bayer, Leverkusen, Germany
Ketavet (Ketamin hydrochlorid)	Pfizer Pharma GmbH, Karlsruhe, Germany
Rompun 2% (Xylazin hyrdochlorid)	Bayer, Leverkusen, Germany
Xylocain® 2% Jelly	Astra Zeneca, Wedel, Germany
Buprenorphine	Temgesic®, Essex Pharma GmbH, Munich, Germany
Dexpanthenol eye ointment	Bayer, Leverkusen, Germany
Sodium hydroxide 1N (1mol/l)	Merck, Darmstadt, Germany
Hydrochloric acid acid 1N (1mol/l)	Merck, Darmstadt, Germany
Heparine Liquemin N 25000®	Roche, Basel, Swiss
Ketamin hydrochloride 100 mg/ mL Ketamin®	Pharmacia, Erlangen, Germany
Ventilation gas, 50% O_2, 50%N_2	Air Liquid, Siegen, Germany
Ventilation gas, 100% O_2	Air Liquid, Siegen, Germany
Glacial acetic acid 100 %	Roth, Karlsruhe, Germany
Haemalaun, Sauer nach Mayer	Waldeck GmbH and Co.KG, Muenster, Germany
Acetone	Mallinckrodt Baker B.V., Deventer, The Netherlands
Ethanol 70%, 95%, 99.6%	Otto Fischer GmbH and CO.KG, Saarbrücken, Germany
Isopropanol (99.8%)	Fluka Chemie, Buchs, Switzerland
Methanol	Sigma-Aldrich Biochemie GmbH, Steinheim, Germany

Formaldehyde alcohol free 3.5%	Roth, Karlsruhe, Germany
Xylol	Roth, Karlsruhe, Germany
Hydrogen peroxide 30%	Merck, Darmstadt, Germany
Picric acid	Fluka Chemie, Buchs, Switzerland
Pertex®	Medite GmbH, Burgdorf, Germany
Natriumchlorid	Roth, Karlsruhe, Germany
Di-Natriumhydrogenphosphat Dihydrat	Merck, Darmstadt, Germany
Trypsin Digest All 2®	Zytomed, Berlin, Germany
Normal Goat Serum	Vector/ Linaris, Wertheim-Bettingen, Germany
Normal Rabbit Serum	Vector/ Linaris, Wertheim-Bettingen, Germany
Vectastain Elite ABC Kits (anti-rabbit, anti-goat)	Vector/ Linaris, Wertheim-Bettingen, Germany
Vector VIP Substrat Kit	Vector/ Linaris, Wertheim-Bettingen, Germany
Sirius red	Niepoetter Labortechnik, Buerstadt, Germany
Toludine blue O, Sigma-Aldrich	Sigma-Aldrich, Steinheim, Germany
Resorcin-Fuschin	Waldeck GmbH and Co.KG, Muenster, Germany
Eosin Y	Thermo scientific, Kalamazoo, USA
Fe-Haematoxilin weigert	Waldeck GmbH and Co.KG, Muenster, Germany
Potassium dihydrogen phosphate	Merk, Darmstad, Germany
Dako Real™ proteinase K	Glostrup, Denmark
Methylgreen Counterstain	Vector/ Linaris, Wertheim-Bettingen, Germany
Tissue-Tek	Sakura Finetek Europe B.V., Alphen Aan den Rijn, The Netherlands
Fluoro Care Anti-Fade Mountant	Biocare Medicals, Pike Lane, Concord, CA, USA
Antibody Diluent	Biocare, Berlin Germany

2.1.2 Consumables

Article name	**Company**
Single use syringes Inject Luer®, 1 mL, 2 mL, 5 ml,10 mL	B. Braun Melsungen, Melsungen, Germany

Single use gloves Transaflex®	Ansell, Surbiton Surrey, UK
Gauze balls size 6	Fuhrman Verrbandstoffe GmbH, Munich, Germany
Disposable feather scalpel	Feather Safety Razor Co, Ltd, Osaka, Japan
Pipette tips, blue, yellow, white	EPPENDORF, Hamburg, Germany
Cell Strainer nylon mesh, 40 µm, 100 µm	BD Biosciences, Bedford, USA
Single use nitrile gloves	Paul Hartmann AG, Heidenheim, Germany
Medical adhesive bands	Durapore® 3M St. Paul, MN, USA
Parafilm	American National Can Menasha, Wisconsin, USA
cover slips	Menzel, Braunschweig, Germany
Microtom blades MX35 Premier	Thermo Scientific
Paraffin embedding medium Paraplast Plus®	Sigma Aldrich, Steinheim, Germany

2.1.3 Surgical instruments, sutures and needles

Company	**Article No.**	**Article name**
FST	11370-31	Moria MC31 Forceps - Serrated Curved
FST	11050-10	Graefe Forceps - 0.8mm Tips Straight
FST	11052-10	Graefe Forceps - 0.8mm Tips Curved
FST	14106-09	Fine Iris Scissors - Large Loops Straight Sharp 9.5cm
FST	11009-13	Semken Forceps: curved, tipps serrated 1.3mmx1mm
FST	12060-01	Castroviejo Micro Needle Holder -Straight w/Lock 9cm
FST	15003-08	Vannas-Tübingen spring scissors, Tip Shape: Sharp/Sharp, Effective Cutting Edge: 5mm
Aesculap	BC313R	Standard Scissors – Blunt
FST	15024-10	Spring Scissors - 8mm Blades Straight Sharp, Length: 10cm, Tip Diameter: 0.2mm, Effective Cutting Edge: 8mm
FST	30087-20	Plastic Caliper
Aesculap	FD562R	Vessel clip Biemer, jaw opening 5 mm, jaw length 9 mm,

		closing force 20-25g
FST	18025-10	Suture Tying Forceps
Beckton Dickinson	304000	BD Microlance™ 3 disposable hypodermic needles, 20 x1½", 0.9 x 40 mm, yellow
Beckton Dickinson	303800	BD Microlance™ 3 disposable hypodermic needles, 26Gx½", 0.45 x 13 mm, brown
Beckton Dickinson	30200	BD Microlance ™ 3 disposable hypodermic needles, 27Gx¾ ", 0.40 x 19 mm, grey
Beckton Dickinson	304000	BD Microlance ™ 3 disposable hypodermic needles, 30Gx½", 0.30 x 13 mm, yellow
Ethickon		Surgical threads non-absorbable ETHIBOND EXCEL®, size 5-0
Ethickon	EH7228H	Prolene 6-0, C-1 13 mm 3/8c, polypropylen, blue monofil suture, non resorbable
Braun Melsungen	4268113S-01	Vasofix® Safety 20Gx1¼", 1.1x33 mm, safety intravenous catheter with injection port
Braun Melsungen	4268210S-01	Vasofix® Safety 14Gx2", 2.2x50 mm, safety intravenous catheter with injection port
Braun Melsungen	8728810F	Perfusor® Syringe 50 mL
Edward Weck		Hemoclip®, ligating clip

2.1.4 Devices for surgery and invasive hemodynamics

Company	**Article Number**	**Article name**
AD Instruments	ML295/M-220	The ML295/M Homeothermic Controller and Plate provides temperature feedback control for controlling small animal (mouse) temperature through a heating plate. The system includes the controller, heating plate and mouse rectal probe.

Leica	Leica M50 with small boomstand	Surgical stereomicroscope
Schott	KL-200	Cold light source
Hugo Sachs Electronics		MiniVent Type 845, a quiet, compact and light weight ventilator designed specifically for mice
VetEquip Inc		Table Top Laboratory Animal Anesthesia System includes a precision, agent-specific vaporizer; oxygen flowmeter; oxygen flush valve; non-rebreathing circuit; mouse- and rat-sized nosecones; induction chamber; waste gas filters; and oxygen supply hose.
Millar Instruments	SPR-671NR	An ultra-miniature pressure catheter (1.1F Nylon) with a single 1.4F pressure sensor side mounted at the tip and is suitable for use in mice.
AD Instruments	ML870B47/M	MPVS-Ultra Single Segment Foundation System for Mice is configured for measurement of ventricular pressure and volume in mice using the appropriate pressure-volume catheter. The system includes a PowerLab, LabChart and LabChart Pro acquisition and analysis software.
Aalborg	PMR1-012148	Model P single flow tube rotameter for low flow rate measurement, 100 mL/min, air

2.1.5 Systems, softwares and machines

- Sakura cassette printer, Sakura finetek Germany GmbH, Staufen, Germany
- Selecta filter paper, Schleicher + Schuell GmbH, Dassel, Germany
- Blood analyzer ABL 330 Radiometer, Copenhagen, Denmark
- Robert: Leica ST5020
- Robert: Leica CV5030
- 100 mL Automated microtom RM 2165, Leica Microsystems, Wetzlar, Germany

- Flattening table HI 1220 Leica Microsystems, Wetzlar, Germany
- Flattening bath for paraffin sections HI 1210 Leica Microsystems, Wetzlar, Germany
- Tissue embedding machine EG 1140H Leica Microsystems, Wetzlar, Germany
- Cooling plate EG 1150C Leica Microsystems, Wetzlar, Germany
- Tissue processing automated machine TP 1050 Leica Microsystems, Wetzlar, Germany
- Stereo light microscope DMLA Leica Microsystems, Wetzlar, Germany
- Digital Camera Microscope DC 300F Leica Microsystems Wetzlar,Germany
- Leica Microsystems, Wetzlar, Germany
- Computer Q 550 IW Leica Microsystems Wetzlar, Germany
- Software Q Win V3 Leica Microsystems Wetzlar, Germany
- Makro for Muscularization degree, Fibrosis, Cardiomyocyte size, Leica Microsystems, Wetzlar, Germany

2.1.6 Antibodies and Lectins

Company	**Company**
Armenian hamster anti-FCεR1	Novus Biologicals, Littleton, CO, 80160 USA
WGA-FITC	Sigma aldrich
IB4-TRITC	Sigma aldrich
Avidin-Rhodamine	Vector Laboratory
p-SMAD	Santa Cruze Biotechnology

2.2 Experimental design

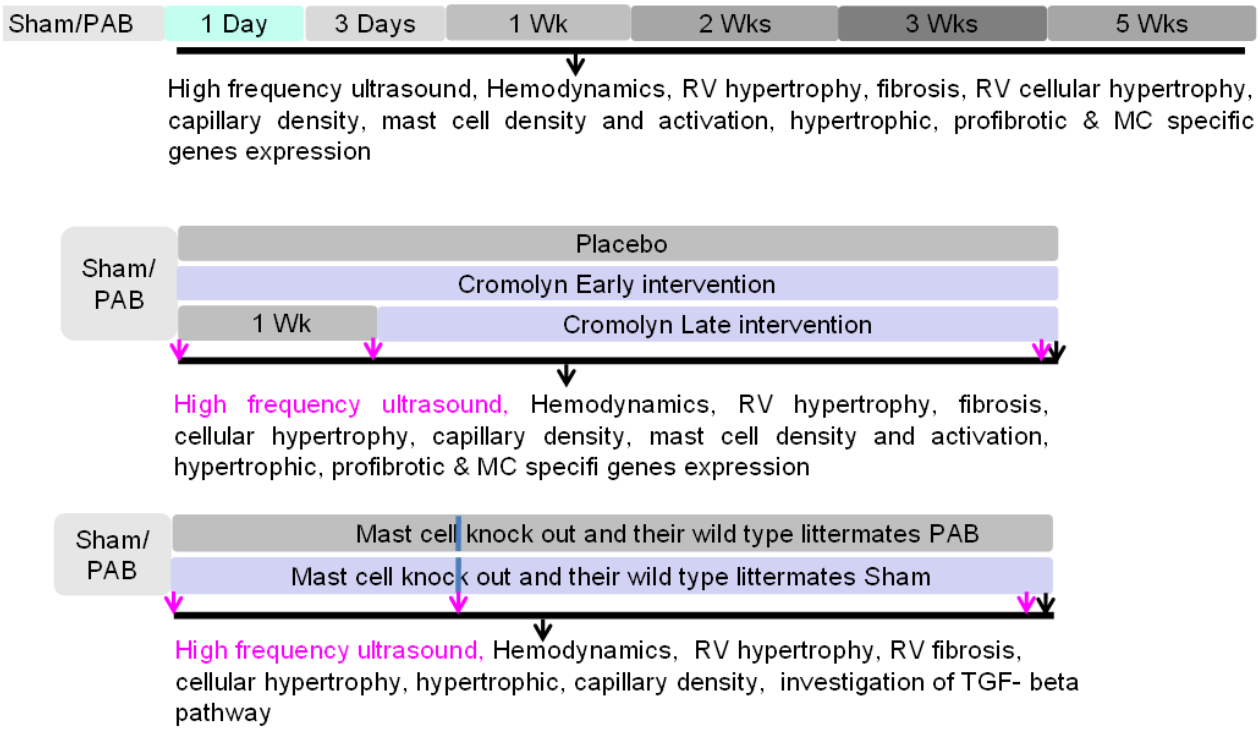

Scheme 5: Experimental design

2.3 Experimental procedures

2.3.1 Animals

Adult C57Bl/6 and WBB6F1/J-*Kit*^{W}/*Kit*$^{W-v}$ mice with the respective wild-type littermates were purchased from Charles River Laboratories (Sulzfeld, Germany). WBB6F1/J-*Kit*^{W}/*Kit*$^{W-v}$ (*Kit*^{W}/*Kit*$^{W-v}$) compound heterozygous mice, which combine the severe *Kit*^{W} mutation with the milder *Kit*$^{W-v}$ mutation, have markedly reduced Kit receptor activity and are severely mast cell-deficient[142]. Because of this deficiency, *Kit*^{W}/*Kit*$^{W-v}$ mice are used to study mast cell biology *in vivo*. *Kit*^{W}/*Kit*$^{W-v}$ mutant mice possess pleiotropic defects in pigment-forming cells, germ cells, red blood cells and mast cells. In addition, they exhibit impaired resistance to parasitic infection and an intrinsic progenitor cell defect. *Kit*$^{W-v}$ homozygotes resemble *Kit*^{W} homozygotes in color, anemia and germ cells, but many of them survive to maturity. The lack of germ cells in mutant mice leads to the development of some ovarian tumors (mesotheliomas and granulosa cell), associated with an

overproduction of pituitary gonadotropic hormone. $Kit^{W/}Kit^{W-v}$ double heterozygotes are viable but sterile because of germ cell deficiency. They are also mast cell deficient. $Kit^{W/}Kit^{W-v}$ double heterozygotes lack intermediate cells, derived from melanoblasts, in the stria vascularis resulting in endocochlear degeneration, loss of endocochlear potential and hearing impairment.

Mice were given free access to water and food and were housed under controlled temperature (22°C) and under standard light-dark cycle (12 hrs each) throughout the experimental period. All experiments were approved by the governmental ethics committee for animal welfare (Regierungspräsidium Giessen (GI 20/10) and Regierungspräsidium Darmstadt (B2/244), Germany.

2.3.2 Orotracheal intubation and ventilation

The intubation and surgical procedures were performed with the aid of a surgical stereomicroscope (Leica Microsystems, Wetzlar, Germany) at 8x magnification. A custom-made endotracheal tube made from an intravenous catheter (Vasofix® Safety 20Gx1¼", 1.1x33 mm, B. Braun Melsungen AG, Melsungen, Germany) with a blunted stylet as a stiff guide to facilitate the introduction of a cannula were prepared. A drop of lidocaine (Xylocain® 2% Jelly, Astra Zeneca GmbH, Wedel, Germany) was put on the tip of the tube to numb the throat and reduce the gag reflex. A blunted stylet (Vasofix® Safety 14Gx2", 2.2x50 mm, B. Braun Melsungen AG, Melsungen, Germany) attached to a 50 mL syringe (Perfusor® Syringe, B. Braun Melsungen AG, Melsungen, Germany), which was held on a retort stand, allowed the mouse to be fixed in a hanging position for the intubation procedure. As intubation requires both hands, the microscope was prefocused approximately 15 mm below the needle to the putative working field, the vocal cords. For illumination a power light with flexible horns (KL-200, Fiber Optics Schott, Mainz, Germany) was used.

For induction of general anesthesia (Table Top Laboratory Animal Anesthesia System, VetEquip Inc, Pleasanton, USA), the animal was placed into a transparent induction chamber, 5% isoflurane (Forene® Abbott, Wiesbach, Germany) in 100% oxygen (Air Liquid, Siegen, Germany) at a flow rate of 2 L/min was used until the animal lost its righting reflex. Thereafter, the mouse was taken out and suspended by the superior incisors on a

blunted needle attached to a 50 mL syringe, which was held on a retort stand. A power light with flexible horns was focused on the ventral neck to transilluminate the trachea. The tongue of the mouse held with the curved forceps held in the operator's right hand, was moved to the left. The forceps held in the left hand are put under the tongue to hold it firmly to the lower jaw. The vocal cords and trachea were then visualized. With the operator's free right hand, the intubation tube was gently inserted into the trachea for 6 mm starting from the vocal cords. Then the guide was removed and the mouse was placed supine on a thermally controlled surgical table and connected to a small animal ventilator MiniVent type 845 (Hugo Sachs Elektronik, March-Hugstetten, Germany), with the exhaust tube immersed in water to confirm the flow of air. The success of the intubation was evaluated by the visual observation of the rhythmic expansion of the thorax synchronous with the ventilator. The ventilation settings for mice were calculated, depending on the animal weight, according the following formulas:

Vt = $0.0062 \times M^{1.01}$, where Vt is tidal volume, and Mb is animal mass in kg;

Ventilation rate (breaths/minutes) = $53.5 \times M^{-0.26}$

Maintenance of anesthesia was provided by continuous inhalation of 2% isoflurane mixed with oxygen. The eyes of animals were protected from drying with dexpanthenol eye ointment (Bepanthen® Bayer, Leverkusen, Germany).

2.3.3 Pulmonary artery banding

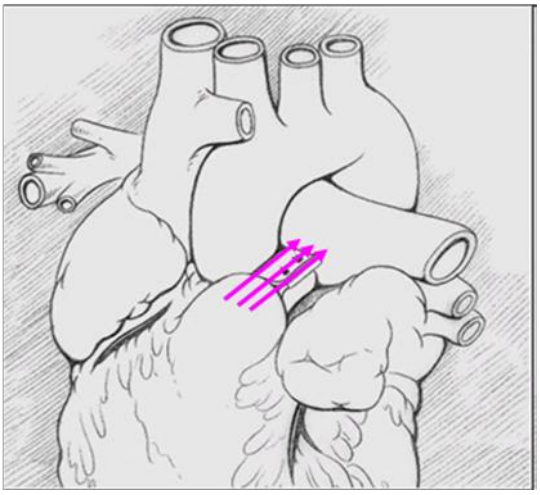

Figure 2: Pulmonary artery banding

Surgery was performed under isoflurane (Forene® Abbott, Wiesbach, Germany) anesthesia (Table Top Laboratory Animal Anesthesia System, VetEquip Inc, Pleasanton, USA) with the aid of a surgical stereomicroscope (Leica Microsystems, Wetzlar, Germany) at 8 x magnification. For illumination a power light with flexible horns (KL-200, Fiber Optics Schott, Mainz, Germany) was used.

After endotracheal intubation the mouse was placed supine on a custome-made homeothermic plate (Keutz Labortechnik, Reisskirchen, Germany) and connected to a small animal ventilator MiniVent type 845 (Hugo Sachs Elektronik, March-Hugstetten, Germany).

Using surgical tape, the four paws of the mouse were taped down to the plate. In an anesthetized and immobilized mouse, the left thoracic wall was shaved and then cleaned with Braunoderm® (B. Braun Melsungen, Melsungen, Germany). A transverse 5 mm incision of the skin was made with scissors 2 mm away from the left sternal border, 2 mm lower than the level of the armpit. Both layers of thoracic muscles were gently pulled apart. The chest cavity was opened with scissors by a small incision at the level of the second intercostal space 2–3 mm from the left sternal border. The chest retractor was gently inserted to spread the wound 4–5 mm in width, taking care to avoid the lungs getting caught in the teeth of the retractor. The thymus and fat were pulled away with forceps to the left arm of the retractor. With two forceps the pericardial sac was gently pulled apart and attached to both arms of the retractor. After a mobilization of the pericardium, the pulmonary trunk was visualized. The pulmonary trunk was bluntly dissected with curved forceps from the aorta and left atrium. To create a tunnel underneath the pulmonary trunk, an L-shaped 26-gauge blunted needle (Becton Dickinson, Drogheda, Ireland) was used. The needle was placed from the side of the pulmonary trunk closest to the left atrium and gently pushed underneath the pulmonary trunk so that the end of the needle appeared between the pulmonary trunk and aortic trunk. A small titanium ligating clip (Hemoclip®, Edward Weck, Research Triangle Park, NC, USA) was placed around the pulmonary trunk with specially adapted appliers set to a width to produce 65-70% constriction. The chest retractor was removed and the thymus was moved back to its physiological position. The lungs were then reinflated by shutting off the outflow on the ventilator for 1–2 sec using a finger. The chest cavity was closed by bringing together the third and fourth ribs with two

6-0 polypropylene sutures (Prolene®, Ethicon, Norderstedt, Germany). While making a knot, slight pressure was applied on the chest with the needle holder to reduce the volume of free air in the chest cavity. All layers of muscle were moved back to their physiological position. Then, the skin was closed with 6-0 polypropylene suture and the wound was treated with Braunoderm® (Braun, Melsungen, Germany).
For the sham operation, dissection of the pulmonary trunk was performed using the curved forceps and the L-shaped needle but a ligating clip was not placed around the pulmonary artery. The lungs were then reinflated and the wound was closed.

Immediately after the operation 0.5 mL of 37°C saline was given intraperitoneally and a dose of analgesic buprenorphine hydrochloride (Temgesic®, 0.1 mg/kg, Essex Pharma GmbH, Munich, Germany) was given subcutaneously after recovery from anesthesia and then every 8 hrs for the next 48 hrs. Once spontaneous respiration resumed, animals were extubated, placed under a heating lamp and were closely observed for 6 hrs to ensure complete recovery from the anesthesia. The mice were then housed to a standard rodent cage with free access to food and water in a room kept at 25°C.

2.3.4 Pharmacological treatments

To investigate the effects of mast cell stabilization in a murine model of pressure overload induced RV hypertrophy, chronic treatment with cromolyn sodium salt (50 mg/kg/day intraperitoneally) was performed. The animals were randomized into placebo, early intervention (starting from day zero for 3 weeks) and late intervention (starting from day 7 after PAB for 2 weeks) groups and were treated intraperitoneally either with placebo (saline) or cromolyn At the end of the experiment (day 21 of PAB), the animals were subjected to hemodynamic measurements. Afterwards the animals were sacrificed and heart tissues were harvested for further analyses.

2.3.5 High frequency ultrasound

Immediately before performing the echocardiographic study, the animal was placed into a transparent induction chamber (Table Top Laboratory Animal Anesthesia System, VetEquip Inc, Pleasanton, USA). For induction of general anesthesia, 5% isoflurane (Forene® Abbott, Wiesbach, Germany) in 100% oxygen (Air Liquid, Siegen, Germany) at a flow rate of 2 L/min was used until the animal lost its righting reflex.

Thereafter, the mouse was taken out and placed in a supine position atop a heating pad with embedded ECG leads. Subsequently, the snout was placed within a nose cone connected to the anesthesia system to maintain a steady-state sedation level throughout the procedure (1.0% to 1.5% isoflurane mixed with 0.5 L/min 100% O_2) while spontaneously breathing. A rectal probe was gently inserted after lubricating to continuously monitor and keep body temperature at 37°C via the heating pad. The eyes of the animal were protected from drying with dexpanthenol eye ointment (Bepanthen® Bayer, Leverkusen, Germany). Using surgical tape, the four paws of the mouse were taped down to the ECG electrode after applying electrode gel to them. Depilatory cream was applied to the chest from the neckline to mid chest level using a cotton applicator tip. The cream was removed after 2 min with a gentle rolling motion of the cotton tips and then the chest was cleaned with distilled water.

To start the transthoracic two-dimensional, M-mode and Doppler imaging, a layer of preheated to body temperature ultrasound gel was applied to the chest of the anesthetized and immobilized mouse, primarily the area overlying the heart. Echocardiographic images were acquired with a commercially available VEVO770 High-Resolution imaging system (VisualSonics, Toronto, Canada) equipped with a 30-MHz transducer. RV free wall thickness (RVWT) was measured in the modified parasternal long-axis view. RV outflow tract (RVOT) dimensions were measured from the RVOT view at the level of the aortic valve. For assessment of right ventricular performance, the RV Tei index and tricuspid annular plane systolic excursion were measured. For determination of TAPSE M-mode cursor was oriented to the junction of the tricuspid valve plane with the RV free wall using the apical four chamber view. RV myocardial performance index (MPI) or Tei index was measured in by Tissue Doppler imaging (TDI) at the lateral part of the tricuspid annulus in the four-chamber view and calculated as the sum of isovolumic contraction time (IVCT) and isovolumic relaxation time (IVRT) divided by the ejection time (ET).

Peak aortic velocity and velocity time integral were determined from a right supraclavicular view. Aortic stroke volume (SVao) was calculated from pulse wave aortic Doppler recordings and measurements of the proximal ascending aortic diameter. The aortic diameter (D) was measured using M-mode echocardiography at the level of the proximal ascending aorta. Because of the pulsatile nature of the cardiovascular system, velocities

are not constant throughout the cardiac cycle, thereby requiring temporal integration of the Doppler velocities known as the time velocity integral (TVI). The cross-sectional area of the aorta (CSAao) was calculated assuming a constant circular orifice throughout the cardiac systole by use of the formula:

$CSAao = (AO\ diameter/2)^2 \times \pi$

$SVao = CSAao \times TVIao$

$COao = SVao \times HR$

$CI = COao/body\ weight,$

where CO is cardiac output, CI is cardiac index and HR is heart rate.

All echocardiographic parameters were calculated off-line using tool section of the Visual Sonics Vevo770 system.

Once the imaging was completed, the restraints were removed from the animal and the electrode gel was wiped off with standard gauze pads. The anesthesia was turned off and the unrestrained animal was allowed to recover on the heated ECG pad. Once the mouse was awake, it was returned to its cage.

2.3.6 Invasive hemodynamic measurements

In vivo cardiac hemodynamic function was assessed in mice following various time periods of pulmonary artery banding and in sham controls. Measurements were preformed under isoflurane (Forene® Abbott, Wiesbach, Germany) anesthesia (Table Top Laboratory Animal Anesthesia System, VetEquip Inc, Pleasanton, USA). Maintenance of anesthesia was provided by continuous inhalation of 1.5% isoflurane mixed with oxygen (Air Liquid, Siegen, Germany). The surgical procedures for catheterization were performed with the aid of a surgical stereomicroscope (Leica Microsystems, Wetzlar, Germany) at 8x magnification. For illumination a power light with flexible horns (KL-200, Fiber Optics Schott, Mainz, Germany) was used.

After endotracheal intubation the mouse was placed supine on a homeothermic plate (AD Instruments, Spechbach, Germany) and connected to a small animal ventilator MiniVent type 845 (Hugo Sachs Elektronik, March-Hugstetten, Germany). The body temperature

was controlled by the rectal probe connected to the control unit (AD Instruments, Spechbach, Germany) and was kept at 37°C during the catheterization.
Using surgical tape, the front paws of the mouse were taped down to the heating blanket. The distal paws were used to monitor the depth of anesthesia. In an immobilized anesthetized animal, the neck and chest area were cleaned with Braunoderm® (Braun, Melsungen, Germany) and then an inverted T-shaped middle-neck incision from mandible to the sternum was made.

2.3.7 Right heart catheterization

The right external jugular vein was carefully exposed by bluntly dissecting the surface of the right neck along the midclavicular line. After careful removal of the connective tissue surrounding the jugular vein, three ligatures of 6-0 polypropylene sutures were placed around the vein. The rostral ligature, placed just below the junction of the internal and external jugular vein, was ligated to prevent bleeding and then gently pulled and taped to the table. A very loose knot was placed to the middle suture. The caudal suture was gently pulled (without securing it) with a needle holder and clamped to the skin of the animal to fix it in the desired position. A couple of drops of physiological saline were put in the vessel area and a small incision was made in between both the rostral and middle ligatures using microincision scissors. Afterwards, the tip of the presoaked (for 30 min into physiological saline solution) high fidelity 1.4F micromanometer catheter (Millar Instruments, Houston, USA), was inserted in the caudal direction into the vein, using a bent 27-gauge needle, followed by gently securing the middle suture. Simultaneously, the caudal suture was released and the catheter was quickly advanced into the right atrium and then RV. After stabilization of the signal, the pressure was recorded. During the data collection, the ventilator was shut off for a few seconds to acquire data without lung motion artifact. The parameters measured were heart rate, RV systolic pressure (RVSP) and end-diastolic pressure (RVEDP), the maximal and minimal first derivative of ventricular pressure (dP/dtMax and dP/dtMin, respectively) and mean right atrial pressure. At the conclusion of the measurements, the catheter was removed by gently pulling it back and was immediately placed into a syringe filled with saline to prevent clotting.

2.3.8 Left heart catheterization

Parotid glands were moved aside and the thin muscle layer around the throat were bluntly dissected with forceps to expose and isolate the right carotid artery. A suture was secured around the distal end of the artery, then gently pulled and taped to the table. An additional suture was inserted beneath carotid artery and a very loose knot was placed. A Biemer microvessel clip (Aesculap, Tuttlingen, Germany) was placed on the proximal part of the carotid artery. A couple of drops of physiological saline were put in the vessel area and a tiny incision was made near the distal end of the artery with a microincision scissors. Using a bent 27-gauge needle, the catheter tip was inserted into the vessel followed by gently securing the second suture. Simultaneously, the clip was released and the high fidelity 1.4F micromanometer catheter (Millar Instruments, Houston, USA) was quickly advanced into the left ventricle until the pressure signal was displayed in the monitor. After stabilization of the signal, the pressure was recorded. During the data collection, the ventilator was shut off for a few seconds to acquire data without lung motion artifact. All data were collected and analyzed using PowerLab data acquisition systems and LabChart 7 for Windows software (MPVS-Ultra Single Segment Foundation System, AD Instruments, Spechbach, Germany). The parameters measured were heart rate, systolic and mean aortic pressure, left ventricular systolic pressure (LVSP) and end-diastolic pressure (LVEDP) and the maximal and minimal first derivative of ventricular pressure (dP/dtMax and dP/dtMin, respectively). At the conclusion of the measurements, the catheter was removed by gently pulling it back and was immediately placed into a syringe filled with saline to prevent clotting.

At the end of the experiment, the mice were sacrificed and the hearts were harvested for further examination.

2.3.9 Tissue processing

The ventricles were dissected out from the great vessels and atria. The RV was isolated from the left ventricle (LV) + septum (LV + S) by dissection along the septal insertion. The RV and (LV + S) were patted dry and weighed. We assessed RV hypertrophy by using the ratios of RV to tibial length and to body weight. The tissue samples were then either fixed in formalin or snap-frozen.

2.4 Histological examinations

2.4.1 Cardiac fibrosis

Heart tissues were immersed in 3.5% formalin for 12 hrs at 4°C. They were then transferred to cold PBS at 4°C overnight and further to 50% alcohol with following dehydration and paraffin embedding. Paraffin embedded blocks were sectioned at a thickness of 3 µm. To detect collagen fibers RV sections were stained with 0.1% Sirius Red (Sirius Red F3B, Niepoetter, Bürstadt, Germany) in picric acid (Fluka). Briefly, sections were deparafinized and rehydrated in xylol and graded ethanol series (99.9%, 96%, 70%), washed with PBS and dipped in 0.1% picrosirius red solution for an hour. Afterwards, excess of picrosirius staining was washed away with 1% glacial acetic acid series, dehydrated with graded ethanol series of increasing concentration from 70% to absolute alcohol. Finally slides were cleared in xylol series and mounted in pertex. The percentage of interstitial collagen area fraction was counted using collagen counting Leica Qwin V3 computer-assisted image analysis software (Leica Microsystem, Wetzlar, Germany). Average data reflect results from at least 5-7 different hearts in each group.

2.4.2 Cardiomyocyte size determination

For cardiomyocyte size determination, 3 µm thin transverse sections of RV were stained with FITC conjugated wheat germ agglutinin (WGA-FITC, Sigma-Aldrich) which specifically binds to the N-acetylglucosamine residue of the cell membrane. Nuclei were stained with 4',6-diamidino-2-phenylindole (DAPI, Invitrogen). Briefly 3 µm thin formalin fixed paraffin embedded transverse sections of RV were deprafinized and rehydrated as mention before. Antigen retrieval was done by digesting with proteinase K for 30 min at room temperature and blocked with 10% BSA to avoid background staining. Sections were incubated with WGA-FITC overnight at 4°C, excess of WGA-FITC was washed for 2 hrs in TBS and finally nuclear staining with DAPI for 10 min at room temperature. Finally, slides were cleaned and mounted in Fluoro Care Anti-Fade Mountant (Biocare, CA, USA). Sections without WGA-FITC and DAPI were used as a negative control. Photomicrographs were quantified to determine the mean cross-sectional area of cardiomyocytes using Leica Qwin V3 computer-assisted image analysis software (Leica Microsystem, Wetzlar, Germany).

Average data reflect results from at least 5-7 different hearts in each group (more than 200 cells for each heart).

2.4.3 Myocardial angiogenesis

To quantify the capillaries, 3 µm thin transverse sections of right ventricles were stained with FITC conjugated wheat germ agglutinin (WGA-FITC, Sigma-Aldrich) for membrane staining and IB4-TRITC staining for endothelial cells. Nuclei were stained with 4',6-diamidino-2-phenylindole (DAPI, Invitrogen) and mounted in Fluoro Care Anti-Fade Mountant (Biocare, CA, USA). Briefly 3 µm thin formalin fixed paraffin embedded transverse sections of RV were deprafinized and rehydrated as mention before. Antigen retrieval was done by digesting the tissue with proteinase K for 30 min at room temperature and blocked with 10% BSA to avoid background staining. Sections were incubated with WGA-FITC (Sigma Aldrich) and IB4-TRITC (Sigma Aldrich) overnight at 4°C, excess of WGA-FITC was washed for 2 hrs in TBS and finally nuclear staining with DAPI for 10 min at room temperature. Finally slides were cleaned and mounted in Fluoro Care Anti-Fade Mountant (Biocare, CA, USA). Sections without WGA-FITC, IB4-TRITC and DAPI were used as a negative control. Photomicrographs were quantified to count the number of cardiomyocytes and capillaries using STEPanizer image analysis tool (University of Bern, Department of Anatomy, Bern, Switzerland) and mean cross-sectional area of cardiomyocytes using Leica Qwin V3 computer-assisted image analysis software (Leica Microsystem, Wetzlar, Germany). Numbers of capillaries per cardiomyocyte and per unit cross sectional area of the cardiomycyte were expressed. Average data reflect results from at least 5-7 different hearts in each group.

2.4.4 Mast cell density and activity

To identify mast cells, toluidine blue staining was performed. Briefly, formalin-fixed RV tissue samples were paraffin embedded and 3 µm sections were stained with toluidine blue. Toluidine blue stock solution (1%) was prepared in 70% ethanol. Toluidine blue working solution was prepared by diluting 10 mL of stock solution in 90 mL of 1% NaCl solution and fixed pH=2.2. Mast cell density was quantified by counting the number of toluidine blue positive cells from each entire RV longitudinal sections (Leica QWin, 200X) in 2 random sections. The mast cell density was expressed as a number of mast cells per

mm^2, Mast cell degranulation was defined by observing the membrane rupture and leakage of the metachromatic granules[143]. The results were expressed as percentage of degranulated mast cell to total amount of mast cells.

2.5 Molecular biology analysis

2.5.1 Reverse transcription polymerase chain reaction

Total RNA was extracted from snap-frozen RV tissue using Quagen RNA isolation kit (Quagen), followed by the synthesis of cDNA using BioRad cDNA synthesis kit (BioRad). cDNA was synthesized with 1 µg of RNA each, using the iScript cDNA Synthesis Kit (Bio-Rad, Munich, Germany). The condition for the reverse transcription was as follows: 1 cycle at 25°C for 5 min; 1 cycle at 42°C for 30 min; 1 cycle at 85°C for 5 min. The real-time PCR was performed with the iQ SYBR Green Supermix according to the manufacturer's instructions (Bio-Rad, Munich, Germany). Briefly, a 25 µL mixture was used containing 12.5 µL iQ SYBR Green Supermix, 0.5 µL forward and reverse primers, 9.5 µL sterile RNAse and DNAase free water and 2 µL of the 1:5 diluted complementary cDNA template. Non-template control was used as a negative control in each run. The intron-spanning primers for ANP, BNP, Col1α1 and Col3α1, TGF-β, HPRT, 18S RNA, MCP-4, MCP-5 (list of primer sequence below in the box), were designed by using sequence information from the NCBI database and obtained from Metabion international AG (Martinsried, Germany).

ANP F-TCTGCCCTCTTGAAAAGCAA, R-TTCGGTACCGGAAGCTGTT
BNP F-GAAGGTGCTGTCCCAGATGA, R-TCCAGCAGCTTCTGCATCTT
Col 1 F-GACGGGAGGGCGAGTGCTGT, R-ACGGGTCCCCTTGGGCCTTG
Col 3 F-AAAGGGTGAAATGGGTCCAG, R-TCACCTGAAGGACCTCGTGT
TGF-beta F-AGAAGGCAAGCCGGAGGGCA, R-TGGGCGGGATGGCATTTTCGG
MCP-4 F-TCTGGGGCTGGAGCTGAGGAGA, R-GCAGCAGTCAACACAAATTGGCGG
MCP-5 F-TGAAGCCTGCAGCAGCCCTG, R-CGTGCCTCCAATGATCTCTCCAGC
HPRT1 F-GCTGACCTGCTGGATTACAT, R-TTGGGGCTGTACTGCTTAAC
18SRNA F-CTTCGCCATCACTGCCATTA, R-CGTGAGTTCTCCAGCCCTCT

The real time PCR was performed with a Mx3000P (Stratagene, Heidelberg, Germany) under the following conditions: 1 cycle at 95°C for 10 min, then 40 cycles at 95°C for 10 sec, 59°C for 10 sec, 72°C for 10 sec, followed by a dissociation curve. PCR products were detected in the ABI-PRISM 7700 sequence detection system (Applied Biosystems) and the results were analyzed using the 2-ΔΔCT method. The level of expression of mRNA was normalized to HPRT and 18S mRNA.

2.6 Statistical analyses

All data are presented as means ± SEM. Comparison of multiple groups was performed by analysis of variance (ANOVA) with the Student–Newman–Keuls post-test. For comparison of two groups Student's *t*-test was performed. *p*-value below 0.05 was considered as statistical significant for all analysis.

3 RESULTS

3.1 Time course of pressure overload-induced right ventricular remodeling

First, we investigated the time course changes in RV remodeling in a murine model of pressure overload induced RV hypertrophy. Animals were investigated at various time points (1, 3, 7, 14, 21 and 35 days) after PAB for assessment of hemodynamics, RV function, expression profile of hypertrophic and profibrotic genes, histological assessment of RV interstitial fibrosis, cellular hypertrophy and capillary density.

3.1.1 Effect of PAB on hemodynamics and cardiac function

To assess the degree of afterload imposed by PAB, we measured RVSP by invasive RV catheterization at various time points after surgery. RVSP significantly increased at all time points compared with sham animals ($p < 0.05$). There were no significant differences in SAP between banded and sham mice at all time points (Figures 3a and 3b).

Cardiac index significantly decreased at postoperative day 1 but partially recovered by day 7 with further gradual decline (Figure 3c). Similar to cardiac index, RV function evaluated by TAPSE and Tei index significantly deteriorated immediately after PAB, but partially recovered on postoperative day 3 with further slow decline (Figures 3d and 3e).

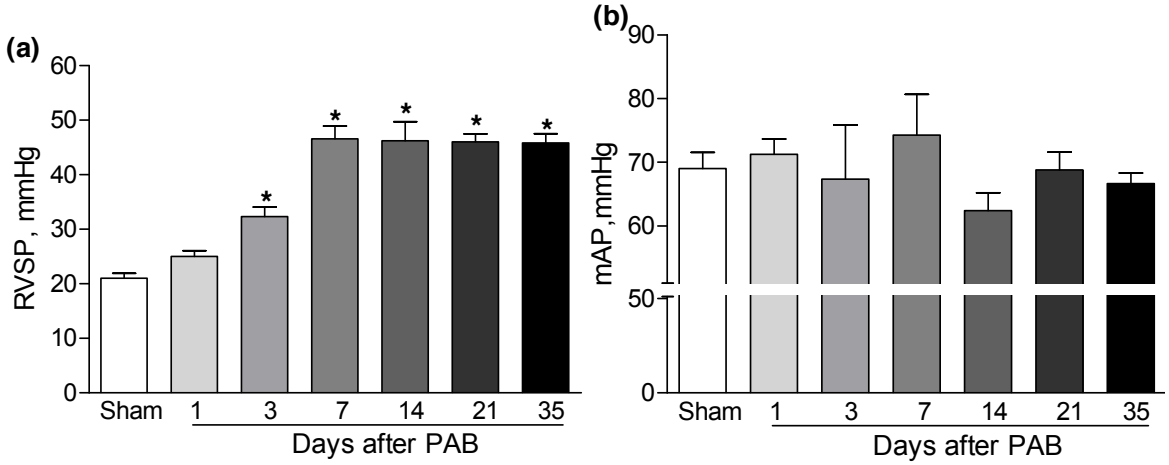

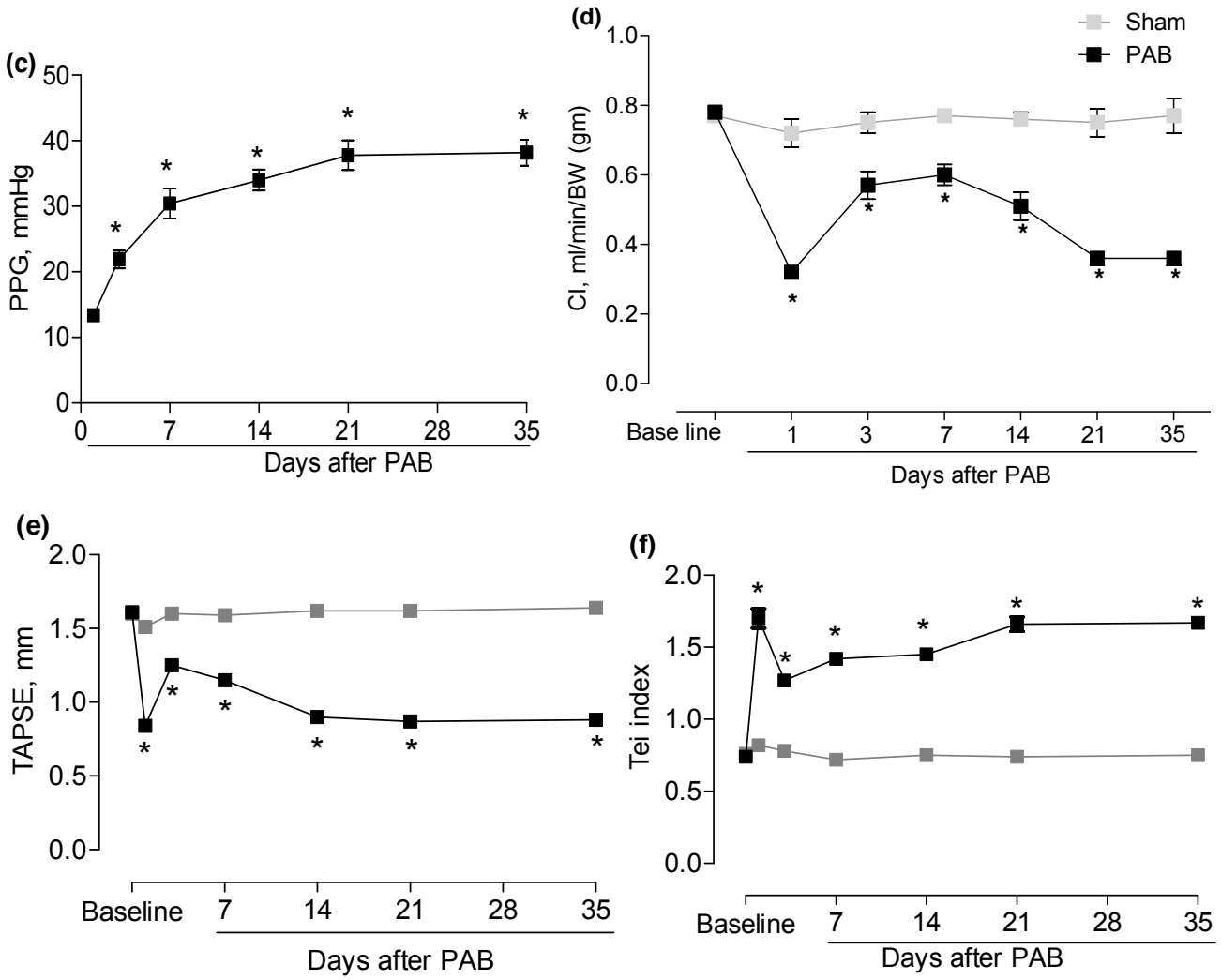

Figure 3: Effect of PAB on hemodynamics and cardiac function
(a) right ventricular systolic pressure (RVSP); (b) mean aortic pressure (mAP); (c) pressure gradient across the PAB; (d) cardiac index (CI); (e) tricuspid annular plane systolic excursion (TAPSE); and (f) Tei index. Data are presented as mean±SEM, $p < 0.05$ compared with sham at corresponding time points, n=8 to 10.

3.1.2 Effect of PAB on RV remodeling

RV hypertrophy developed rapidly after PAB. Although, the RV mass was not significantly different between PAB and sham-operated mice at postoperative day 1, it increased in banded mice after 3 days and continued to increase further up to day 35 (Figure 4e). RV remodeling was characterized by changes in size and shape of the RV. Pressure overload resulted in acute dilatation of the RV chamber with partial reversal on day 3 after PAB and further progressive chamber enlargement (Figure 4c). Significant RV wall thickening

occurred at 3 days after PAB and changed nonsignificantly thereafter (Figure 4b). On a cellular level, significant heart hypertrophy was evident at 7 days after PAB and gradually increased further (Figures 4d and 4f).

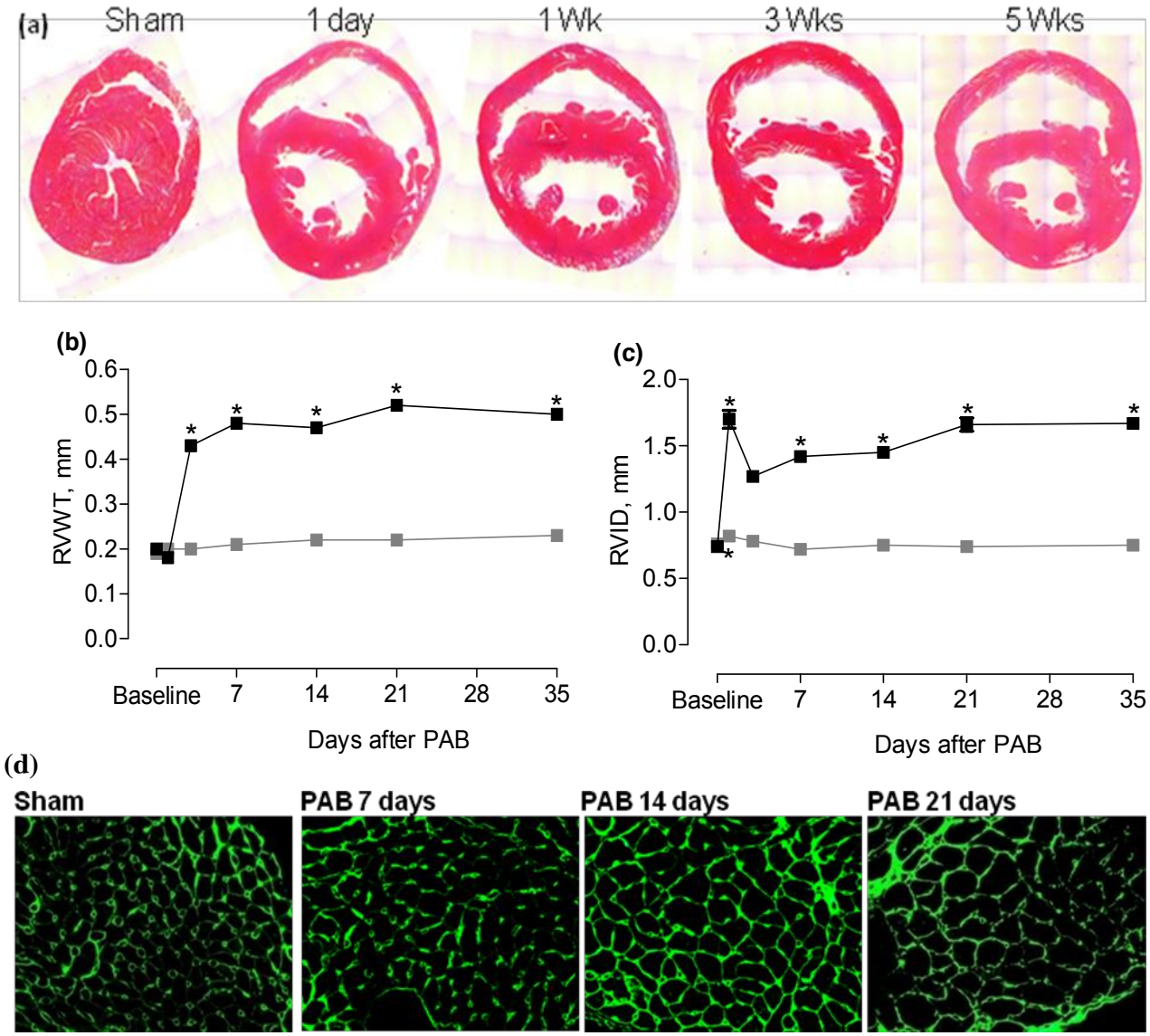

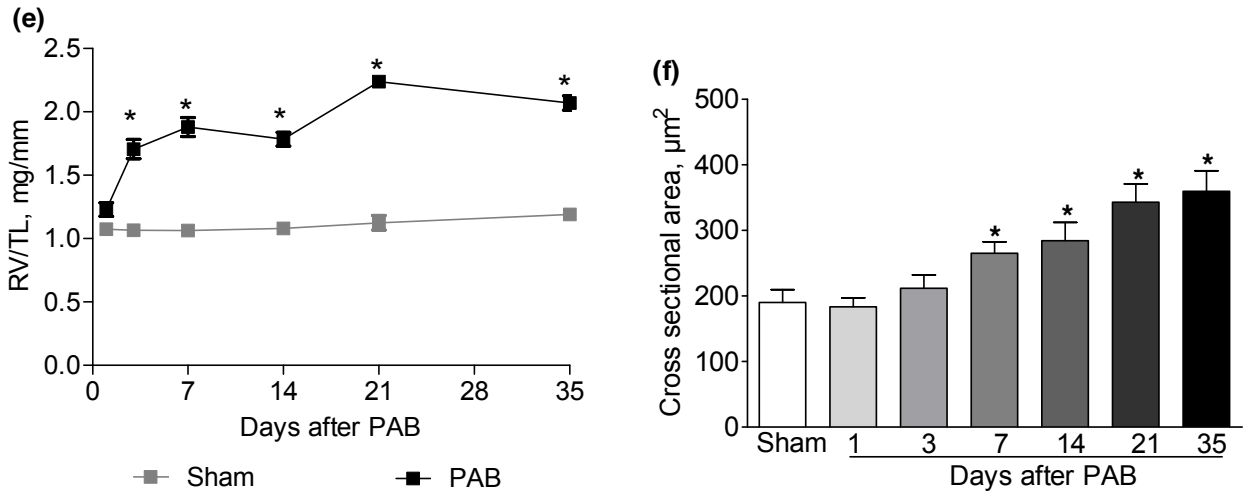

Figure 4: Effect of PAB on right ventricular hypertrophy

(a) HE staining, cross sections of hearts from sham and banded mice; (b) right ventricular wall thickness (RVWT); (c) right ventricular internal dimension (RVID); (d) representative images of right ventricles cut in cross-section and stained with wheat germ agglutinin-FITC conjugate; (e) right ventricular weight/tibial length (RV/TL); and (f) cardiomyocyte cross-sectional area. Data are presented as mean±SEM, $p < 0.05$ compared with sham at corresponding time points, n=8 to 10 for figures b, c, e and n=5 for figures d, f.

3.1.3 Effect of PAB on expression of hypertrophic and profibrotic genes

As RV remodeling comprises of hypertrophy and fibrosis, we investigated the mRNA expression of hypertrophic and profibrotic genes at different time points after PAB. BNP expression increased early after PAB and was maintained at high levels up to 35 days after PAB (Figure 5a). Similarly, TGF-β was up-regulated very early and then remained highly expressed (Figure 5e). In contrast, ANP expression increased only 1 week after PAB and stayed high thereafter (Figure 5b). Similar to ANP, induction of mRNA expression of profibrotic genes collagen 1, collagen 3 and PAI-1 occurred late and then remained high (Figures 5c, 5d and 5f).

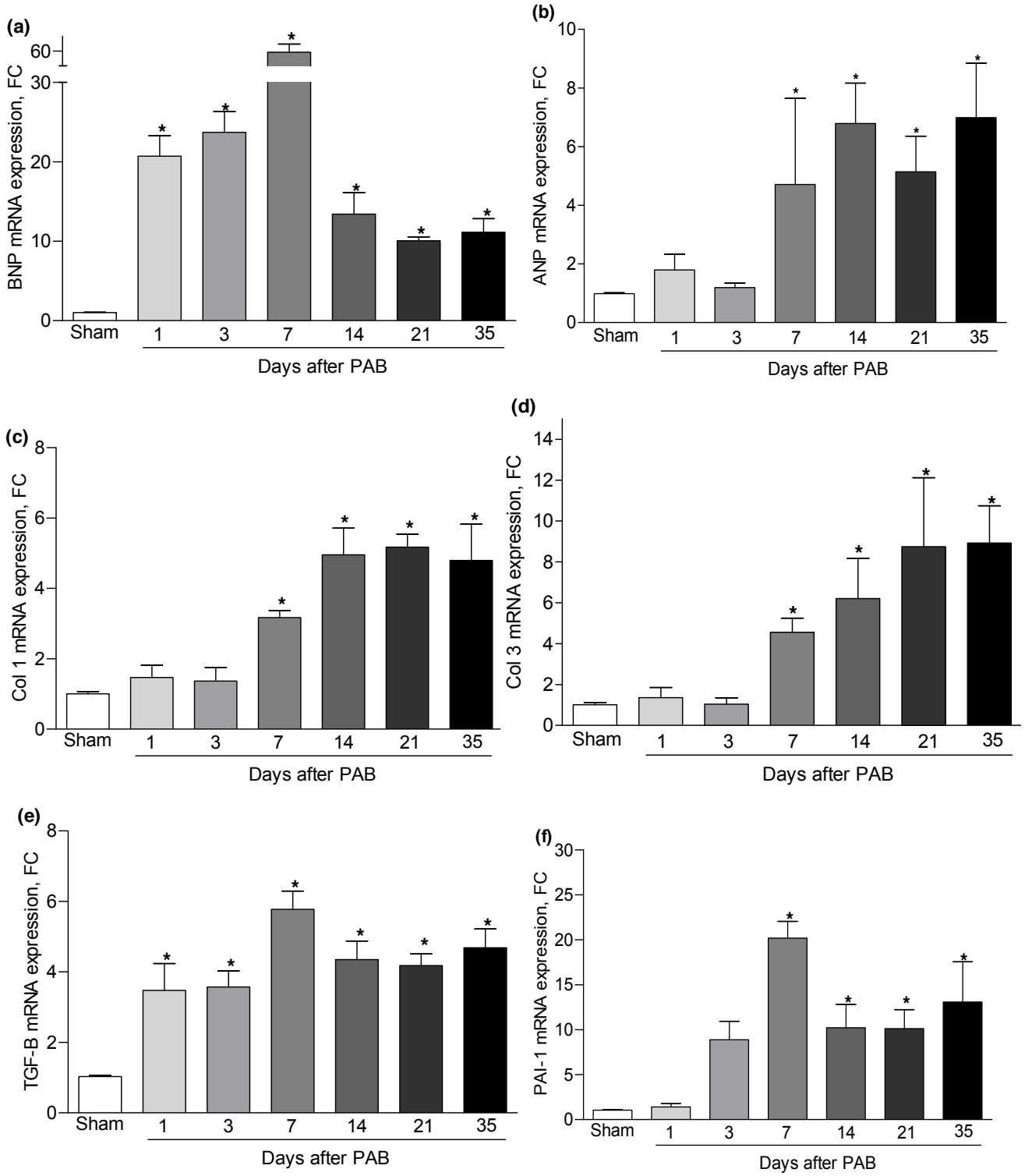

Figure 5: Effect of PAB on the expression of hypertrophic and profibrotic genes
Real-time PCR analysis for hypertrophic and profibrotic markers (a) B-type natriuretic peptide (BNP), (b) atrial natriuretic peptide (ANP), (c) collagen 1 (Col 1) (d) collagen 3 (Col 3) and (e) transforming growth factor 1 (TGF-β), (f) Plasminogen activator inhibitor (PAI-1). Data are presented as mean±SEM, $p<0.05$ compared with sham, n=5 in each group.

3.1.4 Effect of PAB on RV fibrosis

To investigate the effect of PAB in RV remodeling proess, RV fibrosis was assessed by quantifying the fibrosis percentage as decribed in the materials and methods section. Interstitial collagen deposition in banded mice started increasing 1 week after surgery and progressively increased further up to day 35 (Figures 6a and 6b).

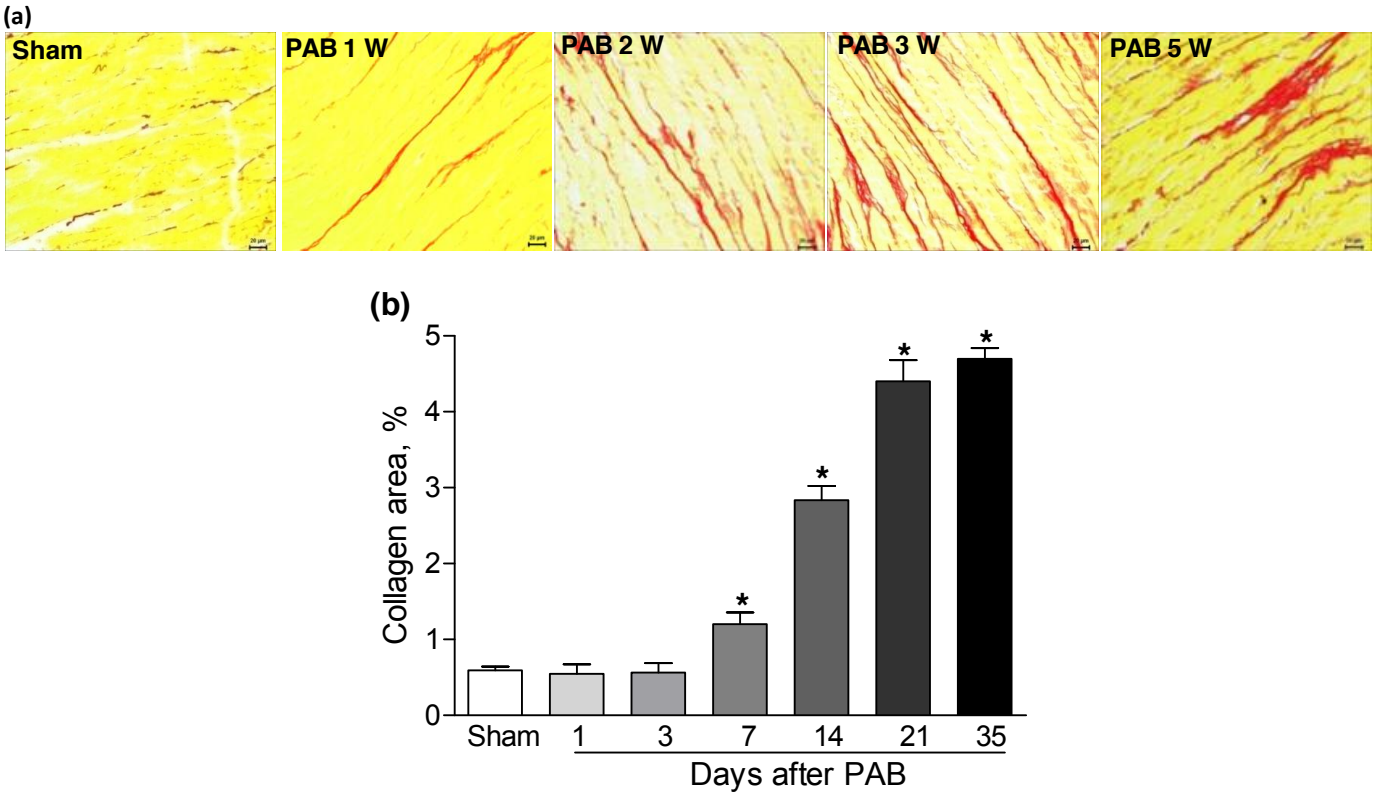

Figure 6: Effect of PAB on RV fibrosis.
(a) representative sirius red staining images of right ventricles. Scale bar, 40 µm; and (b) bar graphs summarizing quantification of interstitial fibrosis. Data are presented as mean±SEM, $p<0.05$ compared with sham, n=5 in each group.

3.1.5 Effect of PAB on RV angiogenesis

The number of microvessels per cardiomyocyte slightly increased until day 7 and did not change thereafter. However, the number of capillaries per cross-sectional area of cardiomyocytes progressively decreased in banded mice (Figure 7c).

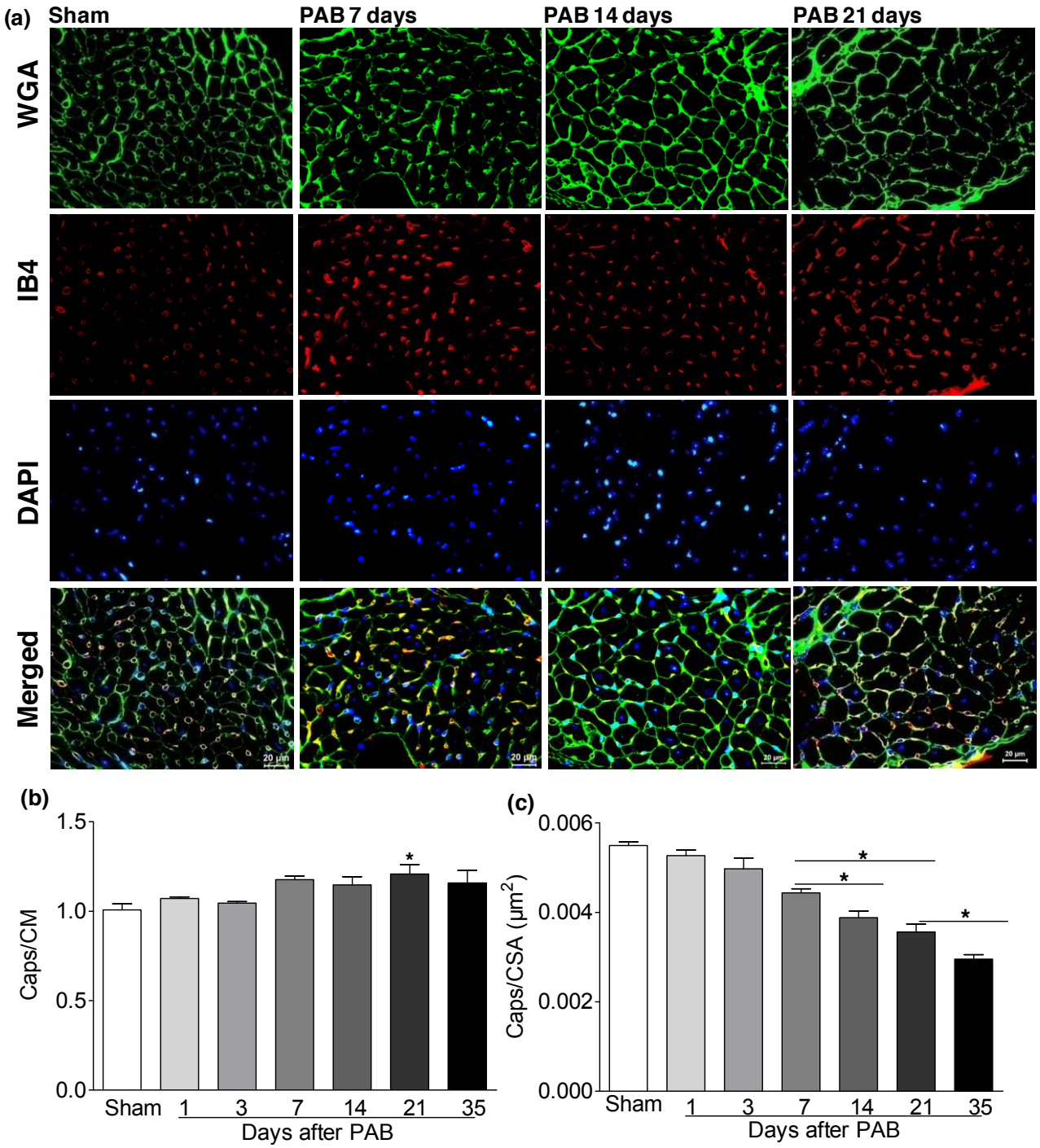

Figure 7: Effect of PAB on RV angiogenesis.
Representative images of right ventricles cut in cross-section and stained with (a) wheat germ agglutinin-FITC conjugate (WGA-FITC), isolectin B4-TRITC conjugate (IB4-TRITC), DAPI and merged. WGA marks cell boundaries (green), isolectin B4 (red) marks endothelial cells, DAPI marks nuclei (blue). Bar graphs summarizing (b) capillaries per cardiomyocytes and (c) capillaries per cross sectional area of cardiomyocytes. Data are presented as mean±SEM, $p<0.05$, n=5 in each group.

3.1.6 Effect of PAB on RV mast cell density and activity

We found time-dependant increase in total number of mast cells (Figure 8b) and a proportion of degranulated mast cells in the RV tissue (Figure 8c). The mast cell density started increasing after 2 weeks and reached maximal values 3 weeks post-surgery. Proportion of degranulated mast cells increased starting from day 1 after PAB and reached a plateau by day 7 (Figures 8a and 8c).

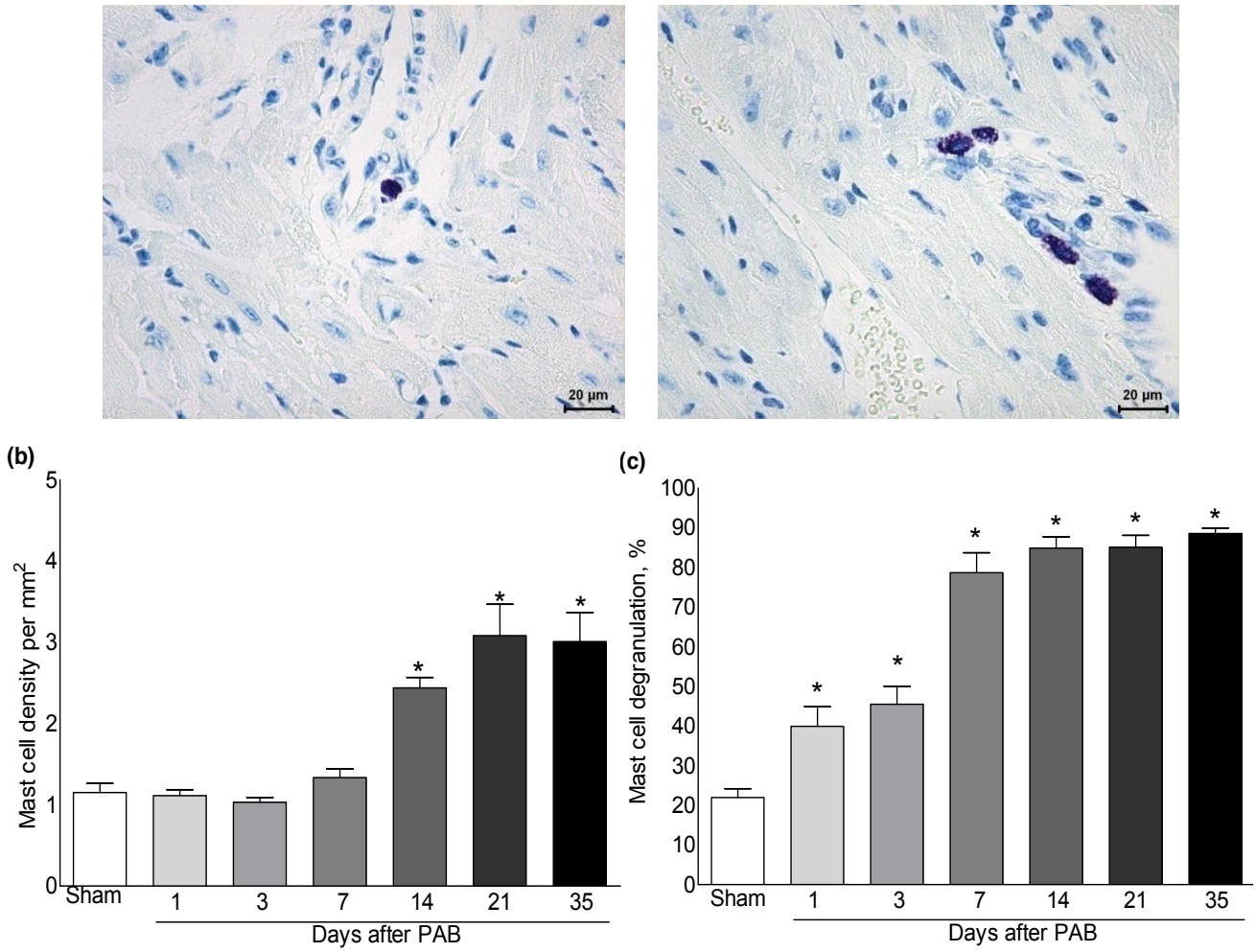

Figure 8: Effect of PAB on RV mast density and activity.
(a) representative images of mast cells in RV tissue from sham and banded mice; (b) mast cell density; and (c) mast cell activity. Data are presented as mean±SEM, $p<0.05$ compared with sham, n=5 in each group.

3.1.7 Effect of PAB on the expression of mast cell specific genes in RV

The increased number of mast cells in pressure overload induced RV hypertrophy was accompanied by increased expression of mast cell specific genes in the RV. There was a 3-

and 6- fold increase in MCP-4 mRNA expression after one week and three weeks of PAB, in the RV from banded mice compared with sham respectively. Similarly, MCP-5 expression was increased 2- and 11- fold in the RV from banded mice after one week and three weeks of PAB, respectively.

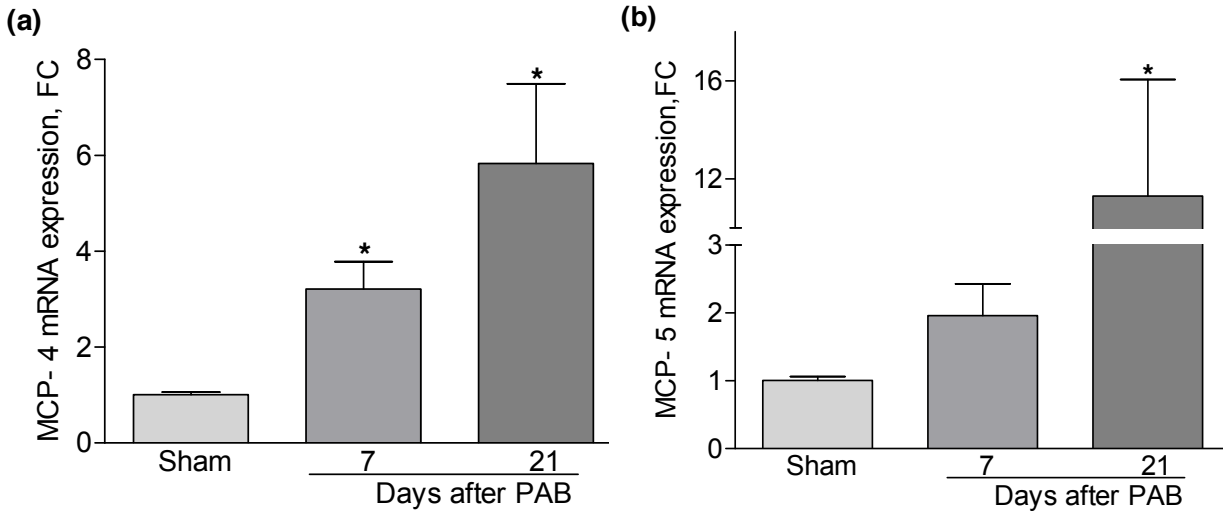

Figure 9: Effect of PAB in the expression of mast cell specific genes in RV.
The mRNA expression of mast cell specific genes (a) mast cell protease 4 (MCP-4) and (b) mast cell protease 5 (MCP-5). Data are presented as mean±SEM, $p<0.05$ compared with sham, n=5 in each group.

3.2 Effects of mast cell stabilization in pressure overload-induced right ventricular remodeling

Banded mice were randomly grouped into placebo and treatment groups (early intervention group which received cromolyn starting from day zero of PAB for 3 weeks and late intervention group which received cromolyn starting from day 7 for 2 weeks). We investigated the effects of mast cell stabilization on hemodynamic, RV remodeling and function.

3.2.1 Effect of cromolyn on hemodynamics and cardiac function

PAB led to significant increase in RVSP compared with sham (Figure 10a). There were no differences in RVSP between placebo and treatment groups indicating comparable levels of pressure overload in those groups. Similarly, there were no significant differences in systemic arterial pressure between the groups (Figure 10b). RV end-diastolic and right atrial

pressures were significantly increased in placebo treated mice (Figures 10c and 10d). Both treatment regimens significantly decreased RVEDP and right atrial pressure. Cardiac output in placebo treated mice was significantly reduced compared with sham animals. Importantly, early as well as late intervention by cromolyn resulted in significant increase in cardiac output compared to placebo treated banded mice (Figure 10e). RV dysfunction evidenced by reduced TAPSE and increased Tei index was observed in banded mice treated with placebo. Cromolyn treatment significantly improved all the parameters of the RV function (Figures 10f and 10g).

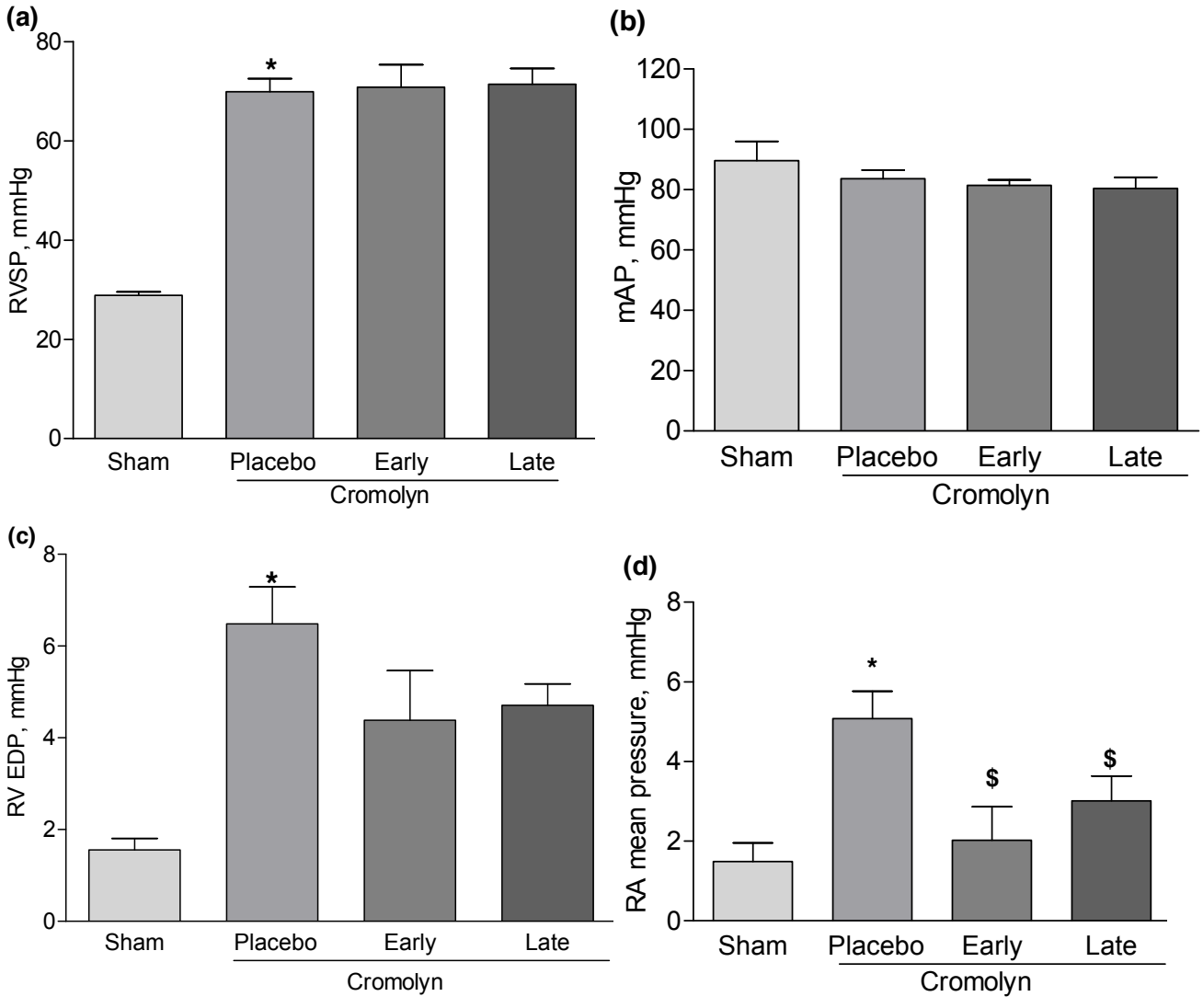

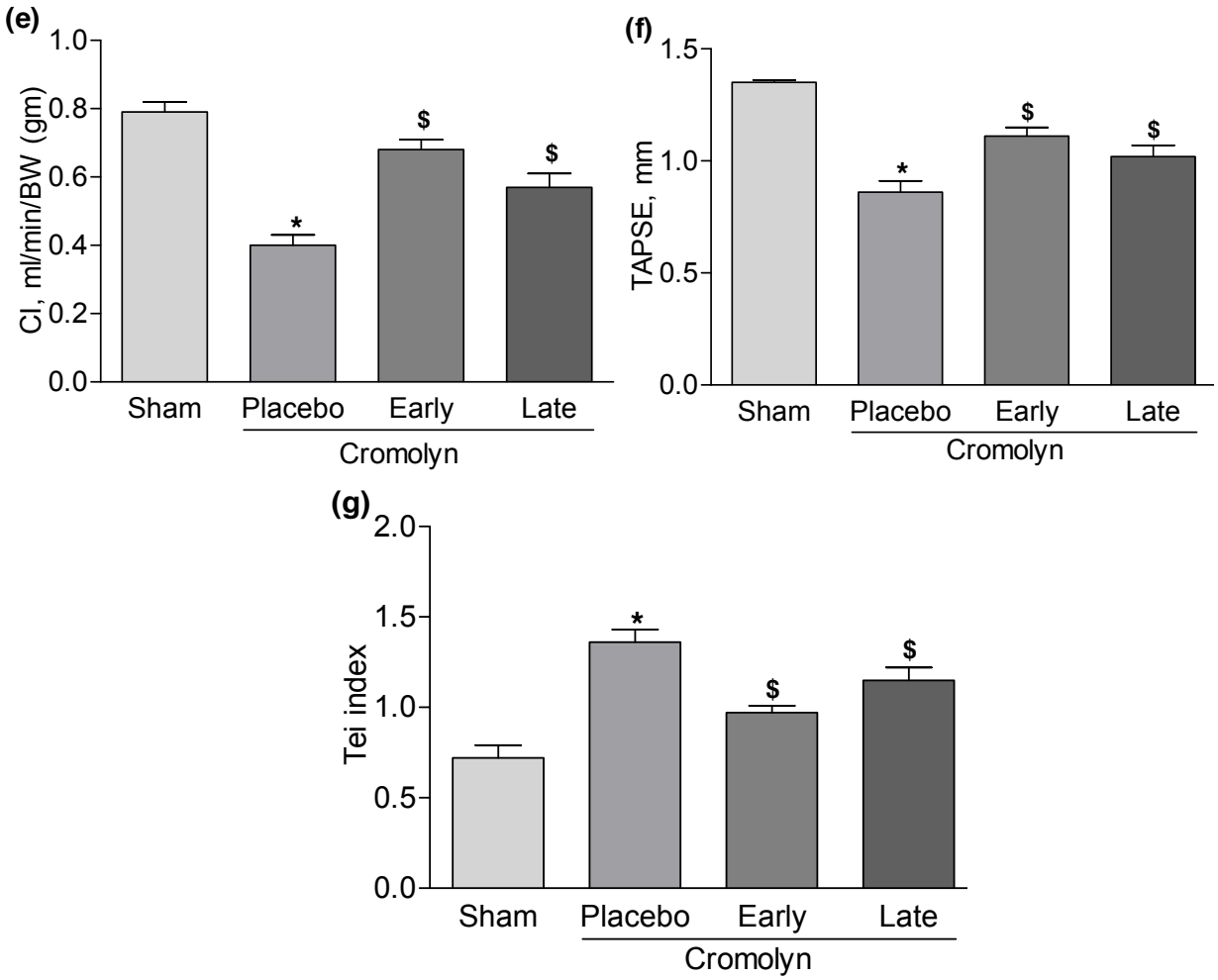

Figure 10: Effect of cromolyn on hemodynamics and cardiac functions.
Treatment with cromolyn was started either from day zero of PAB (early intervention) or at day 7 after PAB (late intervention). (a) right ventricular systolic pressure (RVSP); (b) mean aortic pressure (mAP); (c) right ventricular end-diastolic pressure (RVEDP); (d) mean right atrial pressure; (e) cardiac index (CI); (f) tricuspid annular plane systolic excursion (TAPSE); and (g) Tei index. Data are presented as mean±SEM, *$p<0.05$ compared with sham and $^{\$}p<0.05$ compared with placebo, n=10 in each group.

3.2.2 Effect of cromolyn on RV remodeling

RV remodeling in banded mice was characterized by RV chamber enlargement with thickening of the RV wall and by increased RV mass (Figures 11a, 11b and 11d). Cromolyn prevented significant RV dilatation with wall thickening and attenuated RV mass increase. Although, RV mass and wall thickening were not reduced by late treatment with cromolyn, RV dilatation was slightly but significantly reversed. Interestingly, improvement in RV

remodeling induced by cromolyn treatment was not associated with any effects of therapy on cardiomyocyte hypertrophy (Figures 11c and 11e).

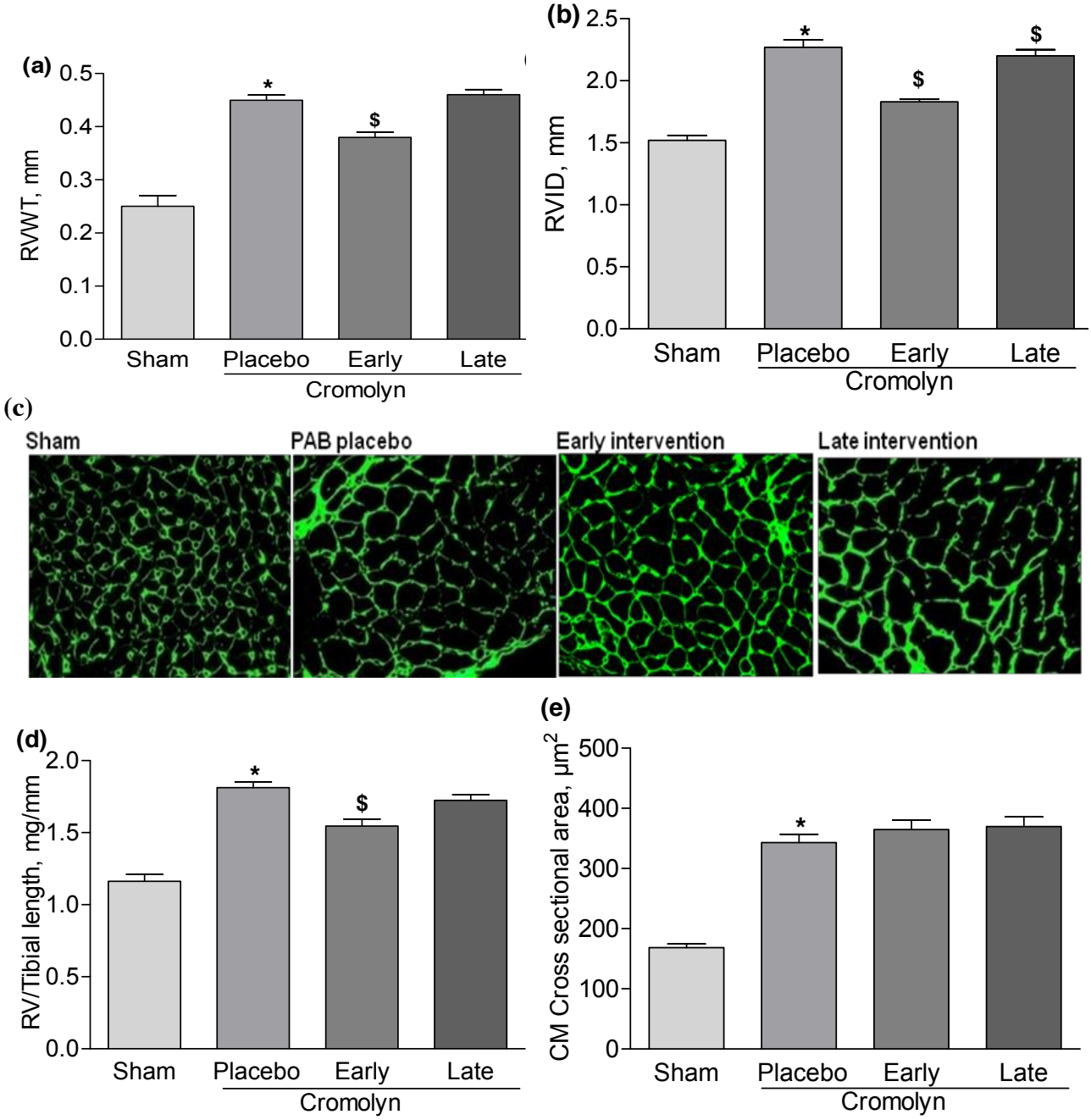

Figure 11: Effect of cromolyn on RV remodeling.
Treatment with cromolyn was started either from day zero of PAB (early intervention) or at day 7 after PAB (late intervention). (a) right ventricular wall thickness (RVWT); (b) right ventricular internal dimension (RVID); (c) representative images of RV cut in cross-section show FITC-conjugated wheat germ agglutinin staining for cross sectional analysis; (d) right ventricular mass/tibial length (RV/TL); and (e) bar graphs summarizing cardiomyocyte (CM) cross sectional area. Data are

presented as mean±SEM, *p<0.05 compared with sham and $p<0.05 compared with placebo, n=10 for figures a, b, d and n=5 for figures c, f.

3.2.3 Effect of cromolyn on expression of hypertrophic and profibrotic genes

Expression of hypertrophic (BNP and ANP) profibrotic markers (collagen 1 and collagen 3) was significantly increased in banded mice receiving placebo compared with shams (Figures 12a, 12b, 12c and 12d). Treatment with cromolyn did not have any effect on the expression of hypertrophic markers. Although, expression of collagen 1 and collagen 3 was significantly decreased in the treatment groups, expression of TGF-β and PAI-1 were not significantly affected (Figures 12 e and 12f).

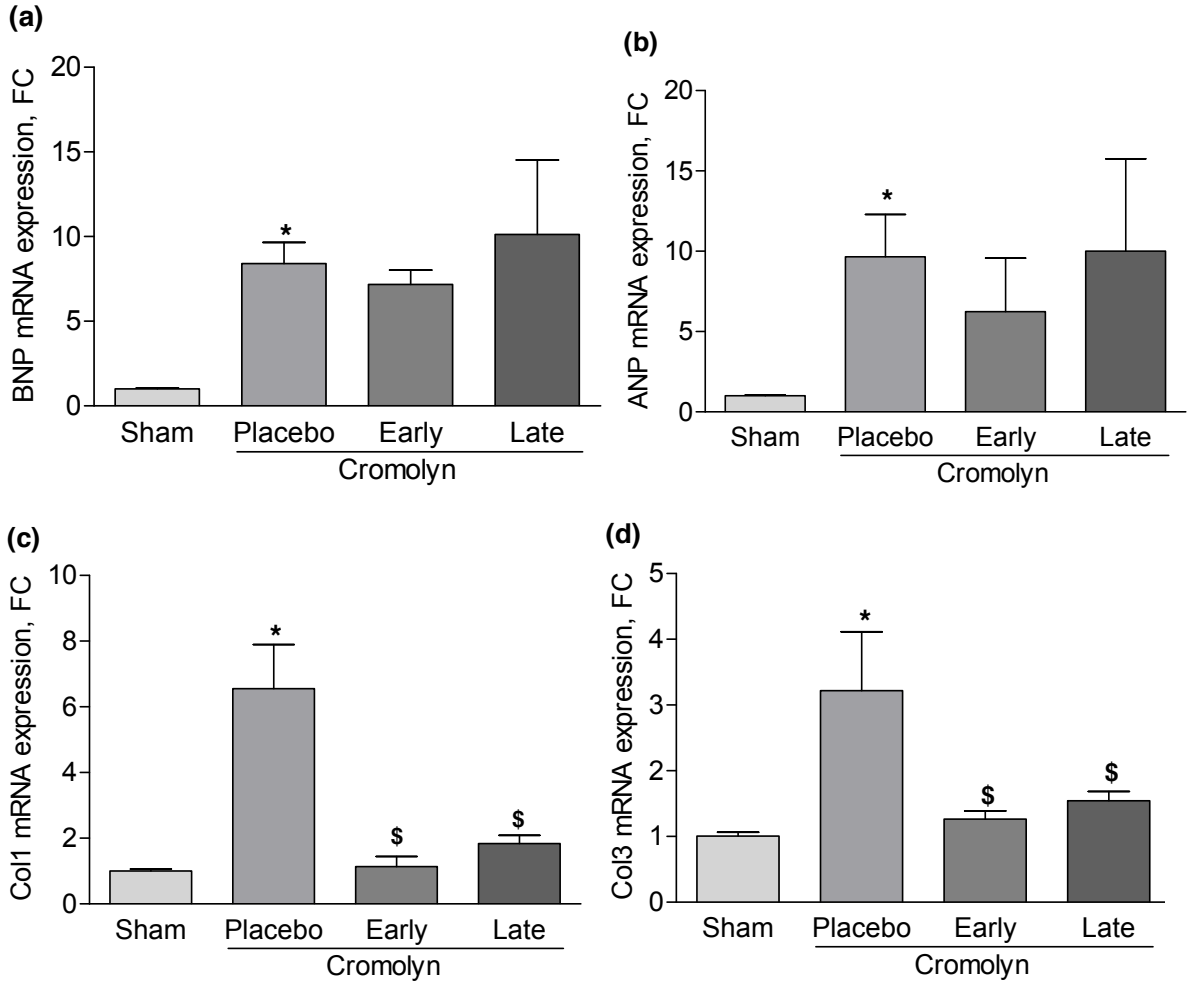

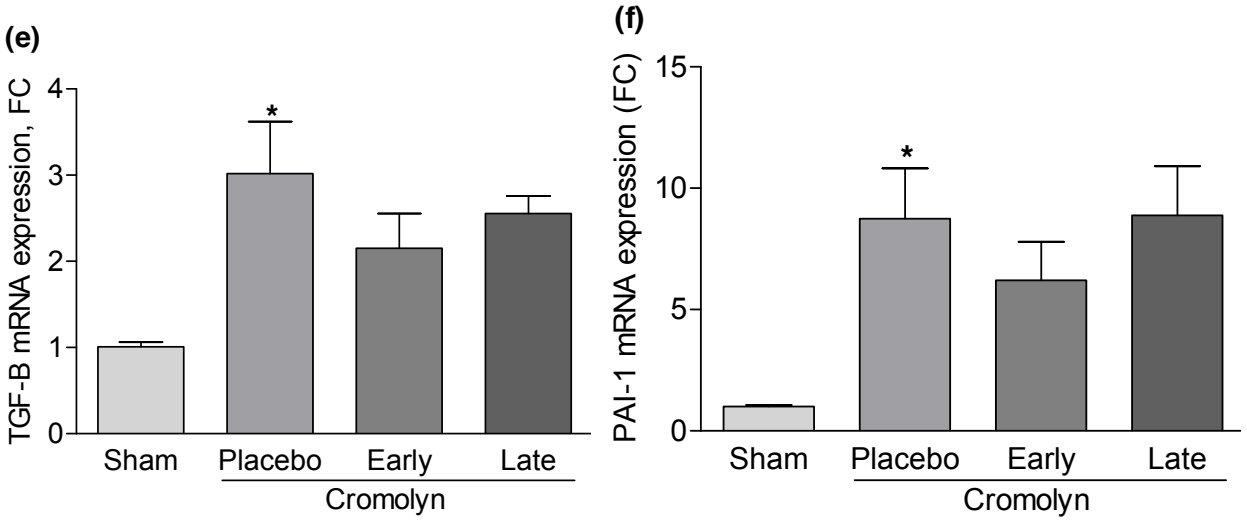

Figure 12: Effect of cromolyn on expression of hypertrophic and profibrotic genes.
Treatment with cromolyn was started either from day zero of PAB (early intervention) or at day 7 after PAB (late intervention). (a) B-type natriuretic peptide (BNP); (b) atrial natriuretic peptide (ANP); (c) collagen 1 (Col1); (d) collagen 3 (Col3); and (e) transforming growth factor β (TGF-β), Plasminogen activator inhibitor (PAI-1). Data are presented as mean±SEM, *p<0.05 compared with sham and $p<0.05 compared with placebo, n=5 in each group.

3.2.4 Effect of cromolyn on mRNA expression mast cell specific genes

The increased mast cell number in PAB placebo was accompanied with increased mRNA expression of the mast cell specific genes in RV. There was significant increase in MCP-4 and MCP-5 mRNA expression in placebo treated mice compared with sham. Treatment with cromolyn significantly decreased expression of these genes (Figures 13a and 13b).

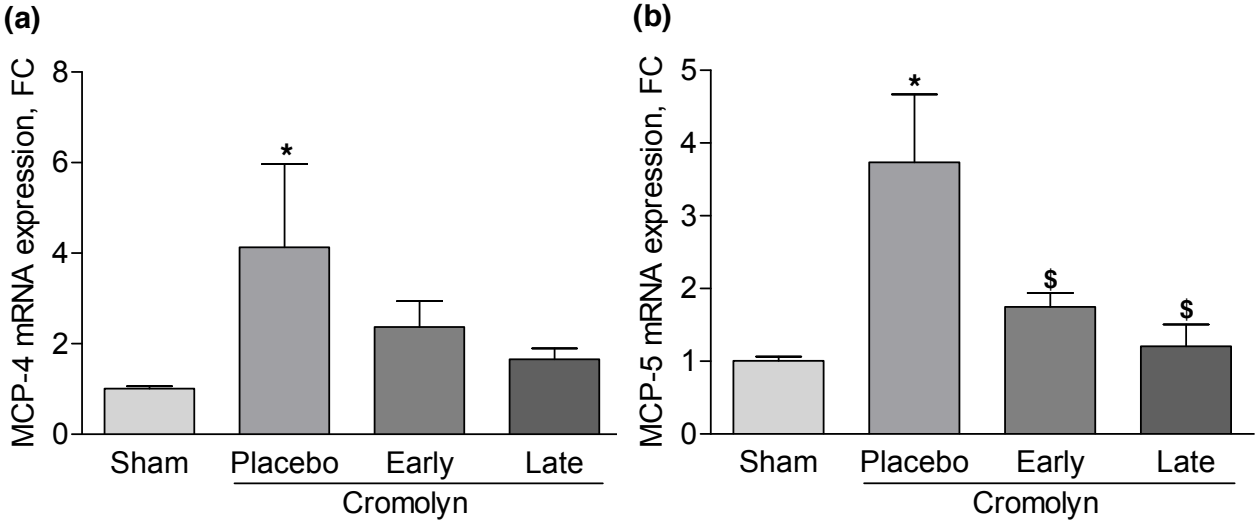

Figure 13: Effect of cromolyn on mRNA expression of mast cell specific genes.
Treatment with cromolyn was started either from day zero of PAB (early intervention) or at day 7 after PAB (late intervention). (a) murine mast cell protease 4 (MCP-4) and (b) murine mast cell protease 5 (MCP-5). Data are presented as mean±SEM, *p<0.05 compared with sham and $p<0.05 compared with placebo, n=5 in each group.

3.2.5 Effect of cromolyn on RV fibrosis

Banded mice receiving placebo showed significantly higher RV interstitial fibrosis compared with sham. Treatment with cromolyn significantly decreased interstitial fibrosis, the effect being more pronounced in the early intervention group (Figures 14a and 14b).

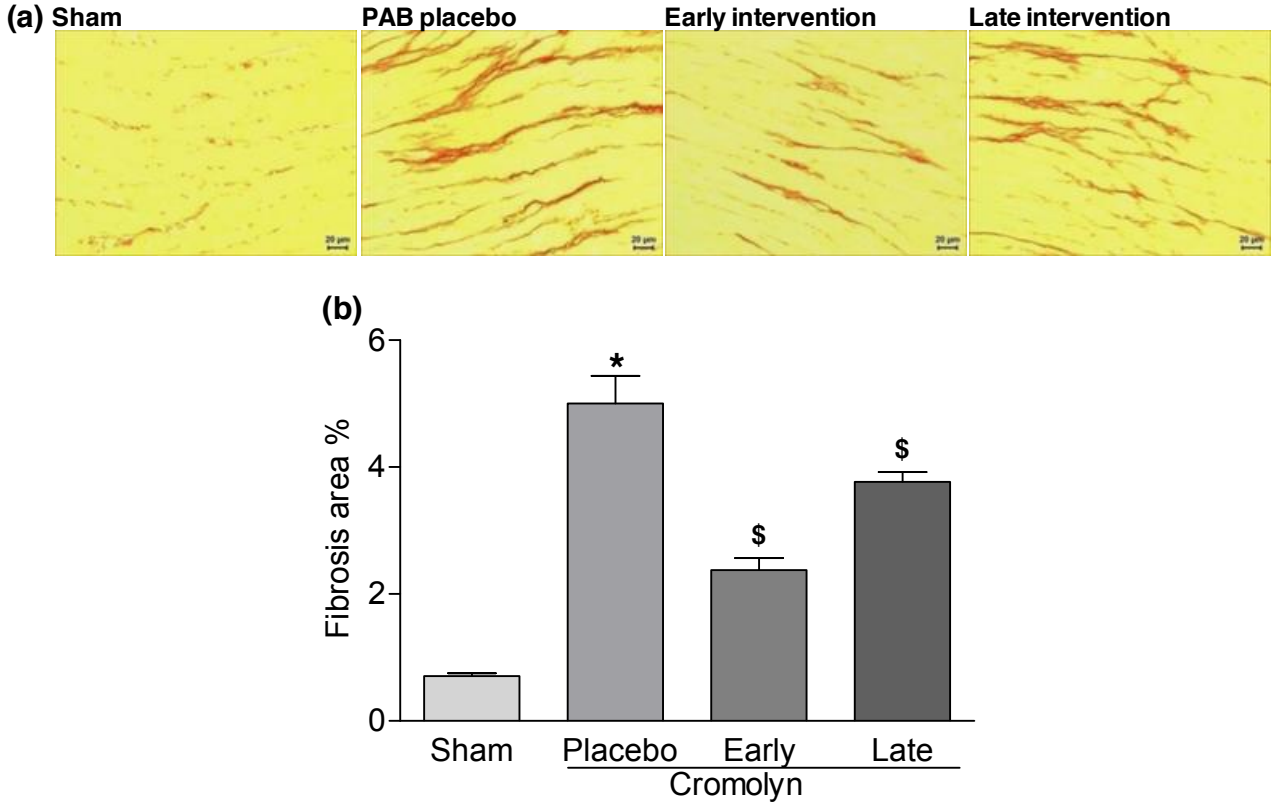

Figure 14: Effect of cromolyn on RV fibrosis.
Treatment with cromolyn was started either from day zero of PAB (early intervention) or at day 7 after PAB (late intervention). (a) representative sirius red staining images of right ventricles. Scale bar, and (b) bar graphs summarizing quantification of interstitial fibrosis. Data are presented as mean±SEM, *p<0.05 compared with sham and $p<0.05 compared with placebo, n=5 in each group.

3.2.6 Effect of cromolyn on RV angiogenesis

There was a slight increase in the capillary density in banded mice compared with sham. However, the number of capillaries per cross-sectional area of cardiomyocytes significantly

decreased in banded mice. Treatment with cromolyn had effects neither on capillary density nor on the relative blood supply (Figures 15b and 15c).

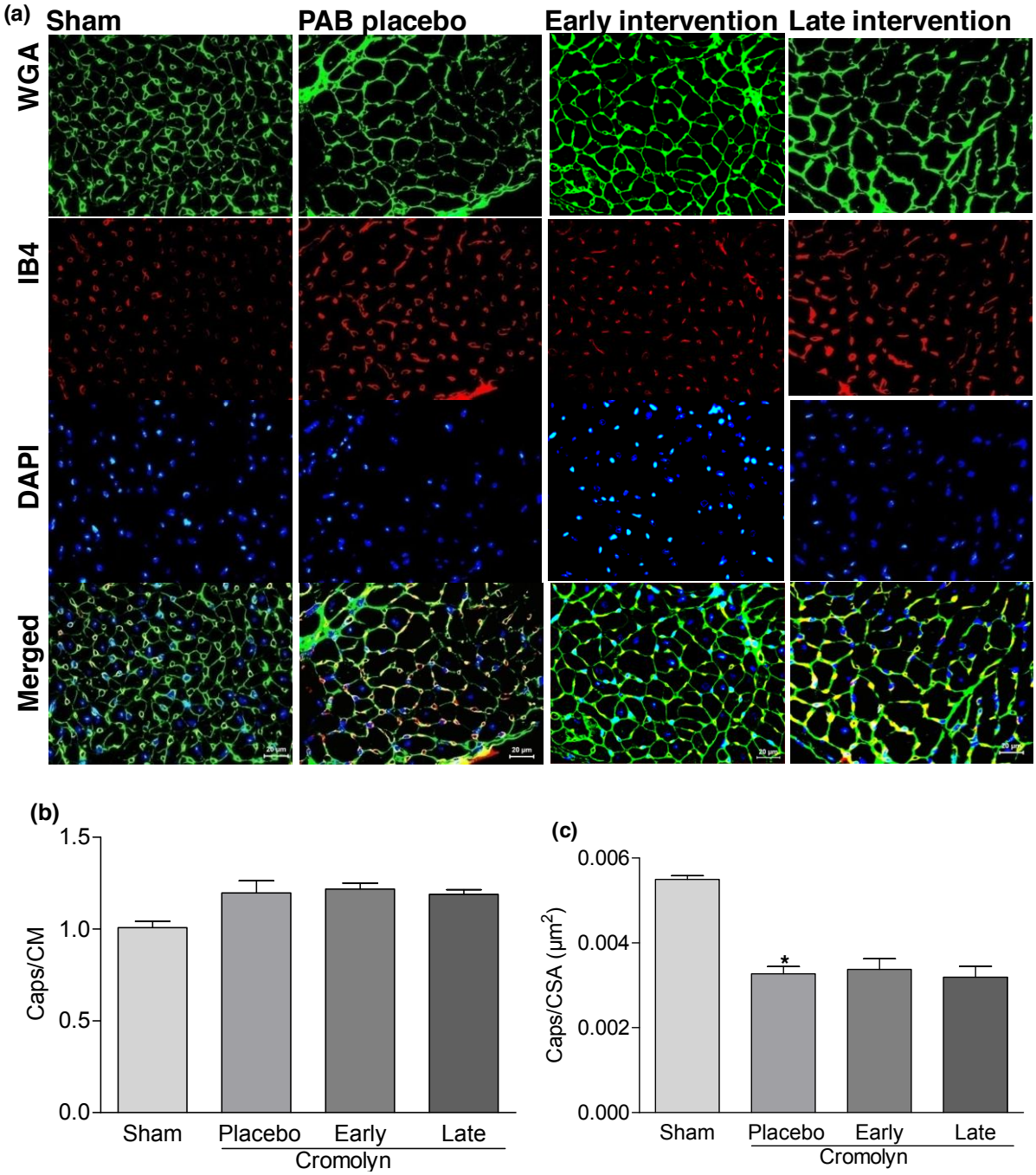

Figure 15: Effect of cromolyn on RV angiogenesis.
Treatment with cromolyn was started either from day zero of PAB (early intervention) or at day 7 after PAB (late intervention). (a) Representative images of right ventricles cut in cross-section and stained with wheat germ agglutinin-FITC conjugate (WGA-FITC), isolectin B4-TRITC conjugate (IB4-TRITC), DAPI and merged. WGA marks cell boundaries (green), isolectin B4 (red) marks endothelial cells, DAPI marks nuclei (blue). Scale bar, 20 µm. Bar graphs summarizing (b) capillaries per

cardiomyocytes and (c) capillaries per cross sectional area of cardiomyocytes. Data are presented as mean±SEM, *p<0.05 compared with sham, n=5 in each group.

3.2.7 Effect of cromolyn on mast cell density and activity

There was an increase in the mast cell density in placebo treated banded mice compared with shams, most of mast cells being degranulated. Treatment with cromolyn resulted in significant reduction of both mast cell density and activity (Figures 16b and 16c).

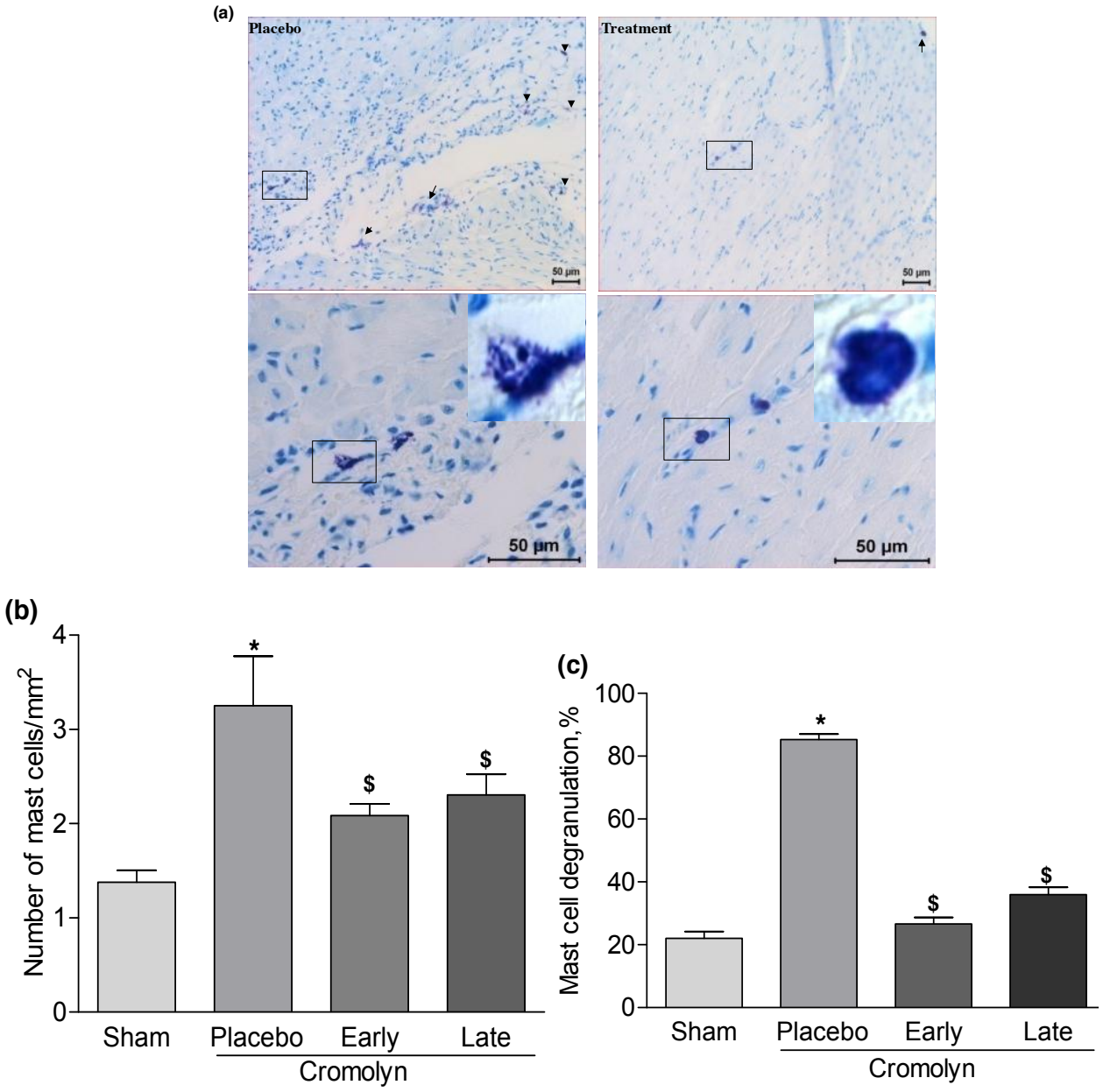

Figure 16: Effect of cromolyn on mast cell density and activity.
Treatment with cromolyn was started either from day zero of PAB (early intervention) or day at 7 after PAB (late intervention). As described in the methods, mast cells were stained with toluidine

blue. (a) representative images of mast cells in RV tissue from placebo and cromolyn treated mice. Scale, bar, 50 µm, (b) mast cell density and (c) mast cell activity. Data are presented as mean±SEM, *p<0.05 compared with sham and $p<0.05 compared with placebo, n=5 in each group.

3.3 Role of mast cells in pressure overload-induced RV remodeling

We investigated the role of MCs in pressure overload induced RV remodeling using mast cell-deficient *WBB6F1-Kit$^{W/W-v}$* (*Kit^{W}*/*Kit^{W-v}*) mice. These *Kit^{W}*/*Kit^{W-v}* mice are compound heterozygous mice, which combine the severe *Kit^{W}* mutation with the milder *Kit^{W-v}* mutation. These animals have markedly reduced Kit receptor activity and are severely mast cell-deficient [142].

3.3.1 Hemodynamics and RV function in banded *Kit^{W}*/*Kit^{W-v}* mice

There were no significant differences in the level of pressure overload imposed on the RV between wild type and *Kit^{W}*/*Kit^{W-v}* mice (Figure 17a). Systemic arterial pressure was not different between the groups (Figure 17b). RV end-diastolic and right atrial pressures non-significantly increased in wild type and *Kit^{W}*/*Kit^{W-v}* mice compared with respective shams (Figures 17c and 17d). Cardiac output significantly decreased in banded wild type mice while in *Kit^{W}*/*Kit^{W-v}* mice cardiac output remained stable (Figure 17e). In wild type mice, PAB led to significant RV dysfunction evidenced by reduced TAPSE and increased Tei index; whereas RV function was preserved in *Kit^{W}*/*Kit^{W-v}* mice (Figures 17f and 17g).

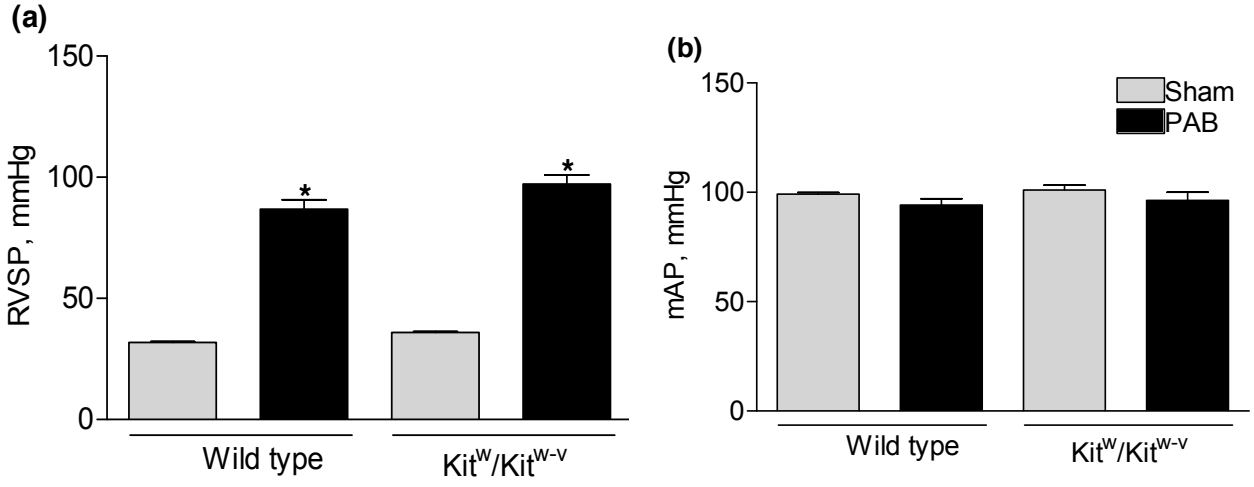

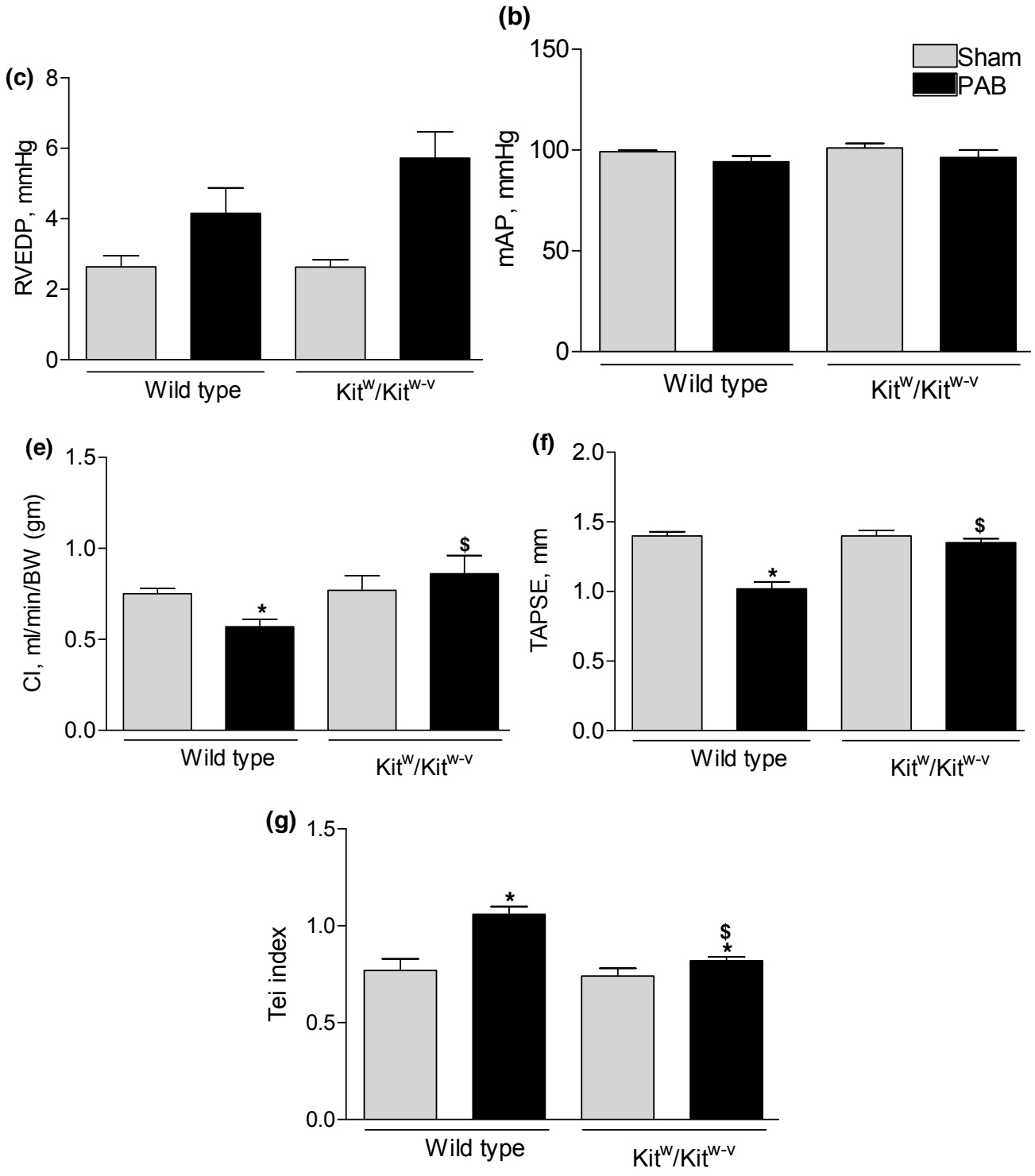

Figure 17: Hemodynamics and RV function in banded *Kit^{W}/Kit^{W-v}* mice

(a) right ventricular systolic pressure (RVSP); (b) mean aortic pressure (mAP); (c) right ventricular end-diastolic pressure (RVEDP); (d) mean right atrial pressure; (e) cardiac index (CI); (f) tricuspid annular plane systolic excursion (TAPSE); and (g) Tei index. Data are presented as mean±SEM, *p<0.05 compared with sham and $p<0.05 compared with banded wild type mice, n=5 for sham and n=10 for PAB in each group.

3.3.2 RV remodeling in banded *Kit*^{W}/*Kit*$^{W-v}$ mice

Although, PAB resulted on increase in RV mass of similar degree in wild type and *Kit*^{W}/*Kit*$^{W-v}$ mice, cardiac remodeling was different in those mice. In wild type mice, RV remodeling was characterized by RV chamber enlargement with thickening of the RV wall and by increased RV mass. In contrast, RV remodeling was characterized by increased RV thickness without RV chamber enlargement in *Kit*^{W}/*Kit*$^{W-v}$ mice (Figures 18a, 18b and 18d). Banded *Kit*^{W}/*Kit*$^{W-v}$ mice showed significantly higher cross sectional area of RV cardiomyocytes compared to banded wild type mice (Figures 18c and 18e).

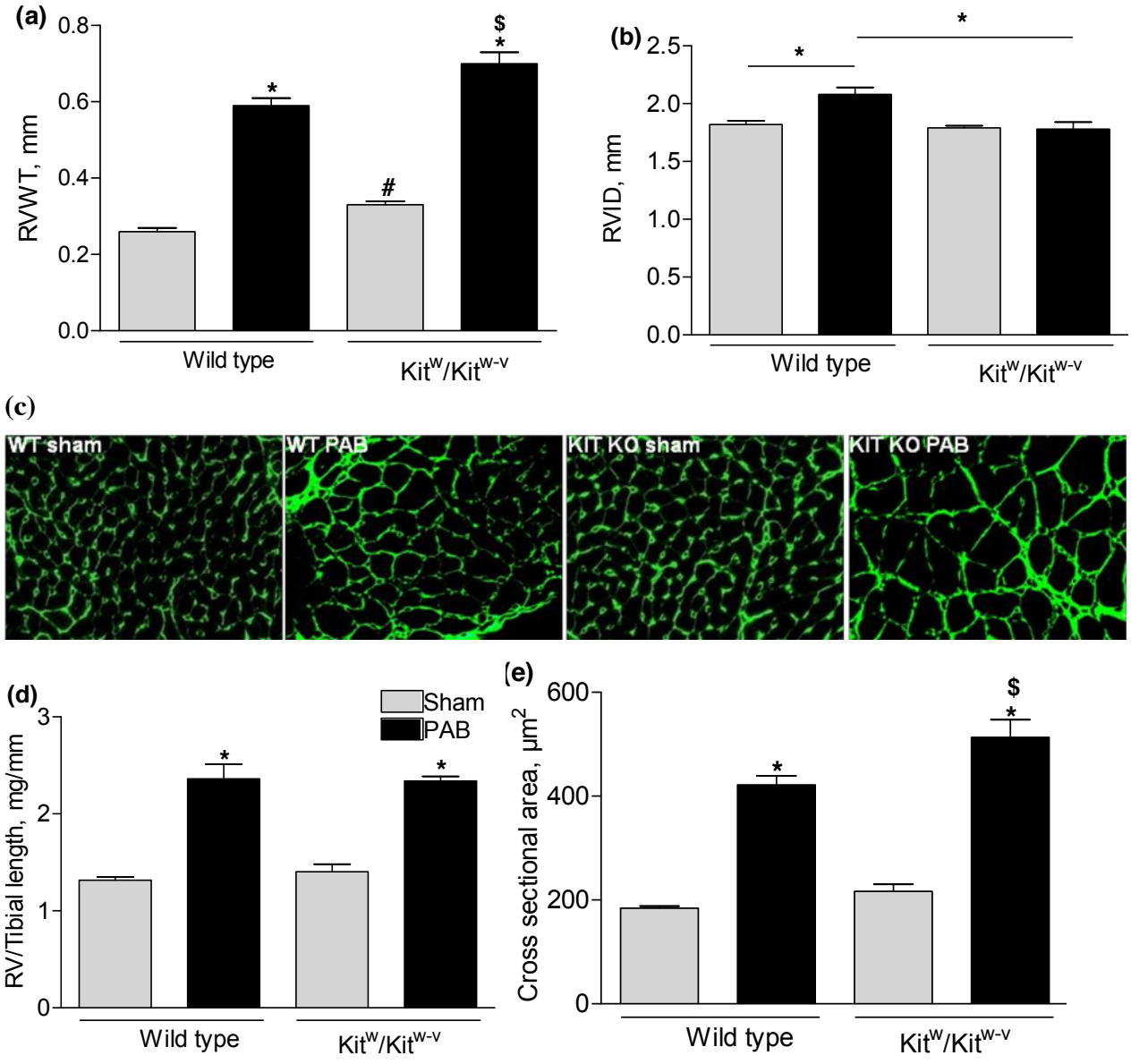

Figure 18: RV remodeling in banded *Kit^{W}/Kit^{W-v}* mice
(a) right ventricular wall thickness (RVWT); (b) right ventricular internal dimension (RVID); (c) representative images of RV cut in cross-section show FITC-conjugated wheat germ agglutinin staining for cross sectional analysis, (d) right ventricular mass/tibial length (RV/TL); and (e) bar graphs summarizing cardiomyocyte (CM) cross sectional area. Data are presented as mean±SEM, *p<0.05 compared with sham, $^{\$}$p<0.05 compared with wild type PAB and $^{\#}$p<0.05 compared with wild type sham, n=5 for sham and n=10 for PAB in each group.

3.3.3 RV fibrosis in banded *Kit^{W}/Kit^{W-v}* mice

Banded wild type mice showed significantly higher RV interstitial fibrosis compared with sham. In contrast, banded *Kit^{W}/Kit^{W-v}* mice displayed significantly decreased RV interstitial fibrosis (Figures 19a and 19b).

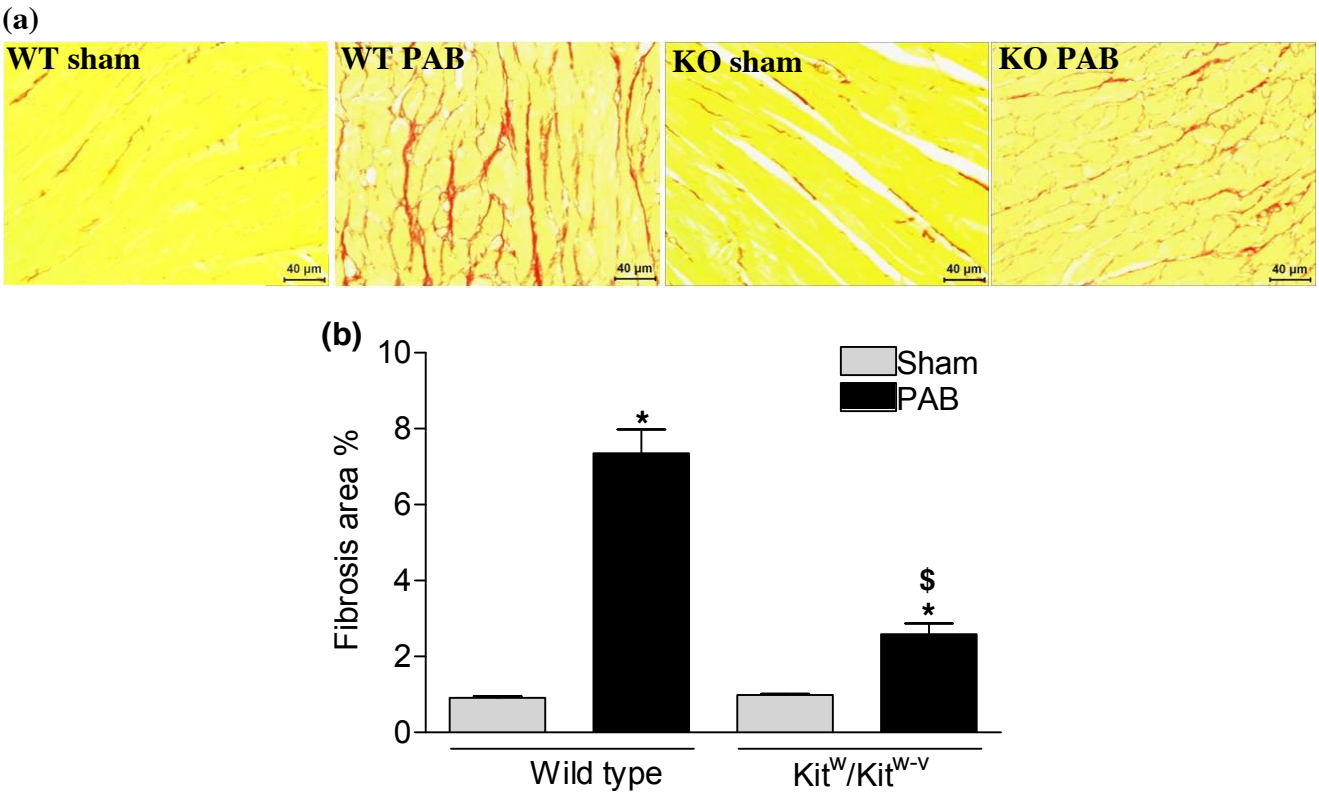

Figure 19: RV fibrosis in banded *Kit^{W}/Kit^{W-v}* mice
(a) representative picrosirius red staining images of right ventricles. Scale bar 40 µm and (b) bar graphs summarizing quantification of interstitial fibrosis. Data are presented as mean±SEM, *p<0.05 compared with sham and $^{\$}$p<0.05 compared with wild type PAB, n=5 for sham and n=10 for PAB in each group.

3.3.4 RV angiogenesis in banded *Kit^{W}/Kit^{W-v}* mice

There was a slight increase in the capillary density in all banded mice compared with shams (Figure 20b). However, the number of capillaries per cross-sectional area of cardiomyocytes significantly decreased in all banded mice (Figure 20c).

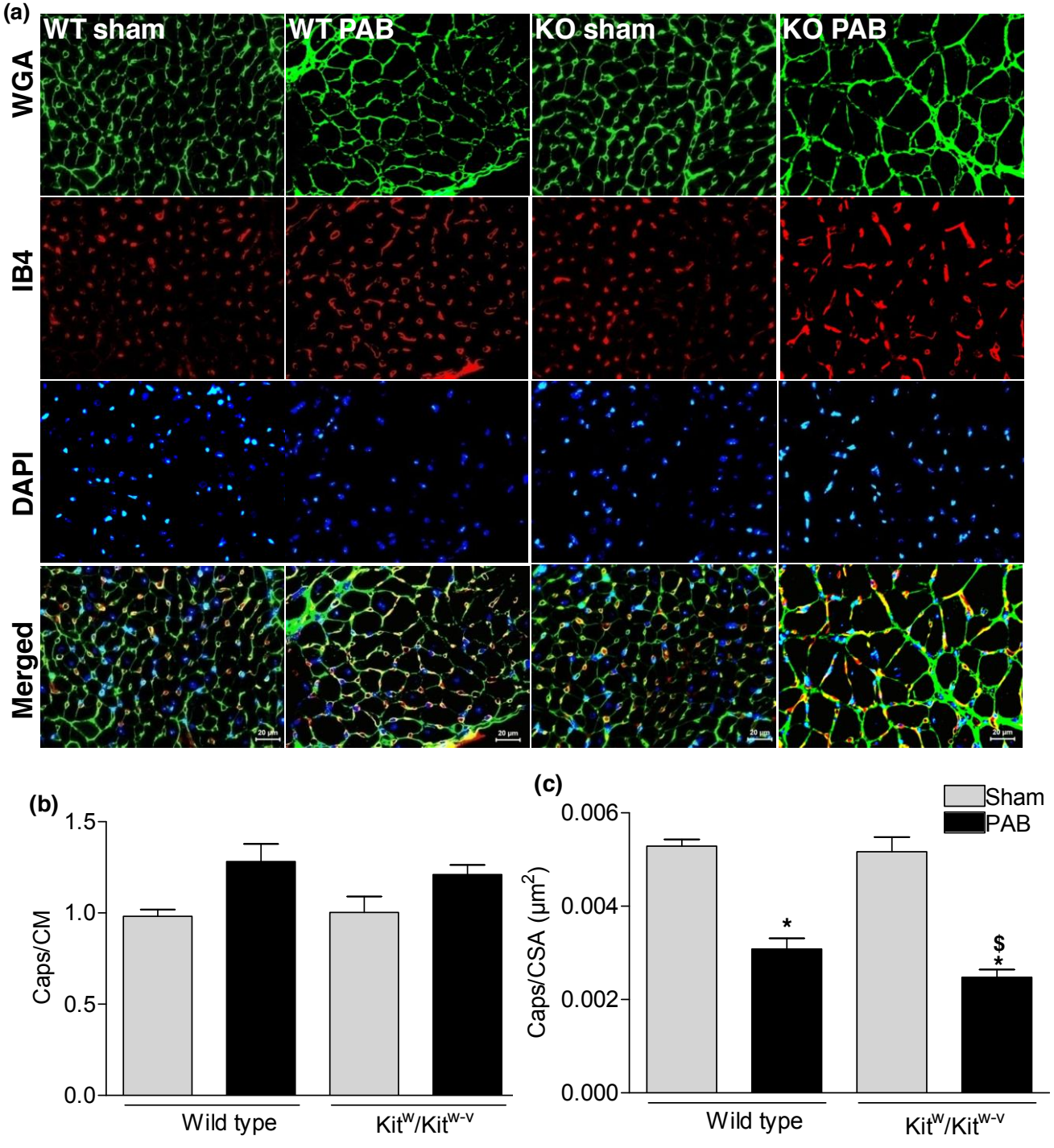

Figure 20: RV angiogenesis in banded *Kit^{W}/Kit^{W-v}* mice
(a) Representative images of right ventricles cut in cross-section and stained with wheat germ agglutinin-FITC conjugate (WGA-FITC), isolectin B4-TRITC conjugate (IB4-TRITC), DAPI and merged. WGA marks cell boundaries (green), isolectin B4 (red) marks endothelial cells, DAPI marks nuclei (blue). Scale bar 20 µm. Bar graphs summarizing (b) capillaries per cardiomyocytes and (c) capillaries per cross sectional area of cardiomyocytes. Data are presented as mean±SEM, *p<0.05 compared with sham and $^{\$}$p<0.05 compared with wild type PAB, n=5 for sham and n=10 for PAB in each group.

3.3.5 RV TGF-β signaling in banded *Kit^{W}/Kit^{W-v}* mice

Immunoreactivity for p-SMAD strongly increased in RV from banded wild type mice compared to the sham. In contrast, immunoreactivity for p-SMAD was strongly reduced in banded *Kit^{W}*/*Kit^{W-v}* mice.

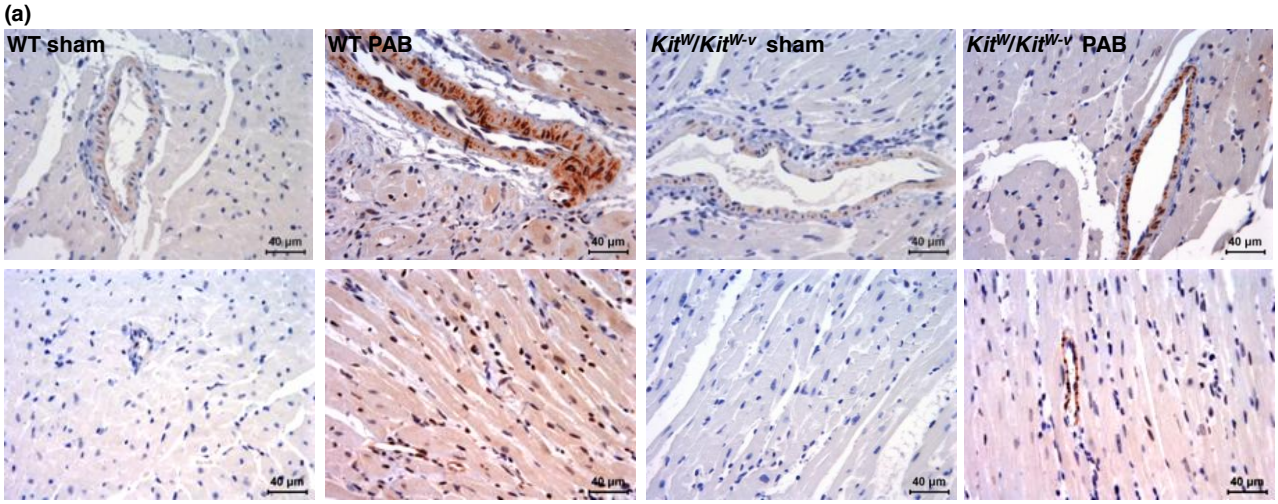

Figure 21: TGF-β signaling in banded *Kit^{W}/Kit^{W-v}* mice
Representative images of RV showing p-SMAD staining in (a) vascular (top) and interstitial (bottom) area, scale bars 40 µm.

4 DISCUSSION

In the present study we demonstrated that mast cells play a role in pressure overload induced RV remodeling. We showed a time-dependent increase in mast cell density and activity in the remodeled RV. Inhibition of mast cell degranulation by a mast cell stabilizer cromolyn significantly improved RV remodeling. Whereas RV remodeling in wild type mice was characterized by chamber enlargement with thickening of the wall and RV dysfunction, in mast cell deficient mice RV remodeling was characterized by a more pronounced increase in wall thickness without chamber enlargement and most importantly preserved RV function.

4.1 Time course of pressure overload-induced RV remodeling

The structural and functional alterations in cardiac tissue after chronic pressure overload have been well characterized and extensively studied using animal models of aortic stenosis[144-148]. Several studies on pressure overload to the RV have been carried out [21,65,20] but systematic time course changes were not investigated so far. We employed a murine model of RV remodeling using PAB. The model of PAB is an emerging model of RV hypertrophy, allowing investigations of the mechanisms of RV hypertrophy and direct effects of therapy on RV remodeling and RV function. Cardiac hypertrophy is normally known as adaptive response where cardiac remodeling comprises cellular, molecular and interstitial alterations resulting in altered shape, size ultimately leading to impaired function[1]. The molecular alterations comprise fetal gene reprogramming, impaired excitation-contraction coupling and cellular metabolic switch[1].

Using the PAB model, we studied the effects of pressure overload on RV performance at early time points after PAB and the time course of the development of RV hypertrophy in mice. To assess the degree of afterload imposed by PAB, we measured peak velocities across the constriction by a Pulse Wave (PW) Doppler. The peak gradient by PW Doppler was measurable in all banded mice and progressively increased. The low gradient early after PAB may be explained by the fact that a thin walled RV is not able to generate high pressures and fails. Indeed, cardiac output significantly decreased at postoperative day 1 but partially recovered by day 7 with further gradual decline. RV mass in banded mice

increased 3 days after PAB and continued to increase further up to day 35. RV remodeling in banded mice was characterized by dilatation and increased free wall thickness of the RV, flattening of the interventricular septum and compression of the left ventricle. Similar to cardiac output, RV function evaluated by TAPSE and Tei index significantly deteriorated immediately after PAB, but partially recovered on postoperative day 3 with further slow decline. Histological examination revealed increased RV cardiomyocyte size. Interstitial collagen deposition in banded mice started increasing 1 week after surgery and progressively increased further up to day 35. RV remodeling was associated with increased expression of hypertrophic and profibrotic markers.

The impaired right ventricular function is also associated with decreased perfusion of RV free wall as a result of massive dilatation of the RV wall and increased systolic compression of the intramural coronary vessels and decreased capillary densities per cross sectional area of the cardiomyocyte as shown in figure 7c . The impaired function is not correlated to the number of capillaries supplied to each cardiomyocytes rather the cardiomyocytes suffered from relative insufficiency because of the increased cell size. Because of the increased RVSP and decreased capillary density per cross sectional area of cardiomyocyte, RV myocardial blood flow fails to increase in proportion to the demand and RV wall turns into ischemic condition it can't work as efficiently as normal RV. Vlahakes *et al*. showed similar results in dog using acute right ventricular hypertension model (Scheme 6)[149].

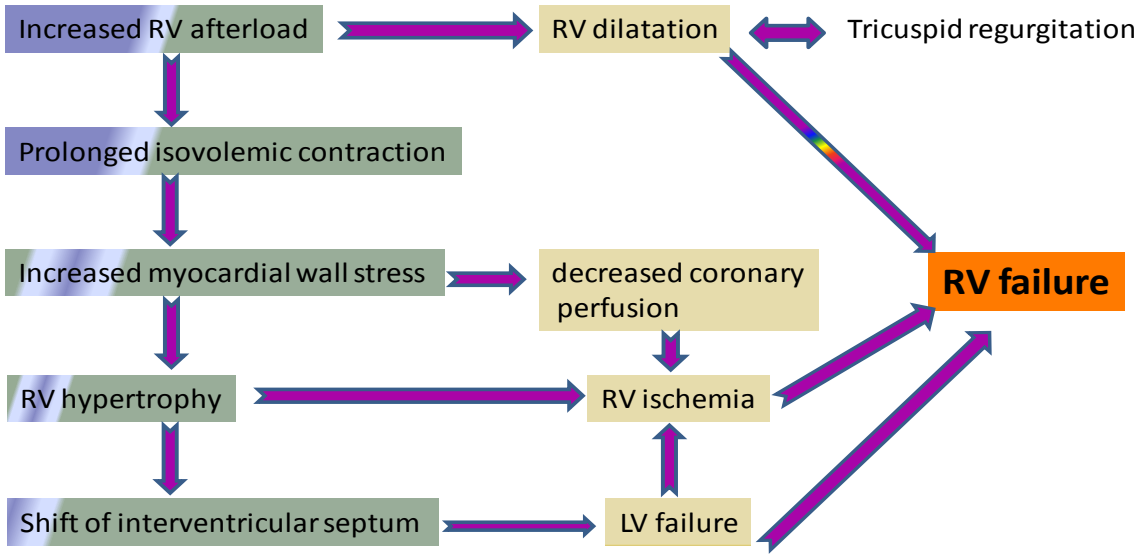

Scheme 6: Progression of pressure overload induced RV remodeling and failure

Recently, it was shown that accumulation and activation of perivascular mast cells in the lungs are the histopathological features present in lungs from idiopathic PAH patients[110]. Moreover, it has been demonstrated that accumulation and activation of mast cells in the lungs contribute to the development of PH using the experimental models of PH in monocrotaline-treated rats [110] and PH secondary to left ventricular pressure overload[111].

Similar increased number of mast cells in the hypertrophied RV was documented after PAB in rats[150]. However, the role of mast cells in the pathogenesis of RV hypertrophy was not investigated. Given the role mast cells play in PH and progression of left ventricular failure[115], we were interested if mast cells are involved in the RV remodeling. Therefore, we investigated the density and activity of mast cells in the RV at different time points after PAB. We found a time-dependent increase in total number of mast cells and proportion of degranulated mast cells in the RV tissue. The mast cell density started increasing after 2 weeks and reached maximal values 3 weeks post-surgery. Proportion of degranulated mast cells increased starting from day 1 after PAB and reached a plateau by day 7. Furthermore, we found upregulation of mMcp-4 and mMcp-5 levels in banded mice on mRNA level.

However, MCs particularly play an important role during tissue repair by stimulating fibroblast proliferation and migration[151,152]. Cardiac MCs are the potential source of TNF-α, TGF-β, bFGF and chymase during different pathological stages of heart failure[140]. Especially prohypertrophic and profibrotic growth factors such as TGF-β and chymase play significant role in cardiac remodeling process. It is reported that mast cell chymase is actively involved in generation of angiotensin II (Ang II) and activation of transforming growth factor TGF-β[126]. MCs themselves are one of the major TGF-β. MC chymase activates latent TGF-β leading to collagen I and III expression in cardiac fibroblast[116].

Taken together, our preliminary data from the study of the time course of RV remodeling suggested possible involvement of mast cells in the RV remodeling process. Mast cells, may thus, represent an interesting target for the development of therapeutic strategies directed specifically at RV and thus improve survival in patients.

4.2 Effects of mast cell stabilization in pressure overload-induced RV remodeling

To investigate the effects of mast cell stabilization in pressure overload induced RV remodeling, we performed treatment with cromolyn. Mast cell stabilizing agents, such as cromolyn, tranilast and ketotifen, are clinically available oral antiallergic drugs. Their antiallergic effects are mainly mediated by the inhibition of the release of chemical mediators from mast cells. As time dependent changes in RV performance and mast cell density and activity in the remodeled RV were observed after PAB, we performed two types of treatment: an early (starting from day zero of PAB for 3 weeks) and late (starting from day 7 of PAB for 2 weeks) interventions. With the early treatment we sought to interfere with early events in the RV remodeling. With the late intervention we sought to affect the mechanisms involved in the transition from compensatory hypertrophy to heart failure. Both treatment options were associated with improvements in major functional parameters such as cardiac output, TAPSE and Tei index. BNP and ANP mRNA expression was not affected by treatment being in line with the absence of effects of cromolyn on cellular hypertrophy. Consistent with the decreased collagen 1 and collagen 3 mRNA expression, there was significant reduction of interstitial fibrosis in the treatment groups. Similarly, prevention of fibrotic deposits with mast cell stabilization was shown in left ventricular hypertrophy in spontaneously hypertensive rats[117]. All these changes may underlie the improved RV remodeling and function in the treated mice (Scheme 7). Santone *et al.* demonstrated improvement of cardiac contractile function by stabilization of mast cells in an animal model of hemorrhagic shock and resuscitation[153].

Interestingly, treatment with cromolyn led also to reduction in mast cell density in the RV. Inhibition of mast cell degranulation might have blocked further homing of mast cells from bone marrow. Similar findings were reported in ischemia-reperfusion-induced cell injury[154,155]. Decreased mast cell density in the treatment groups is accompanied by a significant decrease in mRNA expression of mast cell specific genes MCP-4 and MCP-5. As both early and late interventions resulted in improved RV remodeling and function, we suggest that mast cell are involved in early events initiating adaptive processes to pressure overload as well as in later transition from compensatory hypertrophy to heart failure.

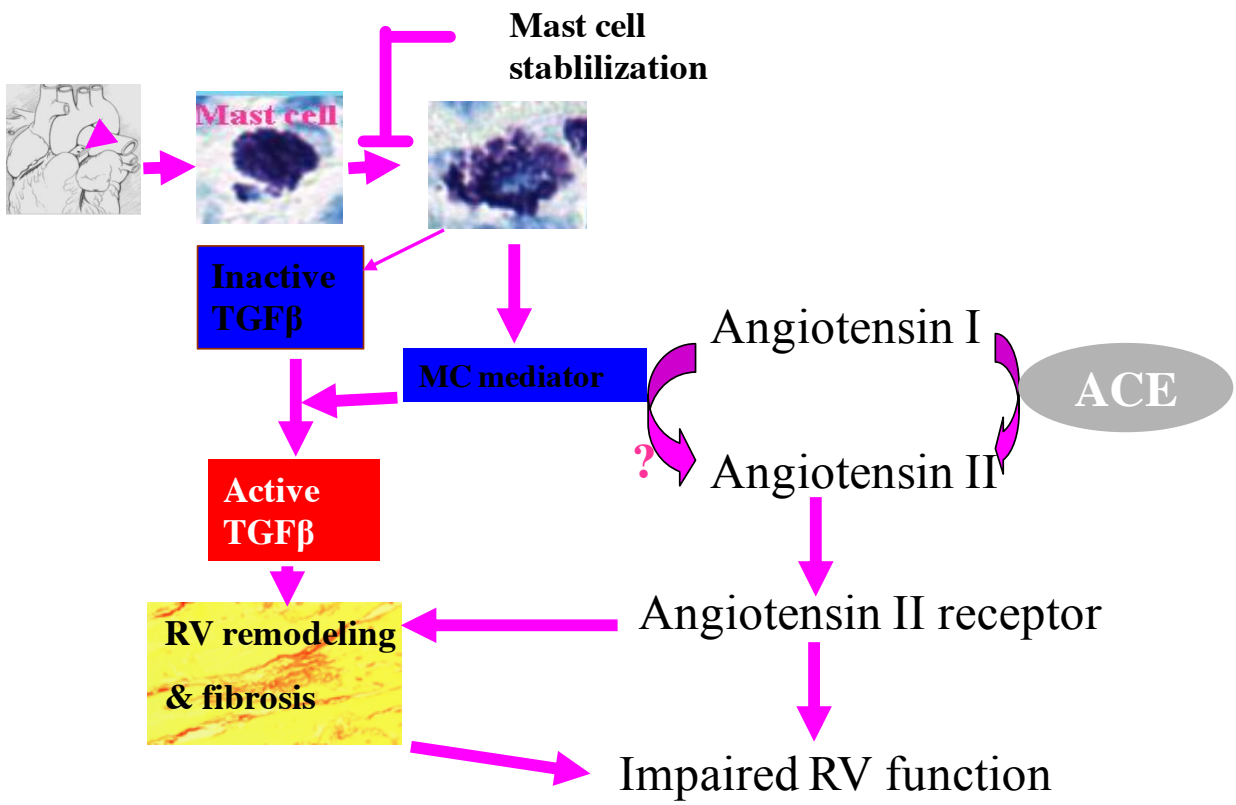

Scheme 7: Effect of mast cell stabilization in pressure overload induced RV remodeling.

4.3 Role of mast cells in pressure overload-induced RV remodeling

To further examine the role of mast cells in RV remodeling, we utilized mast cell–deficient Kit^{W}/Kit^{W-v} mice.

In contrast to wild type mice, RV remodeling Kit^{W}/Kit^{W-v} mice was characterized by increased RV thickness without RV chamber enlargement. Our results are in line with those reporting that Kit^{W}/Kit^{W-v} mice are protected from decompensated LV hypertrophy and chamber dilatation[115]. Moreover, this beneficial type of remodeling was evidenced by absence of interstitial fibrosis and preserved RV function. The absence of interstitial fibrosis in banded Kit^{W}/Kit^{W-v} mice is further supported by the attenuated TGF-β signaling pathway activation in these mice. Mast cells synthesize and store significant amounts of latent TGF-β which is released upon activation/degranulation followed by activation by mast cell chymase[156]. The active TGF-β binds to TGF-βRII present on a cardiac fibroblast[157] thereby stimulating fibroblast proliferation, differentiation to myofibroblast and an increased collagen synthesis (Scheme 8 left panel)[158,159] where as mast cell deficient

mice possesses reduced TGF-β activation (Scheme 8 right panel). In addition, $Kit^{W}/Kit^{W\text{-}v}$ mice displayed a more pronounced cellular hypertrophy. Based on our findings and reports from the literature[66], we assume a presence of a beneficial type of remodeling on a cellular level as well. This type of remodeling is characterized by the increase of cardiomyocyte diameter but not its elongation and is associated with activation of distinct signaling pathways[66].

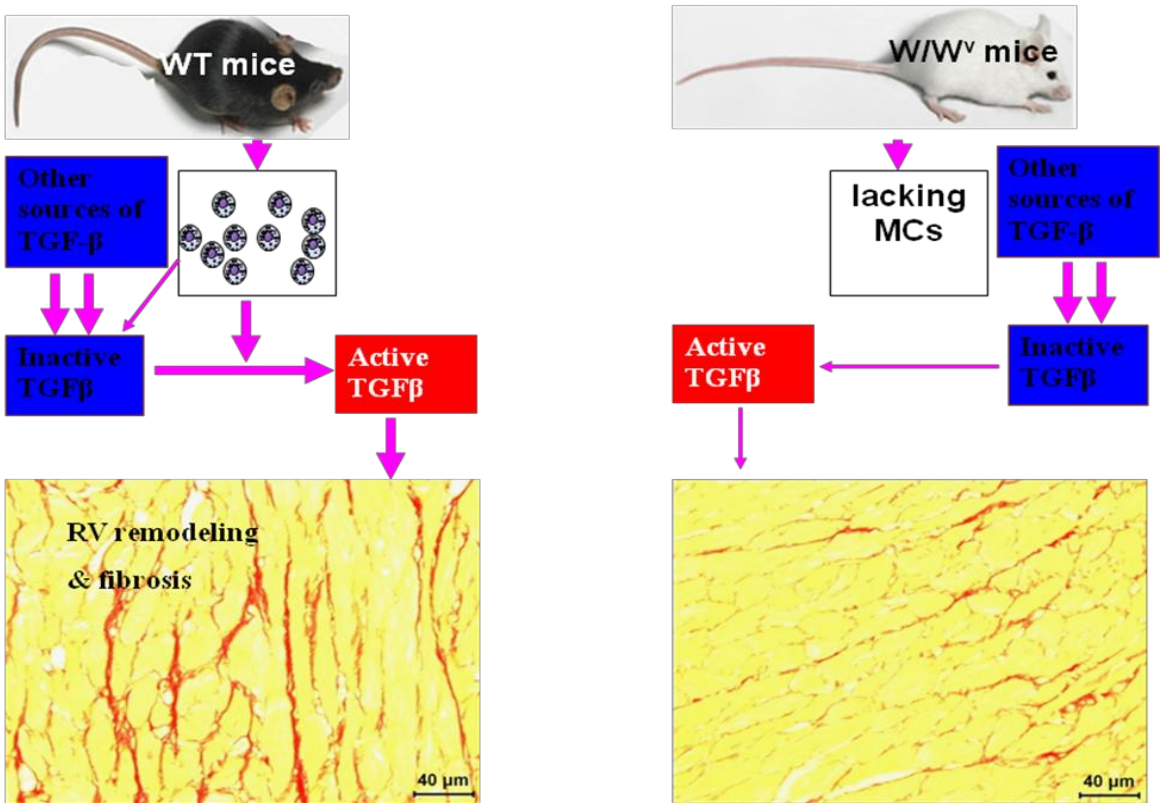

Scheme 8: Role of MCs in pressure overload induced RV remodeling.

4.4 Future prospective

As mast cells contain multiple mediators which may have both beneficial and deleterious effects on RV remodeling, inhibition of mast cell degranulation by mast cell stabilizing agents is rather a nonspecific approach. Identifying those mediators that are involved in the maladaptive remodeling and selective inhibition of them may represent a more specific approach. Based on our findings and data from the literature[160], we believe that mast cells are involved in RV remodeling through their expression of chymase. Human chymases,

which are mast cell-restricted serine proteases, can activate matrix metalloproteinases, convert big endothelin to endothelin I and produce angiotensin II. Therefore, mast cell chymases may contribute to ventricular remodeling. Recently, it was reported that mast cell chymase limits the cardiac efficacy of angiotensin I converting enzyme inhibitor therapy in rodents[126] and demonstrated that combined chymase and ACE inhibition, relative to ACE inhibition alone, improved left ventricular function, decreased adverse cardiac remodeling and improved survival after myocardial infarction in hamsters. It is of interest to utilize mMCP-4 and mMCP-5 knockout mice to delineate the role of chymases in pressure overload induced right ventricular remodeling process.

5 REFERENCES

1. Cohn JN, Ferrari R, Sharpe N. Cardiac remodeling--concepts and clinical implications: a consensus paper from an international forum on cardiac remodeling. Behalf of an International Forum on Cardiac Remodeling. *J Am Coll Cardiol.* 2000;35(3):569-582.
2. Scherrer-Crosbie M, Kurtz B. Ventricular remodeling and function: insights using murine echocardiography. *J Mol Cell Cardiol.*48(3):512-517.
3. Cooper Gt. Cardiocyte adaptation to chronically altered load. *Annu Rev Physiol.* 1987;49:501-518.
4. Sugden PH, Clerk A. Cellular mechanisms of cardiac hypertrophy. *J Mol Med (Berl).* 1998;76(11):725-746.
5. Hunter JJ, Chien KR. Signaling pathways for cardiac hypertrophy and failure. *N Engl J Med.* 1999;341(17):1276-1283.
6. Landmesser U, Wollert KC, Drexler H. Potential novel pharmacological therapies for myocardial remodelling. *Cardiovasc Res.* 2009;81(3):519-527.
7. Mudd JO, Kass DA. Reversing chronic remodeling in heart failure. *Expert Rev Cardiovasc Ther.* 2007;5(3):585-598.
8. Frigerio M, Roubina E. Drugs for left ventricular remodeling in heart failure. *Am J Cardiol.* 2005;96(12A):10L-18L.
9. Eapen Z, Rogers JG. Strategies to attenuate pathological remodeling in heart failure. *Curr Opin Cardiol.* 2009;24(3):223-229.
10. deGoma EM, Vagelos RH, Fowler MB, Ashley EA. Emerging therapies for the management of decompensated heart failure: from bench to bedside. *J Am Coll Cardiol.* 2006;48(12):2397-2409.
11. Mudd JO, Kass DA. Tackling heart failure in the twenty-first century. *Nature.* 2008;451(7181):919-928.
12. McKinsey TA, Kass DA. Small-molecule therapies for cardiac hypertrophy: moving beneath the cell surface. *Nat Rev Drug Discov.* 2007;6(8):617-635.
13. Banerjee D, Haddad F, Zamanian RT, Nagendran J. Right ventricular failure: a novel era of targeted therapy. *Curr Heart Fail Rep.*7(4):202-211.

14. Davlouros PA, Niwa K, Webb G, Gatzoulis MA. The right ventricle in congenital heart disease. *Heart.* 2006;92 Suppl 1:i27-38.
15. D'Alonzo GE, Barst RJ, Ayres SM, Bergofsky EH, Brundage BH, Detre KM, Fishman AP, Goldring RM, Groves BM, Kernis JT, *et al*. Survival in patients with primary pulmonary hypertension. Results from a national prospective registry. *Ann Intern Med.* 1991;115(5):343-349.
16. Assali AR, Teplitsky I, Ben-Dor I, Solodky A, Brosh D, Battler A, Fuchs S, Kornowski R. Prognostic importance of right ventricular infarction in an acute myocardial infarction cohort referred for contemporary percutaneous reperfusion therapy. *Am Heart J.* 2007;153(2):231-237.
17. Ghio S, Gavazzi A, Campana C, Inserra C, Klersy C, Sebastiani R, Arbustini E, Recusani F, Tavazzi L. Independent and additive prognostic value of right ventricular systolic function and pulmonary artery pressure in patients with chronic heart failure. *J Am Coll Cardiol.* 2001;37(1):183-188.
18. Grigioni F, Potena L, Galie N, Fallani F, Bigliardi M, Coccolo F, Magnani G, Manes A, Barbieri A, Fucili A, Magelli C, Branzi A. Prognostic implications of serial assessments of pulmonary hypertension in severe chronic heart failure. *J Heart Lung Transplant.* 2006;25(10):1241-1246.
19. Di Salvo TG, Mathier M, Semigran MJ, Dec GW. Preserved right ventricular ejection fraction predicts exercise capacity and survival in advanced heart failure. *J Am Coll Cardiol.* 1995;25(5):1143-1153.
20. Giovanardi P, Tincani E, Rossi R, Agnoletto V, Bondi M, Modena MG. Right ventricular function predicts cardiovascular events in outpatients with stable cardiovascular diseases: preliminary results. *Intern Emerg Med.* 2012, 7:251–256.
21. Voelkel NF, Quaife RA, Leinwand LA, Barst RJ, McGoon MD, Meldrum DR, Dupuis J, Long CS, Rubin LJ, Smart FW, Suzuki YJ, Gladwin M, Denholm EM, Gail DB. Right ventricular function and failure: report of a National Heart, Lung and Blood Institute working group on cellular and molecular mechanisms of right heart failure. *Circulation.* 2006;114(17):1883-1891.
22. Ghofrani HA, Barst RJ, Benza RL, Champion HC, Fagan KA, Grimminger F, Humbert M, Simonneau G, Stewart DJ, Ventura C, Rubin LJ. Future perspectives for the

treatment of pulmonary arterial hypertension. *J Am Coll Cardiol.* 2009;54(1 Suppl):S108-117.

23. Guglin M, Verma S. Right side of heart failure. *Heart Fail Rev.* 2012, 17:511–527.
24. McLaughlin VV, Davis M, Cornwell W. Pulmonary arterial hypertension. *Curr Probl Cardiol.* 2011, 36(12):461-517.
25. Rosenkranz S. Pulmonary hypertension: current diagnosis and treatment. *Clin Res Cardiol.* 2007;96(8):527-541.
26. Adatia I, Kothari SS, Feinstein JA. Pulmonary hypertension associated with congenital heart disease: pulmonary vascular disease: the global perspective. *Chest.*137(6 Suppl):52S-61S.
27. Hoeper MM. The new definition of pulmonary hypertension. *Eur Respir J.* 2009;34(4):790-791.
28. Chaouat A, Naeije R, Weitzenblum E. Pulmonary hypertension in COPD. *Eur Respir J.* 2008;32(5):1371-1385.
29. Suskovic S, Keser D. Chronic obstructive pulmonary disease status 2011: long walk home. *Respir Med.*105 Suppl 1:S4-6.
30. Hoeper MM, Barbera JA, Channick RN, Hassoun PM, Lang IM, Manes A, Martinez FJ, Naeije R, Olschewski H, Pepke-Zaba J, Redfield MM, Robbins IM, Souza R, Torbicki A, McGoon M. Diagnosis, assessment and treatment of non-pulmonary arterial hypertension pulmonary hypertension. *J Am Coll Cardiol.* 2009;54(1 Suppl):S85-96.
31. Minai OA, Chaouat A, Adnot S. Pulmonary hypertension in COPD: epidemiology, significance and management: pulmonary vascular disease: the global perspective. *Chest.*137(6 Suppl):39S-51S.
32. Guazzi M, Arena R. Pulmonary hypertension with left-sided heart disease. *Nat Rev Cardiol.*7(11):648-659.
33. Guglin M, Khan H. Pulmonary hypertension in heart failure. *J Card Fail.*16(6):461-474.
34. Hoeper MM. Definition, classification and epidemiology of pulmonary arterial hypertension. *Semin Respir Crit Care Med.* 2009;30(4):369-375.
35. Bui AL, Horwich TB, Fonarow GC. Epidemiology and risk profile of heart failure. *Nat Rev Cardiol.*8(1):30-41.

36. Bruce CJ, Connolly HM. Right-sided valve disease deserves a little more respect. *Circulation.* 2009;119(20):2726-2734.
37. Irwin RB, Luckie M, Khattar RS. Tricuspid regurgitation: contemporary management of a neglected valvular lesion. *Postgrad Med J.*86(1021):648-655.
38. Haddad F, Ashley E, Michelakis ED. New insights for the diagnosis and management of right ventricular failure, from molecular imaging to targeted right ventricular therapy. *Curr Opin Cardiol.*25(2):131-140.
39. Guarracino F, Cariello C, Danella A, Doroni L, Lapolla F, Vullo C, Pasquini C, Stefani M. Right ventricular failure: physiology and assessment. *Minerva Anestesiol.* 2005;71(6):307-312.
40. Haddad F, Doyle R, Murphy DJ, Hunt SA. Right ventricular function in cardiovascular disease, part II: pathophysiology, clinical importance and management of right ventricular failure. *Circulation.* 2008;117(13):1717-1731.
41. Esposito G, Rapacciuolo A, Naga Prasad SV, Takaoka H, Thomas SA, Koch WJ, Rockman HA. Genetic alterations that inhibit in vivo pressure-overload hypertrophy prevent cardiac dysfunction despite increased wall stress. *Circulation.* 2002;105(1):85-92.
42. Hill JA, Karimi M, Kutschke W, Davisson RL, Zimmerman K, Wang Z, Kerber RE, Weiss RM. Cardiac hypertrophy is not a required compensatory response to short-term pressure overload. *Circulation.* 2000;101(24):2863-2869.
43. Carreno JE, Apablaza F, Ocaranza MP, Jalil JE. [Cardiac hypertrophy: molecular and cellular events]. *Rev Esp Cardiol.* 2006;59(5):473-486.
44. Marcus ML, Koyanagi S, Harrison DG, Doty DB, Hiratzka LF, Eastham CL. Abnormalities in the coronary circulation that occur as a consequence of cardiac hypertrophy. *Am J Med.* 1983;75(3A):62-66.
45. Tomanek RJ. Response of the coronary vasculature to myocardial hypertrophy. *J Am Coll Cardiol.* 1990;15(3):528-533.
46. Sano M, Minamino T, Toko H, Miyauchi H, Orimo M, Qin Y, Akazawa H, Tateno K, Kayama Y, Harada M, Shimizu I, Asahara T, Hamada H, Tomita S, Molkentin JD, Zou Y, Komuro I. p53-induced inhibition of Hif-1 causes cardiac dysfunction during pressure overload. *Nature.* 2007;446(7134):444-448.

47. Champion HC, Michelakis ED, Hassoun PM. Comprehensive invasive and noninvasive approach to the right ventricle-pulmonary circulation unit: state of the art and clinical and research implications. *Circulation.* 2009;120(11):992-1007.
48. Voelkel NF, Gomez-Arroyo J. The harmonics of rodent pulmonary hypertension models. *Int J Clin Pract Suppl.* (172):1-2.
49. Stenmark KR, Meyrick B, Galie N, Mooi WJ, McMurtry IF. Animal models of pulmonary arterial hypertension: the hope for etiological discovery and pharmacological cure. *Am J Physiol Lung Cell Mol Physiol.* 2009;297(6):L1013-1032.
50. Ciuclan L, Bonneau O, Hussey M, Duggan N, Holmes AM, Good R, Stringer R, Jones P, Morrell NW, Jarai G, Walker C, Westwick J, Thomas M. A Novel Murine Model of Severe Pulmonary Arterial Hypertension. *Am J Respir Crit Care Med.*
51. Burke DL, Frid MG, Kunrath CL, Karoor V, Anwar A, Wagner BD, Strassheim D, Stenmark KR. Sustained hypoxia promotes the development of a pulmonary artery-specific chronic inflammatory microenvironment. *Am J Physiol Lung Cell Mol Physiol.* 2009;297(2):L238-250.
52. Kay JM, Harris P, Heath D. Pulmonary hypertension produced in rats by ingestion of Crotalaria spectabilis seeds. *Thorax.* 1967;22(2):176-179.
53. Reid MJ, Lame MW, Morin D, Wilson DW, Segall HJ. Involvement of cytochrome P450 3A in the metabolism and covalent binding of 14C-monocrotaline in rat liver microsomes. *J Biochem Mol Toxicol.* 1998;12(3):157-166.
54. Lappin PB, Ross KL, King LE, Fraker PJ, Roth RA. The response of pulmonary vascular endothelial cells to monocrotaline pyrrole: cell proliferation and DNA synthesis in vitro and in vivo. *Toxicol Appl Pharmacol.* 1998;150(1):37-48.
55. Okada K, Tanaka Y, Bernstein M, Zhang W, Patterson GA, Botney MD. Pulmonary hemodynamics modify the rat pulmonary artery response to injury. A neointimal model of pulmonary hypertension. *Am J Pathol.* 1997;151(4):1019-1025.
56. White RJ, Meoli DF, Swarthout RF, Kallop DY, Galaria, II, Harvey JL, Miller CM, Blaxall BC, Hall CM, Pierce RA, Cool CD, Taubman MB. Plexiform-like lesions and increased tissue factor expression in a rat model of severe pulmonary arterial hypertension. *Am J Physiol Lung Cell Mol Physiol.* 2007;293(3):L583-590.

57. Akhavein F, St-Michel EJ, Seifert E, Rohlicek CV. Decreased left ventricular function, myocarditis and coronary arteriolar medial thickening following monocrotaline administration in adult rats. *J Appl Physiol.* 2007;103(1):287-295.
58. Dumitrascu R, Koebrich S, Dony E, Weissmann N, Savai R, Pullamsetti SS, Ghofrani HA, Samidurai A, Traupe H, Seeger W, Grimminger F, Schermuly RT. Characterization of a murine model of monocrotaline pyrrole-induced acute lung injury. *BMC Pulm Med.* 2008;8:25.
59. George J, Sun J, D'Armiento J. Transgenic expression of human matrix metalloproteinase-1 attenuates pulmonary arterial hypertension in mice. *Clin Sci (Lond).*122(2):83-92.
60. Cuttica MJ, Langenickel T, Noguchi A, Machado RF, Gladwin MT, Boehm M. Perivascular T-cell infiltration leads to sustained pulmonary artery remodeling after endothelial cell damage. *Am J Respir Cell Mol Biol.*45(1):62-71.
61. Cusimano RJ, Ashe KA, Abel JG, Lichtenstein SV, Salerno TA. A simple model of right ventricular hypertrophy. *J Invest Surg.* 1988;1(1):45-53.
62. Dias CA, Assad RS, Caneo LF, Abduch MC, Aiello VD, Dias AR, Marcial MB, Oliveira SA. Reversible pulmonary trunk banding. II. An experimental model for rapid pulmonary ventricular hypertrophy. *J Thorac Cardiovasc Surg.* 2002;124(5):999-1006.
63. Assad RS, Cardarelli M, Abduch MC, Aiello VD, Maizato M, Barbero-Marcial M, Jatene A. Reversible pulmonary trunk banding with a balloon catheter: assessment of rapid pulmonary ventricular hypertrophy. *J Thorac Cardiovasc Surg.* 2000;120(1):66-72.
64. Gaynor SL, Maniar HS, Bloch JB, Steendijk P, Moon MR. Right atrial and ventricular adaptation to chronic right ventricular pressure overload. *Circulation.* 2005;112(9 Suppl):I212-218.
65. Voeller RK, Aziz A, Maniar HS, Ufere NN, Taggar AK, Bernabe NJ, Jr., Cupps BP, Moon MR. Differential modulation of right ventricular strain and right atrial mechanics in mild vs. severe pressure overload. *Am J Physiol Heart Circ Physiol.* 2011, 301(6):H2362-71.

66. Molkentin JD, Robbins J. With great power comes great responsibility: using mouse genetics to study cardiac hypertrophy and failure. *J Mol Cell Cardiol.* 2009;46(2):130-136.
67. Kreymborg K, Uchida S, Gellert P, Schneider A, Boettger T, Voswinckel R, Wietelmann A, Szibor M, Weissmann N, Ghofrani AH, Schermuly R, Schranz D, Seeger W, Braun T. Identification of right heart-enriched genes in a murine model of chronic outflow tract obstruction. *J Mol Cell Cardiol.*49(4):598-605.
68. Qipshidze N, Tyagi N, Metreveli N, Lominadze D, Tyagi SC. Autophagy mechanism of right ventricular remodeling in murine model of pulmonary artery constriction. *Am J Physiol Heart Circ Physiol.*302(3):H688-696.
69. Urashima T, Zhao M, Wagner R, Fajardo G, Farahani S, Quertermous T, Bernstein D. Molecular and physiological characterization of RV remodeling in a murine model of pulmonary stenosis. *Am J Physiol Heart Circ Physiol.* 2008;295(3):H1351-H1368.
70. Tarnavski O, McMullen JR, Schinke M, Nie Q, Kong S, Izumo S. Mouse cardiac surgery: comprehensive techniques for the generation of mouse models of human diseases and their application for genomic studies. *Physiol Genomics.* 2004;16(3):349-360.
71. Tarnavski O. Mouse surgical models in cardiovascular research. *Methods Mol Biol.* 2009;573:115-137.
72. Rockman HA, Ono S, Ross RS, Jones LR, Karimi M, Bhargava V, Ross J, Jr., Chien KR. Molecular and physiological alterations in murine ventricular dysfunction. *Proc Natl Acad Sci U S A.* 1994;91(7):2694-2698.
73. Bartelds B, Borgdorff MA, Smit-van Oosten A, Takens J, Boersma B, Nederhoff MG, Elzenga NJ, van Gilst WH, De Windt LJ, Berger RM. Differential responses of the right ventricle to abnormal loading conditions in mice: pressure vs. volume load. *Eur J Heart Fail.*13(12):1275-1282.
74. Vistnes M, Waehre A, Nygard S, Sjaastad I Andersson KB, Husberg C, Christensen G. Circulating cytokine levels in mice with heart failure are etiology dependent. *J Appl Physiol.*108(5):1357-1364.

75. Fang YH, Piao L, Hong Z, Toth PT, Marsboom G, Bache-Wiig P, Rehman J, Archer SL. Therapeutic inhibition of fatty acid oxidation in right ventricular hypertrophy: exploiting Randle's cycle. *J Mol Med (Berl).*90(1):31-43.
76. Vida VL, Rizzo S, Maschietto N, Boccuzzo G, Milanesi O, Thiene G, Stellin G, Basso C. Age is a risk factor for maladaptive changes of the pulmonary root in rats exposed to increased pressure loading. *Cardiovasc Pathol.*
77. Harston RK, McKillop JC, Moschella PC, Van Laer A, Quinones LS, Baicu CF, Balasubramanian S, Zile MR, Kuppuswamy D. Rapamycin treatment augments both protein ubiquitination and Akt activation in pressure-overloaded rat myocardium. *Am J Physiol Heart Circ Physiol.*300(5):H1696-1706.
78. Bogaard HJ, Mizuno S, Hussaini AA, Toldo S, Abbate A, Kraskauskas D, Kasper M, Natarajan R, Voelkel NF. Suppression of histone deacetylases worsens right ventricular dysfunction after pulmonary artery banding in rats. *Am J Respir Crit Care Med.*183(10):1402-1410.
79. Bogaard HJ, Natarajan R, Henderson SC, Long CS, Kraskauskas D, Smithson L, Ockaili R, McCord JM, Voelkel NF. Chronic pulmonary artery pressure elevation is insufficient to explain right heart failure. *Circulation.* 2009;120(20):1951-1960.
80. Piao L, Fang YH, Cadete VJ, Wietholt C, Urboniene D, Toth PT, Marsboom G, Zhang HJ, Haber I, Rehman J, Lopaschuk GD, Archer SL. The inhibition of pyruvate dehydrogenase kinase improves impaired cardiac function and electrical remodeling in two models of right ventricular hypertrophy: resuscitating the hibernating right ventricle. *J Mol Med (Berl).*88(1):47-60.
81. Schafer S, Ellinghaus P, Janssen W, Kramer F, Lustig K, Milting H, Kast R, Klein M. Chronic inhibition of phosphodiesterase 5 does not prevent pressure-overload-induced right-ventricular remodelling. *Cardiovasc Res.* 2009;82(1):30-39.
82. Galli SJ. Mast cells and basophils. *Curr Opin Hematol.* 2000;7(1):32-39.
83. Marone G, de Crescenzo G, Adt M, Patella V, Arbustini E, Genovese A. Immunological characterization and functional importance of human heart mast cells. *Immunopharmacology.* 1995;31(1):1-18.
84. Shelburne CP, Abraham SN. The mast cell in innate and adaptive immunity. *Adv Exp Med Biol.*716:162-185.

85. Bradding P, Holgate ST. Immunopathology and human mast cell cytokines. *Crit Rev Oncol Hematol.* 1999;31(2):119-133.
86. Younan GJ, Heit YI, Dastouri P, Kekhia H, Xing W, Gurish MF, Orgill DP. Mast cells are required in the proliferation and remodeling phases of microdeformational wound therapy. *Plast Reconstr Surg.*128(6):649e-658e.
87. Parkin J, Cohen B. An overview of the immune system. *Lancet.* 2001;357(9270):1777-1789.
88. Asai K, Kitaura J, Kawakami Y, Yamagata N, Tsai M, Carbone DP, Liu FT, Galli SJ, Kawakami T. Regulation of mast cell survival by IgE. *Immunity.* 2001;14(6):791-800.
89. Kalesnikoff J, Huber M, Lam V, Damen JE, Zhang J, Siraganian RP, Krystal G. Monomeric IgE stimulates signaling pathways in mast cells that lead to cytokine production and cell survival. *Immunity.* 2001;14(6):801-811.
90. Klueh U, Kaur M, Qiao Y, Kreutzer DL. Critical role of tissue mast cells in controlling long-term glucose sensor function in vivo. *Biomaterials.*31(16):4540-4551.
91. Krishnaswamy G, Ajitawi O, Chi DS. The human mast cell: an overview. *Methods Mol Biol.* 2006;315:13-34.
92. Metz M, Maurer M. Mast cells--key effector cells in immune responses. *Trends Immunol.* 2007;28(5):234-241.
93. Galli SJ, Maurer M, Lantz CS. Mast cells as sentinels of innate immunity. *Curr Opin Immunol.* 1999;11(1):53-59.
94. Theoharides TC, Cochrane DE. Critical role of mast cells in inflammatory diseases and the effect of acute stress. *J Neuroimmunol.* 2004;146(1-2):1-12.
95. Gordon JR, Galli SJ. Mast cells as a source of both preformed and immunologically inducible TNF-alpha/cachectin. *Nature.* 1990;346(6281):274-276.
96. McLachlan JB, Hart JP, Pizzo SV, Shelburne CP, Staats HF, Gunn MD, Abraham SN. Mast cell-derived tumor necrosis factor induces hypertrophy of draining lymph nodes during infection. *Nat Immunol.* 2003;4(12):1199-1205.
97. Marshall JS, Jawdat DM. Mast cells in innate immunity. *J Allergy Clin Immunol.* 2004;114(1):21-27.

98. Swindle EJ, Metcalfe DD, Coleman JW. Rodent and human mast cells produce functionally significant intracellular reactive oxygen species but not nitric oxide. *J Biol Chem.* 2004;279(47):48751-48759.
99. Malaviya R, Ikeda T, Ross E, Abraham SN. Mast cell modulation of neutrophil influx and bacterial clearance at sites of infection through TNF-alpha. *Nature.* 1996;381(6577):77-80.
100. Frandji P, Tkaczyk C, Oskeritzian C, David B, Desaymard C, Mecheri S. Exogenous and endogenous antigens are differentially presented by mast cells to CD4+ T lymphocytes. *Eur J Immunol.* 1996;26(10):2517-2528.
101. Poncet P, Arock M, David B. MHC class II-dependent activation of CD4+ T cell hybridomas by human mast cells through superantigen presentation. *J Leukoc Biol.* 1999;66(1):105-112.
102. Marshall JS. Mast-cell responses to pathogens. *Nat Rev Immunol.* 2004;4(10):787-799.
103. Puxeddu I, Piliponsky AM, Bachelet I, Levi-Schaffer F. Mast cells in allergy and beyond. *Int J Biochem Cell Biol.* 2003;35(12):1601-1607.
104. Dvorak AM. Mast-cell degranulation in human hearts. *N Engl J Med.* 1986;315(15):969-970.
105. Rakusan K, Sarkar K, Turek Z, Wicker P. Mast cells in the rat heart during normal growth and in cardiac hypertrophy. *Circ Res.* 1990;66(2):511-516.
106. Bot I, Biessen EA. Mast cells in atherosclerosis. *Thromb Haemost.*106(5):820-826.
107. Sun J, Sukhova GK, Yang M, Wolters PJ, MacFarlane LA, Libby P, Sun C, Zhang Y, Liu J, Ennis TL, Knispel R, Xiong W, Thompson RW, Baxter BT, Shi GP. Mast cells modulate the pathogenesis of elastase-induced abdominal aortic aneurysms in mice. *J Clin Invest.* 2007;117(11):3359-3368.
108. Sun J, Zhang J, Lindholt JS, Sukhova GK, Liu J, He A, Abrink M, Pejler G, Stevens RL, Thompson RW, Ennis TL, Gurish MF, Libby P, Shi GP. Critical role of mast cell chymase in mouse abdominal aortic aneurysm formation. *Circulation.* 2009;120(11):973-982.

109. Sun J, Sukhova GK, Wolters PJ, Yang M, Kitamoto S, Libby P, MacFarlane LA, Mallen-St Clair J, Shi GP. Mast cells promote atherosclerosis by releasing proinflammatory cytokines. *Nat Med.* 2007;13(6):719-724.

110. Dahal BK, Kosanovic D, Kaulen C, Cornitescu T, Savai R, Hoffmann J, Reiss I, Ghofrani HA, Weissmann N, Kuebler WM, Seeger W, Grimminger F, Schermuly RT. Involvement of mast cells in monocrotaline-induced pulmonary hypertension in rats. *Respir Res.*12:60.

111. Hoffmann J, Yin J, Kukucka M, Yin N, Saarikko I, Sterner-Kock A, Fujii H, Leong-Poi H, Kuppe H, Schermuly RT, Kuebler WM. Mast cells promote lung vascular remodelling in pulmonary hypertension. *Eur Respir J.*37(6):1400-1410.

112. Frangogiannis NG, Lindsey ML, Michael LH, Youker KA, Bressler RB, Mendoza LH, Spengler RN, Smith CW, Entman ML. Resident cardiac mast cells degranulate and release preformed TNF-alpha, initiating the cytokine cascade in experimental canine myocardial ischemia/reperfusion. *Circulation.* 1998;98(7):699-710.

113. Somasundaram P, Ren G, Nagar H, Kraemer D, Mendoza L, Michael LH, Caughey GH, Entman ML, Frangogiannis NG. Mast cell tryptase may modulate endothelial cell phenotype in healing myocardial infarcts. *J Pathol.* 2005;205(1):102-111.

114. Kitaura-Inenaga K, Hara M, Higuchi K, Yamamoto K, Yamaki A, Ono K, Nakano A, Kinoshita M, Sasayama S, Matsumori A. Gene expression of cardiac mast cell chymase and tryptase in a murine model of heart failure caused by viral myocarditis. *Circ J.* 2003;67(10):881-884.

115. Hara M, Ono K, Hwang MW, Iwasaki A, Okada M, Nakatani K, Sasayama S, Matsumori A. Evidence for a role of mast cells in the evolution to congestive heart failure. *J Exp Med.* 2002;195(3):375-381.

116. Shiota N, Rysa J, Kovanen PT, Ruskoaho H, Kokkonen JO, Lindstedt KA. A role for cardiac mast cells in the pathogenesis of hypertensive heart disease. *J Hypertens.* 2003;21(10):1935-1944.

117. Levick SP, McLarty JL, Murray DB, Freeman RM, Carver WE, Brower GL. Cardiac mast cells mediate left ventricular fibrosis in the hypertensive rat heart. *Hypertension.* 2009;53(6):1041-1047.

118. Batlle M, Roig E, Perez-Villa F, Lario S, Cejudo-Martin P, Garcia-Pras E, Ortiz J, Roque M, Orus J, Rigol M, Heras M, Ramirez J, Jimenez W. Increased expression of the renin-angiotensin system and mast cell density but not of angiotensin-converting enzyme II in late stages of human heart failure. *J Heart Lung Transplant.* 2006;25(9):1117-1125.

119. Theoharides TC, Kempuraj D, Tagen M, Conti P, Kalogeromitros D. Differential release of mast cell mediators and the pathogenesis of inflammation. *Immunol Rev.* 2007;217:65-78.

120. Lees M, Taylor DJ, Woolley DE. Mast cell proteinases activate precursor forms of collagenase and stromelysin, but not of gelatinases A and B. *Eur J Biochem.* 1994;223(1):171-177.

121. Fang KC, Raymond WW, Blount JL, Caughey GH. Dog mast cell alpha-chymase activates progelatinase B by cleaving the Phe88-Gln89 and Phe91-Glu92 bonds of the catalytic domain. *J Biol Chem.* 1997;272(41):25628-25635.

122. Tchougounova E, Lundequist A, Fajardo I, Winberg JO, Abrink M, Pejler G. A key role for mast cell chymase in the activation of pro-matrix metalloprotease-9 and pro-matrix metalloprotease-2. *J Biol Chem.* 2005;280(10):9291-9296.

123. Urata H, Ganten D. Cardiac angiotensin II formation: the angiotensin-I converting enzyme and human chymase. *Eur Heart J.* 1993;14 Suppl I:177-182.

124. Urata H, Hoffmann S, Ganten D. Tissue angiotensin II system in the human heart. *Eur Heart J.* 1994;15 Suppl D:68-78.

125. Jenne DE, Tschopp J. Angiotensin II-forming heart chymase is a mast-cell-specific enzyme. *Biochem J.* 1991;276 (Pt 2):567-568.

126. Wei CC, Hase N, Inoue Y, Bradley EW, Yahiro E, Li M, Naqvi N, Powell PC, Shi K, Takahashi Y, Saku K, Urata H, Dell'italia LJ, Husain A. Mast cell chymase limits the cardiac efficacy of Ang I-converting enzyme inhibitor therapy in rodents. *J Clin Invest.*120(4):1229-1239.

127. Gusev K, Domenighetti AA, Delbridge LM, Pedrazzini T, Niggli E, Egger M. Angiotensin II-mediated adaptive and maladaptive remodeling of cardiomyocyte excitation-contraction coupling. *Circ Res.* 2009;105(1):42-50.

128. Kim S, Ohta K, Hamaguchi A, Yukimura T, Miura K, Iwao H. Angiotensin II induces cardiac phenotypic modulation and remodeling in vivo in rats. *Hypertension.* 1995;25(6):1252-1259.

129. Lijnen PJ, Petrov VV, Fagard RH. Angiotensin II-induced stimulation of collagen secretion and production in cardiac fibroblasts is mediated via angiotensin II subtype 1 receptors. *J Renin Angiotensin Aldosterone Syst.* 2001;2(2):117-122.

130. Kim S, Iwao H. Molecular and cellular mechanisms of angiotensin II-mediated cardiovascular and renal diseases. *Pharmacol Rev.* 2000;52(1):11-34.

131. Schnee JM, Hsueh WA. Angiotensin II, adhesion and cardiac fibrosis. *Cardiovasc Res.* 2000;46(2):264-268.

132. Kanemitsu H, Takai S, Tsuneyoshi H, Nishina T, Yoshikawa K, Miyazaki M, Ikeda T, Komeda M. Chymase inhibition prevents cardiac fibrosis and dysfunction after myocardial infarction in rats. *Hypertens Res.* 2006;29(1):57-64.

133. Matsumoto T, Wada A, Tsutamoto T, Ohnishi M, Isono T, Kinoshita M. Chymase inhibition prevents cardiac fibrosis and improves diastolic dysfunction in the progression of heart failure. *Circulation.* 2003;107(20):2555-2558.

134. Takai S, Jin D, Sakaguchi M, Katayama S, Muramatsu M, Matsumura E, Kim S, Miyazaki M. A novel chymase inhibitor, 4-[1-([bis-(4-methyl-phenyl)-methyl]-carbamoyl)3-(2-ethoxy-benzyl)-4-oxo-azetidin e-2-yloxy]-benzoic acid (BCEAB), suppressed cardiac fibrosis in cardiomyopathic hamsters. *J Pharmacol Exp Ther.* 2003;305(1):17-23.

135. Joseph J, Kennedy RH, Devi S, Wang J, Joseph L, Hauer-Jensen M. Protective role of mast cells in homocysteine-induced cardiac remodeling. *Am J Physiol Heart Circ Physiol.* 2005;288(5):H2541-2545.

136. Boerma M, Wang J, Wondergem J, Joseph J, Qiu X, Kennedy RH, Hauer-Jensen M. Influence of mast cells on structural and functional manifestations of radiation-induced heart disease. *Cancer Res.* 2005;65(8):3100-3107.

137. Scandiuzzi L, Beghdadi W, Daugas E, Abrink M, Tiwari N, Brochetta C, Claver J, Arouche N, Zang X, Pretolani M, Monteiro RC, Pejler G, Blank U. Mouse mast cell protease-4 deteriorates renal function by contributing to inflammation and fibrosis in immune complex-mediated glomerulonephritis. *J Immunol.*185(1):624-633.

138. Crivellato E, Beltrami CA, Mallardi F, Ribatti D. The mast cell: an active participant or an innocent bystander? *Histol Histopathol.* 2004;19(1):259-270.

139. Akgul A, Skrabal CA, Thompson LO, Loebe M, Lafuente JA, Noon GP, Youker KA. Role of mast cells and their mediators in failing myocardium under mechanical ventricular support. *J Heart Lung Transplant.* 2004;23(6):709-715.

140. Balakumar P, Singh AP, Ganti SS, Krishan P, Ramasamy S, Singh M. Resident cardiac mast cells: are they the major culprit in the pathogenesis of cardiac hypertrophy? *Basic Clin Pharmacol Toxicol.* 2008;102(1):5-9.

141. Paul M, Poyan Mehr A, Kreutz R. Physiology of local renin-angiotensin systems. *Physiol Rev.* 2006;86(3):747-803.

142. Galli SJ, Kitamura Y. Genetically mast-cell-deficient W/Wv and Sl/Sld mice. Their value for the analysis of the roles of mast cells in biologic responses in vivo. *Am J Pathol.* 1987;127(1):191-198.

143. Chen R, Ning G, Zhao ML, Fleming MG, Diaz LA, Werb Z, Liu Z. Mast cells play a key role in neutrophil recruitment in experimental bullous pemphigoid. *J Clin Invest.* 2001;108(8):1151-1158.

144. Musumeci M, Maccari S, Corritore E, Massimi A, Stati T, Marano G, Catalano L. Signaling pathway-focused gene expression profiling in pressure overloaded hearts. *Ann Ist Super Sanita.*47(3):290-295.

145. Reddy DS, Singh M, Ghosh S, Ganguly NK. Role of cardiac renin-angiotensin system in the development of pressure-overload left ventricular hypertrophy in rats with abdominal aortic constriction. *Mol Cell Biochem.* 1996;155(1):1-11.

146. Heymans S, Lupu F, Terclavers S, Vanwetswinkel B, Herbert JM, Baker A, Collen D, Carmeliet P, Moons L. Loss or inhibition of uPA or MMP-9 attenuates LV remodeling and dysfunction after acute pressure overload in mice. *Am J Pathol.* 2005;166(1):15-25.

147. Muller P, Kazakov A, Semenov A, Bohm M, Laufs U. Pressure-induced cardiac overload induces upregulation of endothelial and myocardial progenitor cells. *Cardiovasc Res.* 2008;77(1):151-159.

148. Henderson BC, Tyagi N, Ovechkin A, Kartha GK, Moshal KS, Tyagi SC. Oxidative remodeling in pressure overload induced chronic heart failure. *Eur J Heart Fail.* 2007;9(5):450-457.

149. Vlahakes GJ, Turley K, Hoffman JI. The pathophysiology of failure in acute right ventricular hypertension: hemodynamic and biochemical correlations. *Circulation.* 1981;63(1):87-95.

150. Olivetti G, Lagrasta C, Ricci R, Sonnenblick EH, Capasso JM, Anversa P. Long-term pressure-induced cardiac hypertrophy: capillary and mast cell proliferation. *Am J Physiol.* 1989;257(6 Pt 2):H1766-1772.

151. Trautmann A, Toksoy A, Engelhardt E, Brocker EB, Gillitzer R. Mast cell involvement in normal human skin wound healing: expression of monocyte chemoattractant protein-1 is correlated with recruitment of mast cells which synthesize interleukin-4 in vivo. *J Pathol.* 2000;190(1):100-106.

152. Kupietzky A, Levi-Schaffer F. The role of mast cell-derived histamine in the closure of an in vitro wound. *Inflamm Res.* 1996;45(4):176-180.

153. Santone DJ, Shahani R, Rubin BB, Romaschin AD, Lindsay TF. Mast cell stabilization improves cardiac contractile function following hemorrhagic shock and resuscitation. *Am J Physiol Heart Circ Physiol.* 2008;294(6):H2456-2464.

154. Singh M, Saini HK. Resident cardiac mast cells and ischemia-reperfusion injury. *J Cardiovasc Pharmacol Ther.* 2003;8(2):135-148.

155. Parikh V, Singh M. Cardiac mast cell stabilization and cardioprotective effect of ischemic preconditioning in isolated rat heart. *J Cardiovasc Pharmacol.* 1998;31(5):779-785.

156. Lindstedt KA, Wang Y, Shiota N, Saarinen J, Hyytiainen M, Kokkonen JO, Keski-Oja J, Kovanen PT. Activation of paracrine TGF-beta1 signaling upon stimulation and degranulation of rat serosal mast cells: a novel function for chymase. *Faseb J.* 2001;15(8):1377-1388.

157. Chen K, Mehta JL, Li D, Joseph L, Joseph J. Transforming growth factor beta receptor endoglin is expressed in cardiac fibroblasts and modulates profibrogenic actions of angiotensin II. *Circ Res.* 2004;95(12):1167-1173.

158. Leask A. TGFbeta, cardiac fibroblasts and the fibrotic response. *Cardiovasc Res.* 2007;74(2):207-212.

159. Eghbali M, Tomek R, Woods C, Bhambi B. Cardiac fibroblasts are predisposed to convert into myocyte phenotype: specific effect of transforming growth factor beta. *Proc Natl Acad Sci U S A.* 1991;88(3):795-799.

160. Zhao XY, Zhao LY, Zheng QS, Su JL, Guan H, Shang FJ, Niu XL, He YP, Lu XL. Chymase induces profibrotic response via transforming growth factor-beta 1/Smad activation in rat cardiac fibroblasts. *Mol Cell Biochem.* 2008;310(1-2):159-166.

6 ACKNOWLEDGEMENTS

I would like to express my gratitude to all those who encouraged and helped me to complete this work.

First of all, I wish to express sincere thanks to my supervisors, Prof. Dr. HA Ghofrani and Prof. Dr. RT Schermuly, for providing the opportunity to join their research group. Their valuable guidance and support throughout the study made me able to complete the work. Their team work and concept of scientific work to give freedom to the group members will be my source of inspiration to keep enthusiasm to move forward in my research carrier.

I would like to express my special gratitude and thanks to Prof. Dr. Werner Seeger, head of internal medicine II, UGMLC and ECCPS. My sincere thanks also go to Prof. Norbert Wiessmann for providing direct and indirect support.

I am exceptionally thankful Dr. Akylbek Sydykov for his outstanding scientific support and for shaping me into admirable scientist. Thank you very much Akyl.

I would like to thank Dr. B. Kojonazarov for sharing his expertise in echocardiography, Dr. Bhola Kumar Dahal, Dr. Djuro Kosanovic for their continuous suggestions in every aspect, Julia Neumann for translating the German version of summary here in this thesis.

My sincere gratitude goes to Ewa Bieniek, Chirstina Vroom, Stephanie Viehmann, Lisa Fröhlich for their valuable technical supports and thanks for creating friendly environment every time.

I am deeply thankful to the faculty and administrative members of MBML and GGL graduate programs. Thanks for organizing highly scientific and specialized courses from experts and participatory model of tutorials (MBML).

Last but not the least, it would be impossible to complete my PhD research without love and support from my mom Tika Luitel, wife Roshana Kandel, lovely daughter Himashana Luitel and all of my family members. Thank you for your love and support.

Thank you

7 CURRICULUM VITAE

Himal Luitel, 11 February, 1979, Married

Unterhof-69, App. Nr. 1007, 935392, Giessen, Germany

Phone: +496413405815 (Fixed); +4917682135827 (Cell)

E-mail: Himal.Luitel@innere.med.uni-giessen.de

Academic Qualification

Year	Qualification	Board/University	Remarks
2008-2012	Dr. hum.biol.	Justus-Liebig University Giessen, Germany	Ongoing
2006-2008	Master of Science in Molecular Biology	Free University Brussels (VUB), Katholieke University Leuven, University of Antwerpen (UA); Belgium	2 yrs
1998-2003	Doctor in Veterinary Medicine	Tribhuvan University (TU), Institute of Agriculture & Animal Science (IAAS), Rampur, Chitwan, Nepal	5.5 yrs
1995-1997	Intermediate Science in Agriculture	TU, Paklihawa Campus, Bhairahawa, Nepal.	2 yrs
1994	School Leaving Certificate	Government of Nepal, Ministry of Education, Janasewa Secondary School, Syangja, Nepal.	10 yrs schooling

Language Proficiency

Nepali (Native), English (Advanced), Hindi (average) and German (fair)

Skills

Statistical analysis using Microsoft Excel, Graph Pad Prism and SPSS, Hemodyanamic measurements of mouse (both right and left heart catheterization with fluid filled and miller catheter system), histology and tissue stereology, cell culture techniques, molecular biological tools (PCR, RT-PCR, western blot, northern blot, chip assay)

Scholarships/Awards/Grants

1. Molecular Biology and Medicine of the Lungs (MBML) scholarship for PhD study (2008 October to September 2011) in Justus Liebig University, Giessen, Germany.
2. MBML travel grants (2011) for attending American Thoracic Society Conference in Denver, Colorado held on 13-18 May, 2011.
3. VLIR (Flemish Interuniversity Council, Belgium) scholarship for Master of Science in Molecular Biology (September 2006 to September 2008) in Free University Brussels (VUB), Katholieke University Leuven, University of Antwerpen (UA); Belgium
4. Full Scholarship in Bachelor of Veterinary Science & Animal Husbandry in Tribhuvan University, Nepal (1998 to 2003)

Work experience

SN	Designation	Duration	Institute	Responsibilities
1	Lecturer	April, 2005 to September, 2006	Himalayan College of Agricultural Sciences and Technology (HICAST), Bhaktapur, Nepal.	Faculty and Veterinary clinician at HICAST veterinary teaching hospital
2	Veterinary officer	August, 2004 to April 2005	Livestock & Poultry Disease Diagnostic Clinic, Chitwan, Nepal	Disease diagnosis and treatment of domesticated animals, pets and poultry birds
3	Research assistant	April 2002 to September, 2004	Food safety	Analysis of milk, egg and fecal samples from dairy, meat and poultry industries.
4	Instructor	November 2003 to April 2005.	Kantipur College of Medical Sciences, Bharatpur, Chitwan, Nepal.	Theoretical as well as practical courses for Junior Technical Assistant

Trainings

SN	Name of the training	Duration	Organizer
1	SPSS	10th, 19th, 21st, 24th, 26th Jan, 2011	University of Giessen, International Giessen Graduate School for Life Sciences (GGL)
2	Biostatistics	13-17th July, 2009	University of Giessen, Molecular Biology and Medicine of the Lungs (MBML)
3	Tissue stereology course	29th Aug to 6th Sept 2011	University of Bern, Department of Anatomy, Switzerland
4	Federation of European Laboratory Animal Associations (FELASA) Course	19-23 Sept, 2011	Charite University Berlin, Germany

Conferences, Seminars and workshops

1. Molecular Biology and Medicine of the Lungs (MBML) annual retreat, University of Giessen, Germany, 20-22 June 2011, **Oral talk:** "Role of Mast cell in pressure overload induced right ventricular hypertrophy."
2. 2nd international conference, Excellence Cluster Cardio-pulmonary System (ECCPS), Bad Nauheim, Germany, 16-18 June 2011, **Poster:** "Role of Mast cell in pressure overload induced right ventricular hypertrophy."
3. American Thoracic Society (ATS) 2011 International Conference, Denver, Colorado, USA, 13-18 May, 2011, **Poster:** "Contribution of Progenitor Cells in Pressure Induced Right Ventricular Hypertrophy."
4. MBML annual retreat, 9-11 august 2010, **Oral talk:** "Contribution of Progenitor Cells in Pressure Induced Right Ventricular Hypertrophy."

Co-author in published abstracts

1. Effects of the multikinase inhibitor Sunitinib on right ventricular remodeling in an experimental model of right heart hypertrophy. S.S. Pullamsetti, B. Kojonazarov, A.

Sydykov, **H. Luitel,** D. Kosanovic, *et al*. (A6592, Oral presentation, ATS conference **2010**, New Orleans, USA)

2. Improvement of right heart structure and function by Bay 41-8543 in pulmonary artery banded mice. Wiebke Janssen**,** Yves Schymura**,** Astrid Wietelmann**,** Johannes-Peter Stasch**, Himal Luitel,** Norbert Weissmann**,** Hossein A Ghofrani**,** Friedrich Grimminger**,** Thomas Braun**,** Werner Seeger and Ralph T Schermuly, 5th International Conference on cGMP: Generators, Effectors and Therapeutic Implications, June 24-26, 2011, Halle (Saale)/Germany

Research works

1. Contribution of progenitor cells in pressure overload induced right ventricular hypertrophy, research going on, Justus Liebig University, Giessen, Germany.
2. Role of mast cells in pressure overload induced right ventricular hypertrophy, research going on, Justus Liebig University, Giessen, Germany.
3. "Expression and purification of recombinant Shiga-like toxin of Enterohemorrhagic *E. coli*". As a part of Master's thesis in University of Ghent, Faculty of Veterinary Science, Department of Parasitology, Virology and Immunology, Salisburylaan 133, 9820 Merelbeke, Belgium. (September 2007 Sept. 1008).
4. Seroprevalence of Brucellosis & E coli O157:H7 strain in slaughtered animals in Chitwan district, Nepal, Research conducted under joint collaboration of Veterinary Teaching Hospital, Tribhuvan University, Institute of Agriculture Science and Animal Husbandry and Tuft University School of Veterinary medicine, Massachusetts, NE, USA (July to October, 2004).
5. Prevalence of Zoonotic Salmonellosis in poultry industry in Chitwan district, Nepal, Research conducted under joint collaboration of Veterinary Teaching Hospital, Tribhuvan University, Institute of Agriculture Science and Animal Husbandry and Tuft University School of Veterinary medicine, Massachusetts, NE, USA (November 2004 to may, 2005).

Publications

1. Kosanovic D, Kojonazarov B, **Luitel H**, Dahal BK, Sydykov A, Cornitescu T, Jansen W, Brandes RP, Ghofrani HA, Weissmann N, Grimminger F, Seeger W, Schermuly

RT, Therapeutic efficacy of TBC3711 in monocrotaline-induced pulmonary hypertension. Respir Res., 2011 June 23;12(1):87.

2. Effects of multikinase inhibitors on pulmonary vascular and right ventricular remodeling. Kojonazarov B, Sydykov A, Pullamsetti SS, **Luitel H**, Dahal BK, Kosanovic D, Tian X, Majewski M, Baumann C, Evans S, Phillips P, Fairman D, Davie N, Wayman C, Kilty I, Weissmann N, Grimminger F, Seeger W, Ghofrani HA, Schermuly RT. 2011 **(accepted International Journal of Cardiology**)
3. Intratracheal application of soluble guanylyl cyclase stimulator BAY41-8543 for treatment of pulmonary arterial hypertension. Amirjanians V, Egemnazarov B, Sydykov A, **Luitel H**, Pradhan K, Stasch JP, Redlich G, Weissmann N, Grimminger F, Seeger W, Ghofrani HA, Schermuly RT. 2011 **(submitted**)
4. Laboratory Manual of Livestock production and management, Veterinary theriogenology published by Himalayan College of Agricultural Sciences and Technology (HICAST), Purbanchal University, Bhaktapur, Nepal. (2005)
5. Parturient Paresis in Dairy Cow: Case report, The Blue Cross, The annual Bulletin of Nepal Veterinary Students Association (NVSA), Tribhuvan University, Institute of Agriculture and Animal Sciences (IAAS), Rampur, Chitwan, Nepal. (2003)
6. Sero-prevelance of Brucellosis and E. coli O157:H7 strain in slaughtered animals in Chitwan District, Nepal, Thesis work of Bachelor of Veterinary Sciences and Animal Husbandry (B.V.Sc. & A.H.), Tribhuvan University, Institute of Agriculture and Animal Science (IAAS), Rampur, Chitwan, Nepal. (2004)

8 STATEMENT/ERKLÄRUNG AN EIDES STATT

“I declare that I have completed this dissertation single-handedly without the unauthorized help of a second party and only with the assistance acknowledged therein. I have appropriately acknowledged and referenced all text passages that are derived literally from or are based on the content of published or unpublished work of others and all information that relates to verbal communications. I have abided by the principles of good scientific conduct laid down in the charter of the Justus Liebig University of Giessen in carrying out the investigations described in the dissertation.”

“Ich erkläre: Ich habe die vorgelegte Dissertation selbständig, ohne unerlaubte fremde Hilfe und nur mit den Hilfen angefertigt, die ich in der Dissertation angegeben habe. Alle Textstellen, die wörtlich oder sinngemäß aus veröffentlichten oder nicht veröffentlichten Schriften entnommen sind, und alle Angaben, die auf mündlichen Auskünften beruhen, sind als solche kenntlich gemacht. Bei den von mir durchgeführten und in der Dissertation erwähnten Untersuchungen habe ich die Grundsätze guter wissenschaftlicher Praxis, wie sie in der „Satzung der Justus-Liebig-Universität Gießen zur Sicherung guter wissenschaftlicher Praxis“ niedergelegt sind, eingehalten.“

Himal Luitel

Giessen

21.08.2012